Engineering Journal

American Institute of Steel Construction

Fourth Quarter 2012 Volume 49, No. 4

www.aisc.org

ENGINEERING JOURNAL

AMERICAN INSTITUTE OF STEEL CONSTRUCTION

Dedicated to the development and improvement of steel construction, through the interchange of ideas, experiences and data.

ENGINEERING JOURNAL (ISSN 0013-8029) is published quarterly. Subscriptions: Members: one subscription, $40 per year, included in dues; Additional Member Subscriptions: $40 per year. Non-Members U.S.: $160 per year. Foreign (Canada and Mexico): Members $80 per year. Non-Members $160 per year. Published by the American Institute of Steel Construction at One East Wacker Drive, Suite 700, Chicago, IL 60601.

Periodicals postage paid at Chicago, IL and additional mailing offices. **Postmaster:** Send address changes to ENGINEERING JOURNAL in care of the American Institute of Steel Construction, One East Wacker Drive, Suite 700, Chicago, IL 60601.

Message from the Editor

A privilege of being the editor of *Engineering Journal* is that I get to work with the best and brightest of the structural steel industry, such as Reidar Bjorhovde, Dr.-Ing., Ph.D., P.E., Research Editor of *Engineering Journal*. His "Current Steel Structures Research" column has been a feature of our journal for eight years now. However, starting in 2013 his column—a quarterly snapshot of steel research around the globe—will appear semi-annually, rather than quarterly.

Dr. Bjorhovde will continue to travel around the world (no exaggeration) to participate in a wide variety of industry events. If you haven't already done so, check out his 2011 interview with AISC's Margaret Matthew (Podcast No. 11 at www.aisc.org/podcasts) for highlights from past travels. We are pleased that Dr. Bjorhovde can continue his efforts for us. Watch for his next columns in the second and fourth quarter issues in 2013.

I would also like to thank our reviewers for their contributions to the success of our journal. A list of our 2012 reviewers is posted on our web site at www.aisc.org/ej.

Sincerely,

Keith A. Grubb, P.E., S.E.
Editor

Axial Capacities of Eccentrically Loaded Equal-Leg Single Angles: Comparisons of Various Design Methods

YUWEN LI

ABSTRACT

For most structural engineers, the design of an eccentrically loaded single angle without lateral restraint along its length was considered to be a formidable task prior to the publication of the 2005 AISC *Specification for Structural Steel Buildings*. According to Section E5 of the 2005 *Specification*, the effects of eccentricity on single-angle members are permitted to be neglected by using the effective slenderness ratio as specified, provided that members are loaded at the ends in compression through the same leg; members are attached by welding or by a minimum of two-bolt connections; there are no intermediate transverse loads; the leg length ratio is less than 1.7, if angles are connected through the shorter leg; and the modified *KL/r* is less than or equal to 200.

Table 4-12 of the 13th edition AISC *Steel Construction Manual* provided the available strengths in axial compression of eccentrically loaded single angles, with the assumption that the compressive force is applied at the geometric *y-y* axis at a distance of 0.75*t* from the back of the connected leg, where *t* is the angle thickness. Table 4-12 has been revised in the 14th edition AISC *Steel Construction Manual*. The new table corrects some numerical errors in the calculations and moves the compressive force to the midpoint of the connected leg. The values of the axial compressive design strength in Table 4-12 are developed on the basis of bending about the principal axes *w-w* and *z-z*.

Keywords: eccentrically loaded single angles, design tables.

INTRODUCTION

Single angles are commonly used as secondary bracing members for bridges and other structures, as web members for small or medium-sized truss structures, and in latticed structures, such as transmission towers. In structural analysis, single-angle members are always treated as "truss members" that can take only axial loads, either in tension or in compression. However, because single angles are connected to gusset plates through one leg using welding or bolting, the members are subjected to both axial and flexural demands resulting from the eccentric connection. Although the single angle is the most basic shape of hot-rolled steel sections, its behavior under eccentric force is complex and difficult to predict due to the fact that its geometric axes do not align with its principal axes. Therefore, the design method for predicting the axial strength of single angles evolves with the better understanding of its behavior, and it is evident in specification revisions over the years.

A design example of eccentrically loaded equal-leg single angles was presented in the 1st edition AISC *Manual of Steel Construction*, *LRFD* (AISC, 1986). However, there was not a specification specifically for single angles. The stand-alone *Specification for Allowable Stress Design of Single-Angle Members* was first introduced by the 9th edition AISC *Steel Construction Manual*, *ASD* (AISC, 1989). In 1993, AISC introduced the first stand-alone *Specification for Load and Resistance Factor Design of Single-Angle Members* (AISC, 1993), and this specification was included in the 2nd edition AISC *Manual of Steel Construction, LRFD* (AISC, 1994). The same specification was updated in 2000 and was included in the 3rd edition of the AISC *Manual of Steel Construction, LRFD* (AISC, 2001). Single-angle design was finally incorporated into the 2005 AISC *Specification for Structural Steel Buildings* (AISC, 2005a) with additional improvements. For instance, the slenderness ratio of eccentrically loaded single-angle members was modified to make use of the formulas applicable to concentrically loaded members.

Design tables for equal-leg single angles in compression based on the 1989 ASD *Specification* were developed by Walker (1991). Tables for the design strength of concentrically loaded single-angle struts based on the 1986 LRFD *Specification* were presented by Zureick (1993). Tables for the design strength of eccentrically loaded single angle struts based on the 1993 LRFD *Specification* were prepared by Sakla (2001). The 13th edition AISC *Manual* (AISC, 2005b) provided a table of available strengths for eccentrically loaded single angles in axial compression (Table 4-12), with an assumption that the compressive force is applied at

YuWen Li, P.E., Principal Structural Engineer, Gannett Fleming, Inc., Audubon, PA. E-mail: yli@gfnet.com

the geometric *y-y* axis at a distance of 0.75*t* from the back of the connected leg. Table 4-12 has been completely updated in the 14th edition *Manual* (AISC, 2011) with the introduction point of the compressive force moved to the mid-point of the connected leg, *b*/2.

DESIGN CONSIDERATIONS OF SINGLE ANGLES IN COMPRESSION

Slenderness Ratio Requirement

The slenderness ratio *KL/r* requirement differs among the design codes. For members designed on the basis of compression, the user note in Section E2 of the 2010 AISC *Specification* indicates that the slenderness ratio preferably should satisfy $KL/r \leq 200$. However, the *KL/r* ratio requirement is more stringent for steel bridges: the slenderness ratio should satisfy $KL/r \leq 120$ for main members and $KL/r \leq 140$ for bracing members according to Section 6.9.3 of AASHTO (2004). It should be noted that bracing for curved girder bridges are considered main members.

Effective Length Factor

The effective length factor $K = 1.0$ should be used to determine the unbraced length of single angles in compression based on Chapter C of the 2010 AISC *Specification*. The effective length factor $K = 0.75$ for bolted or welded end connections at both ends has been used by AASHTO (2004). However, a change was made in AASHTO (2007) to use $K = 1.0$ for single angles, regardless of end connection types.

Minimum Size of Single Angles

The minimum size of angles is not stipulated AISC specifications. Although AASHTO does not specifically limit the minimum angle size, it does limit the minimum thickness of most structural steels to 5/16 in., including angles. However, the designer should check with owners about the requirements for the minimum sizes of single angles that they may have. For example, MassDOT requires a minimum size of L3×3×3/8, PennDOT and NJDOT require L3½×3½×3/8 as a minimum, and VDOT requires L5×3×3/8 as a minimum.

Connection to Gusset Plate

Single-angle members are attached to the gusset plate by either welding or bolting. Connection type and details affect how the axial load is transferred through the connection from the gusset plate to the angle members. For welded connections where fillet welds are placed on two sides of the connected leg, conventional wisdom says to place the welds in such a way that the center of gravity of weld resistance coincides with the centroid of the member (Figure 1a vs. Figure 1b) in order to minimize the torsion induced in the

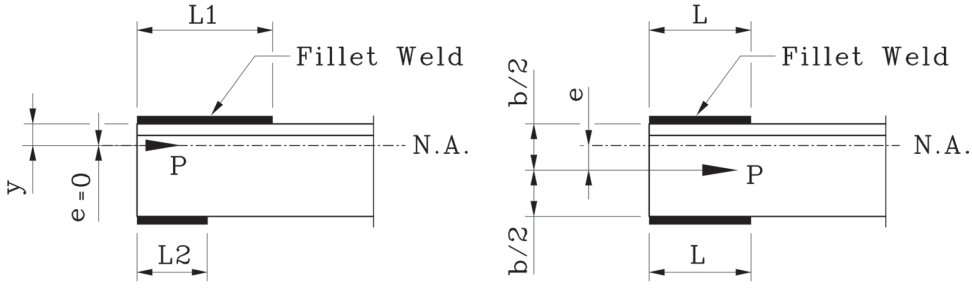

Fig. 1. Welded connection.

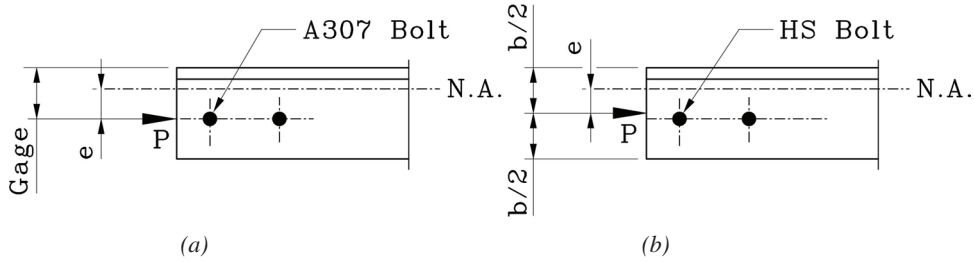

Fig. 2. Bolted connection.

connection. It is suggested that this is even more desirable when the member is subjected to repeated or reversed stress.

For bolted connections, a minimum of two bolts are required per connection per AISC and AASHTO. Bolt holes often follow the gage line of the angle. If ASTM A307 bolts are used (Figure 2), the axial force is applied to the angle members through the bolt line. The axial force can be considered applied through the mid-point of the bolted leg if high-strength bolted connections are designed as slip critical joints and the friction between the connected leg and gusset plate is uniformly distributed.

Placement of welds and bolts is stipulated in Chapter J of the 2010 AISC *Specification* and has evolved over the years. The provision of arranging the center of gravity of the welds or bolts group to coincide with the center of gravity of the member is not applicable to statically loaded single angles according to the 1989 AISC ASD *Specification*, the 1986, 1998 and 2001 AISC LRFD *Specifications*, and the 2005 AISC *Specification*. The wording "statically loaded" is eliminated from Section J1.7 of the 2010 AISC *Specification*. However, the requirement for balancing the welds about the neutral axis of the angle is still warranted when the members are subjected to cyclic loading. Therefore, one can assume that the static axial load is applied at the mid-point of the connected leg, as it generates larger axial compressive design strength (Example 3), and the cyclic axial load is applied at neutral axis because it generates smaller and conservative axial compressive design strength (Example 4).

Eccentricity

As previously discussed, an end connection through one leg creates the eccentricity for the applied axial load that induces the end moment and, therefore, affects the load carrying capacity of either the connection or the member, or both. The effect of connection eccentricity is a function of connection and member stiffness, the proper eccentricity should be assumed when computing the axial capacity of single angles. Blodgett (1966) concluded that if the gusset plate is very flexible and offers no restraining action at the end of the member, the moment due to connection eccentricity must be resisted by the member, not by the connection. On the other hand, if the gusset plate is rigid enough so that there is no end rotation of the member, the moment due to connection eccentricity must be resisted by the connection, not by the member. The same concept is now presented in Figure C-D3.3 of the 2010 AISC *Specification* Commentary.

The actual eccentricity in the angle is less than the distance from the gusset centerline if there is any restraint from the gusset (Lutz, 2006). Woolcock and Kitipornchai (1986) recommended reduction of the eccentricity to $y - t/2$, where t is the angle thickness. Because the eccentricity will affect the capacity of the single angle, if a larger capacity is required, the connection should be evaluated to see if the eccentricity can be minimized. Three scenarios of end connections are summarized as follows:

- ***Figure 3a.*** When the end connection is flexible relative to the single-angle member, the eccentricity in the angle can be assumed as $e = y$ or $e = y + t_1/2$, with the latter being more conservative, and used to generate Table 4-12 in the 13th and 14th editions of the AISC *Manual*.

- ***Figure 3b.*** When the end connection is rigid relative to the single-angle member, the eccentricity in the angle can be assumed as $e = y$ or $e = y - t/2$, with the former being more conservative.

- ***Figure 3c.*** When the end connection is similar to that shown, eccentricity in the angle can be assumed as $e = y - t_1/2$, which is measured from the mid-thickness of gusset plate to the neutral axis of the angle.

DESIGN EXAMPLES

Four methods are presented here to illustrate the design procedures involved with the eccentrically loaded single angle. Equation and section references in these examples refer to the 2010 AISC *Specification*.

- **Method 1.** Axial capacities of equal-leg angle (L4×4×⅜) based on Section E5, the effects of eccentricity and end restraint are incorporated by using the effective slenderness ratio.

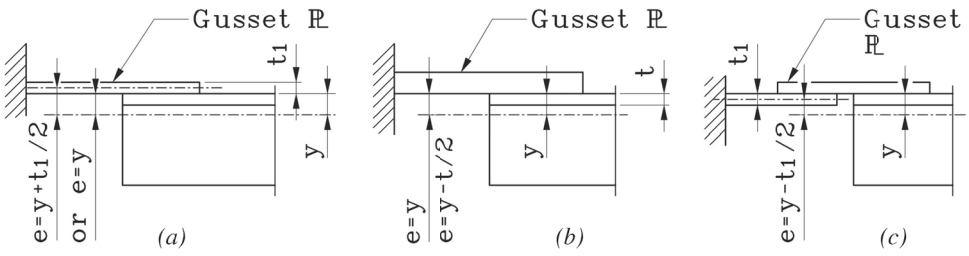

Fig. 3. Eccentricity.

- **Method 2.** Axial capacities of equal-leg angle (L4×4×⅜) based on Sections E7, F10 and H2, assuming that bending is about the one of the geometric axes, and the eccentricity is $e = y + t_1/2$, where $t_1 = 1.5t$ and t is the angle thickness.

- **Method 3.** Axial capacities of equal-leg angle (L4×4×⅜) based on Sections E7, F10 and H2, assuming that bending is about the principal axes and axial load is applied at mid-point of the connected leg, and the eccentricity is $e = y + t_1/2$, where $t_1 = 1.5t$ and t is the angle thickness.

- **Method 4.** Axial capacities of equal-leg angle (L4×4×⅜) based on Sections E7, F10 and H2, assuming that bending is about the principal axes and axial load is applied at one of the geometric axis of the angle, and the eccentricity is $e = y + t_1/2$, where $t_1 = 1.5t$ and t is the angle thickness.

Method 1

L4×4×⅜, connected one leg. See Figure 4.

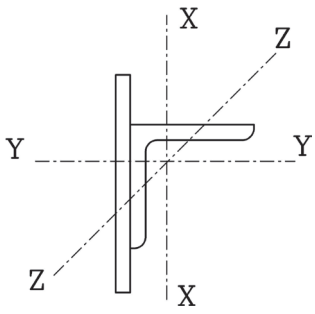

Fig. 4. Method 1.

L = 72 in.
K = 1.0
F_y = 36 ksi
E = 29,000 ksi
A_g = 2.86 in.^{2}
b = 4.0 in.
t = 0.375 in.
r_x = 1.230 in.
r_z = 0.779 in.
KL/r ≤ 200
ϕ_c = 0.90
Ω_c = 1.67

Solution

Check the required radius of gyration, r_{min}:

$$r_{min} = KL/200 = 1.0(72)/200 = 0.360 \text{ in}$$

0.360 in. < r_z = 0.779 in. **OK**

Determine the effective slenderness ratio, *KL/r*. For equal-leg angles or unequal-leg angles connected through the longer leg that are individual members:

$$\frac{L}{r_x} = \frac{72}{1.23} = 58.5 \le 80$$

Therefore, from Equation E5-1:

$$\frac{KL}{r} = 72 + 0.75\frac{L}{r_x} = 72 + 0.75(58.5) = 116$$

Determine if reduction factor Q, for unstiffened elements is applicable [Section E7.1(c)]:

$$b/t = 4.0/0.375 = 10.7$$

From *Specification* Table B4.1a:

$$\lambda_r = 0.45\sqrt{\frac{E}{F_y}} = 0.45\sqrt{\frac{29{,}000}{36}} = 12.8$$

Because $b/t < \lambda_r$, the member is classified as a non-slender section and $Q_s = 1.0$ (Equation E7-10).

Therefore, $Q = Q_s = 1.0$.

From Equation E3-4, the elastic buckling stress, F_e, is:

$$F_e = \frac{\pi^2 E}{\left(\frac{KL}{r}\right)^2} = \frac{\pi^2(29{,}000)}{116^2} = 21.2 \text{ ksi}$$

For calculating the critical stress, F_{cr}, Equation E3-2 is essentially a special case of Equation E7-2, when the member is classified as a non-slender section.

$$KL/r \le 4.71\sqrt{\frac{E}{QF_y}} = 4.71\sqrt{\frac{29{,}000}{1.0(36)}} = 134$$

Therefore, using Equation E3-2 or E7-2:

$$F_{cr} = Q\left[0.658^{\frac{QF_y}{F_e}}\right]F_y$$

$$= 1.0\left[0.658^{1.0(36)/21.31}\right](36) = 17.8 \text{ ksi}$$

The nominal compressive strength may be calculated from Equations E3-1 or E7-1:

$$P_n = F_{cr}A_g = 17.8(2.86) = 50.8 \text{ kips}$$

Calculate the design compressive strength, $\phi_c P_n$, and the allowable compressive strength, P_n/Ω_c, using Section E1:

$\phi_c P_n = 0.90(50.8) = 45.7$ kips (LRFD)

$P_n/\Omega_c = 50.8/1.67 = 30.4$ kips (ASD)

Method 2

L4×4×⅜, connected to one leg, axial load is applied at the middle thickness of the gusset plate. The angle is designed on the basis of geometric axis (*x*-*x*) bending. See Figure 5.

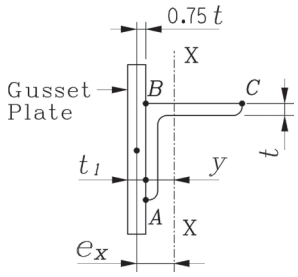

Fig. 5. Method 2.

t_1 = $1.5t = 9/16$ in.
I_x = 4.32 in.^{4}
S_x = 1.50 in.^{3}
y = 1.13 in.
$S_{x(A,B)}$ = I_x/y = 3.82 in.^{3}
e_x = $0.75t + y$ = 1.41 in.
ϕ_b = 0.90

See Method 1 for additional information.

Solution

1. Calculate the design axial stress, F_{ca}.

Determine the maximum slenderness ratio, *KL/r*:

$$\frac{KL}{r} = \frac{KL}{r_z} = \frac{72}{0.779} = 92.4 \le 200, \textbf{ OK}$$

Determine the reduction factor Q, for unstiffened element from Section E7.1(c):

Same as Method 1, $Q = Q_s = 1.0$

Determine the elastic buckling stress, F_e from Equation E3-4:

$$F_e = \frac{\pi^2 E}{\left(\frac{KL}{r}\right)^2} = \frac{\pi^2 (29{,}000)}{92.4^2} = 33.5 \text{ ksi}$$

Determine the critical stress, F_{cr}:

$$KL/r \le 4.71\sqrt{\frac{E}{QF_y}} = 4.71\sqrt{\frac{29{,}000}{1.0(36)}} = 134$$

Therefore, using Equation E3-2 or E7-2:

$$F_{cr} = Q\left[0.658^{\frac{QF_y}{F_e}}\right]F_y$$

$$= 1.0\left[0.658^{1.0(36)/33.5}\right](36) = 23.0 \text{ ksi}$$

Determine the design axial stress, F_{ca}, using Section H2:

$F_{ca} = \phi_c F_{cr} = 0.90(22.7) = 20.7$ ksi

Determine the required axial stress, f_{ra}:

$f_{ra} = P_r/A_g = P_r/2.86$ ksi

2. Calculate the design flexural stress, F_{cbx} (Section F10).

Check angle leg compactness for flexure (Table B4.1b):

$$\lambda_p = 0.54\sqrt{E/F_y} = 0.54\sqrt{29{,}000/36} = 15.3$$

$$\lambda_r = 0.91\sqrt{E/F_y} = 0.91\sqrt{29{,}000/36} = 25.8$$

Because $b/t < \lambda_p$, member is classified as a compact section.

Determine flexural strength based on leg local buckling (Section F10.3):

Because the member is a compact section, the limit state of local buckling does not apply.

Determine flexural strength based on yielding (Section F10-1):

$M_y = F_y S_x = 36(1.50) = 54.0$ kip-in.

$M_n = 1.5M_y = 1.5(54.0) = 81.0$ kip-in

Determine flexural strength based on lateral-torsional buckling for bending about one of the geometric axes (Section F10.2):

Calculate the elastic lateral-torsional buckling moment, M_e (Equation F10-6b):

$$M_e = \frac{0.66Eb^4 tC_b}{L_b^2}\left(\sqrt{1+0.78\left(\frac{L_b t}{b^2}\right)^2}+1\right)$$

$$= \frac{0.66(29{,}000)(4)^4(0.375)(1.0)}{72^2}$$

$$\times\left(\sqrt{1+0.78\left(\frac{72(0.375)}{4^2}\right)^2}+1\right)$$

$$= 991 \text{ kip-in}$$

Because $M_e > M_y = 0.8F_yS_x = 0.8(36)(1.50) = 43.2$ kip-in, use Equation F10-3:

$$M_n = \left(1.92 - 1.17\sqrt{\frac{M_y}{M_e}}\right)M_y \le 1.5M_y$$

$$= \left(1.92 - 1.17\sqrt{\frac{43.2}{991}}\right)(43.2)$$

$$= 72.39 \le 1.5(43.20) = 64.8 \text{ kip-in}$$

Determine the controlling nominal flexure strength, M_n:

$M_n = \min [81.0,64.8] = 64.8$ kip-in.

Determine the design flexure strength, $\phi_b M_n$:

$\phi_b M_n = 0.90(64.8) = 58.3$ kip-in.

Determine the design flexure stresses, $F_{cbx(C)}$ and $F_{cbx(A,B)}$:

$F_{cbx(C)} = \phi_b M_n/S_x = 58.3/1.50 = 38.9$ ksi

$F_{cbx(A,B)} = \phi_b M_n/S_{x(A,B)} = 58.3/3.82 = 15.3$ ksi

3. Calculate the interaction of flexure and axial stresses.

Because the angle is a non-symmetric section subject to compression and single-axis bending about one of the geometric axes, Equation H2-1 should be used and can be written as:

$$\left|\frac{f_{ra}}{F_{ca}} + \frac{f_{rbx}}{F_{cbx}}\right| \le 1.0$$

This can be rewritten based on signs of bending stress at the points of consideration as follows:

Points A and B:

$$\left|\frac{f_{ra}}{F_{ca}} + \frac{f_{rbx(A,B)}}{F_{cbx(A,B)}}\right| \le 1.0$$

Point C:

$$\left|\frac{f_{ra}}{F_{ca}} - \frac{f_{rbx(C)}}{F_{cbx(C)}}\right| \le 1.0$$

where

f_{ra} = required axial stress

$f_{rbx(A,B)}$, $f_{rbx(C)}$ = required flexure stresses

Determine moment due to axial load, $M_{rx} = B_{1x}(e_xP_r)$ from Equation A-8-1, where:

B_{1x} = multiplier to account for P-δ effect based on Section 8.2 of Appendix 8.

$$B_{1x} = \frac{C_m}{1 - \alpha P_r / P_{e1x}} \ge 1.0 \quad \text{(Equation A-8-3)}$$

α = 1.0 (LRFD) or 1.6 (ASD)

$C_m = 1.0$ (conservative)

$$P_{e1x} = \frac{\pi^2 EI^*}{(K_1L)^2} \quad \text{(Equation A-8-5)}$$

$EI^* = 0.8\tau_b EI_x$

τ_b = 1.0, when $\alpha P_r/P_y \le 0.5$

$= 4(\alpha P_r/P_y)[1-(\alpha P_r/P_y)]$ otherwise

$\alpha P_r/P_y = 1.0(P_r)/[(36)(2.86)] = P_r/103$

$$P_{e1x} = \frac{\pi^2 EI^*}{(K_1L)^2} = \frac{\pi^2(0.8)\tau_b(29{,}000)(4.32)}{[1.0(72)]^2} = 191\tau_b$$

$$B_{1x} = \frac{C_m}{1 - \alpha P_r/P_{e1x}} = \frac{1.0}{1 - 1.0(P_r)/191\tau_b} = \frac{191\tau_b}{191\tau_b - P_r}$$

Determine the required second-order flexural strength, M_{rx}, as follows:

$$M_{rx} = B_{1x}(e_xP_r) = \left[\frac{191\tau_b}{191\tau_b - P_r}\right](e_xP_r)$$

Apply Equation H2-1 at points A and B:

$$\left|\frac{f_{ra}}{F_{ca}} + \frac{f_{rbx(A,B)}}{F_{cbx(A,B)}}\right| = \left|\frac{P_r/2.86}{20.7} + \frac{\left[\frac{191\tau_b(e_xP_r)}{191\tau_b - P_r}\right]\frac{1}{3.82}}{15.3}\right| \le 1.0$$

Solving the previous equation, $P_r = 22.5$ kips.

Apply Equation H2-1 at point C:

$$\left|\frac{f_{ra}}{F_{ca}} - \frac{f_{rbx(C)}}{F_{cbx(C)}}\right| = \left|\frac{P_r/2.86}{20.7} - \frac{\left(\frac{191\tau_b(e_xP_r)}{191\tau_b - P_r}\right)\frac{1}{1.50}}{38.9}\right| \le 1.0$$

Solving the previous equation, $P_r = 56.7$ kips.

Determine the design compressive strength, $\phi_c P_n$, and the allowable compressive strength, P_n/Ω_c:

$\phi_c P_n = P_r = \min(22.5, 56.7) = 22.5$ kips (LRFD)

$P_n/\Omega_c = (P_r/\phi_c)/\Omega_c = (22.5/0.9)/1.67 = 15.0$ kips (ASD)

Method 3

L4×4×⅜, connected to one leg, axial load is applied at mid-point of angle leg and mid-thickness of gusset plate. The angle is designed on the basis of principal axes (*w-w, z-z*) bending. See Figure 6.

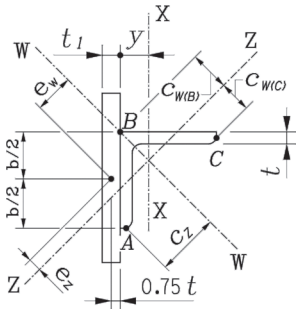

Fig. 6. Method 3.

t_1 = $1.5t$ = 9/16 in.
I_x = 4.32 in.^{4}
I_y = 4.32 in.^{4}
e_w = 1.613 in.
e_z = 0.382 in.
I_z = $A_g(r_z)^2$ =1.74 in.^{4}
I_w = $I_x + I_y - I_z$ = 6.90 in.^{4}
r_w = $\sqrt{I_w / A_g}$ = 1.55 in.^{4}

See Methods 1 and 2 for additional information.

Solution

1. Calculate the angle concentric design axial stress, F_{ca}:

Same as Method 2.

F_{ca} = 20.7 ksi

Determine the required axial stress, f_{ra}:

$f_{ra} = P_r/A_g = P_r/2.86$ ksi

2. Calculate the angle flexural strength about major principal axis, $\phi_b M_{nw}$.

Angle leg compactness for flexure is same as Method 2. Because $b/t < \lambda_p$, the limit state of local buckling does not apply.

Determine the flexural strength based on yielding (Section F10-1):

Points A and C:

$C_z = \sin 45°(b - t/2) = (0.707)(4 - 0.375/2) = 2.70$ in.

$S_w = I_w/C_z$ = 6.90/2.70 = 2.56 in.^{3} (compare to 2.56 in.^{3} from AISC Shapes Database V14.0)

$M_{yw} = F_y S_w = 36(2.56) = 92.2$ kip-in.

$M_{nw} = 1.5M_{yw} = 1.5(92.2) = 138$ kip-in.

Determine the flexural strength based on lateral-torsional buckling for bending about the major principal axis (Section F10.2):

The elastic lateral-torsional buckling moment, M_e, from Equation F10-4, is:

$$M_e = \frac{0.46Eb^2t^2C_b}{L}$$
$$= \frac{0.46(29{,}000)(4)^2(0.375)^2(1.0)}{72}$$
$$= 417 \text{ kip-in}$$

Because $M_e > M_{yw}$, use Equation F10-3 to calculate M_{nw}:

$$M_{nw} = \left(1.92 - 1.17\sqrt{\frac{M_{yw}}{M_e}}\right)M_{yw} \le 1.5M_{yw}$$
$$= \left(1.92 - 1.17\sqrt{\frac{92.2}{417}}\right)92.2 \le 138$$
$$= 126 \le 138$$
$$= 126 \text{ kip-in.}$$

Determine the controlling nominal flexure strength, M_{nw}:

M_{nw} = min [138, 126] = 126 kip-in.

Determine the design flexure strength, $\phi_b M_{nw}$:

$\phi_b M_{nw} = 0.90(126) = 113$ kip-in.

Determine the design flexure stresses, $F_{cbw(A)}$ and $F_{cbw(C)}$:

$F_{cbw(A)} = F_{cbw(C)} = \phi_b M_{nw}/S_w = 113/2.56 = 44.1$ ksi

3. Calculate the angle flexural strength about minor principal axis, $\phi_b M_{nz}$.

Determine flexural strength based on yielding (Section F10-1):

Point B

$C_{w(B)} = y/\sin 45° = 1.13/0.707 = 1.60$ in.

$S_{z(B)} = I_z/C_{w(B)} = 1.74/1.60 = 1.09$ in.^{3} (compare to 1.08 in.^{3} from AISC Shape Database V14.0)

Points A and C

$$C_{w(A,C)} = \sin 45°(b + t/2) - C_{w(B)}$$
$$= 0.707(4 + 0.375/2) - 1.60 = 1.36 \text{ in.}$$

$S_{z(A,C)} = I_z/C_{w(A,C)} = 1.74/1.36 = 1.27$ in.^{3} (compare to 1.27 in.^{3} from AISC Shape Database V14.0)

Thus,

$$M_{yz} = F_y S_{z(B)} = 36(1.080) = 38.9 \text{ kip-in.}$$

Determine the nominal flexure strength, M_{nz}:

$$M_{nz} = 1.5\, M_{yz} = 1.5(38.9) = 58.3 \text{ kip-in.}$$

Determine the design flexure strength, $\phi_b M_{nz}$:

$$\phi_b M_{nz} = 0.90(58.3) = 52.5 \text{ kip-in.}$$

Determine the design flexure stresses $F_{cbx(B)}$, $F_{cbx(A)}$ and $F_{cbx(C)}$:

$$F_{cbz(B)} = \phi_b M_{nz}/S_{z(B)} = 52.5/1.08 = 48.6 \text{ ksi}$$

$$F_{cbz(A)} = F_{cbz(C)} = \phi_b M_{nz}/S_{z(A,C)} = 52.5/1.27 = 41.3 \text{ ksi}$$

4. Calculate the interaction of flexure and axial stresses.

Because the angle is a non-symmetric section subject to compression and bi-axis bending about the major and minor principal axes of the angle, Equation H2-1 should be used:

$$\left|\frac{f_{ra}}{F_{ca}} + \frac{f_{rbw}}{F_{cbw}} + \frac{f_{rbz}}{F_{cbz}}\right| \le 1.0$$

which can be rewritten based on the signs of bending stress at points A, B and C, respectively, as follows:

$$\left|\frac{f_{ra}}{F_{ca}} + \frac{f_{rbw(A)}}{F_{cbw(A)}} - \frac{f_{rbz(A)}}{F_{cbz(A)}}\right| \le 1.0$$

$$\left|\frac{f_{ra}}{F_{ca}} + \frac{f_{rbz(B)}}{F_{cbz(B)}}\right| \le 1.0$$

$$\left|\frac{f_{ra}}{F_{ca}} - \frac{f_{rbw(C)}}{F_{cbw(C)}} - \frac{f_{rbz(C)}}{F_{cbz(C)}}\right| \le 1.0$$

where

f_{ra} = required axial stress

$f_{rbw(A,\,C)}, f_{rbz(A,\,B,\,C)}$ = required flexure stresses

Determine moments due to axial load M_{rw} and M_{rz} from Equation A-8-1:

$$M_{rw} = B_{1w}(e_w P_r)$$

$$M_{rz} = B_{1z}(e_z P_r)$$

where

B_{1w}, B_{1z} = multiplier to account for P-δ effect based on Section 8.2 of Appendix 8

$$B_1 = \frac{C_m}{1 - \alpha P_r / P_{e1}} \ge 1.0 \qquad \text{(Equation A-8-3)}$$

$\alpha = 1.0$ (LRFD) or 1.6 (ASD)

$C_m = 1.0$ (conservative)

$$P_{e1} = \frac{\pi^2 EI^*}{(K_1 L)^2} \qquad \text{(Equation A-8-5)}$$

$EI^* = 0.8\tau_b EI$

$\tau_b = 1.0$, when $\alpha P_r/P_y \le 0.5$, otherwise

$\tau_b = 4(\alpha P_r/P_y)[1 - (\alpha P_r/P_y)]$

$\alpha P_r/P_y = 1.0(P_r)/[(36)(2.86)] = P_r/103$

$$P_{e1w} = \frac{\pi^2 EI_w^*}{(K_1 L)^2} = \frac{\pi^2 (0.8)\tau_b (29{,}000)(6.90)}{[1.0(72)]^2} = 305\tau_b \text{ kips}$$

$$P_{e1z} = \frac{\pi^2 EI_z^*}{(K_1 L)^2} = \frac{\pi^2 (0.8)\tau_b (29{,}000)(1.74)}{[1.0(72)]^2} = 76.7\tau_b \text{ kips}$$

$$B_{1w} = \frac{C_m}{1 - \alpha P_r / P_{e1w}} = \frac{1.0}{1 - 1.0(P_r)/305\tau_b} = \frac{305\tau_b}{305\tau_b - P_r}$$

$$B_{1z} = \frac{C_m}{1 - \alpha P_r / P_{e1z}} = \frac{1.0}{1 - 1.0(P_r)/76.7\tau_b} = \frac{76.7\tau_b}{76.7\tau_b - P_r}$$

The required second-order flexural strengths M_{rw} and M_{rz} for checking stress at points A, B and C are:

$$M_{rw} = B_{1w}(e_w P_r) = \left(\frac{305\tau_b}{305\tau_b - P_r}\right)(e_w P_r)$$

$$M_{rz} = B_{1z}(e_z P_r) = \left(\frac{76.7\tau_b}{76.7\tau_b - P_r}\right)(e_z P_r)$$

Apply Equation H2-1 at point A:

$$\left|\frac{f_{ra}}{F_{ca}}+\frac{f_{rbw(A)}}{F_{cbw(A)}}-\frac{f_{rbz(A)}}{F_{cbz(A)}}\right|=$$

$$\left|\frac{\dfrac{P_r/2.86}{20.7}+\dfrac{\left(\dfrac{305\tau_b(e_wP_r)}{305\tau_b-P_r}\right)\Big/2.56}{44.4}}{-\dfrac{\left(\dfrac{76.7\tau_b(e_zP_r)}{76.7\tau_b-P_r}\right)\Big/1.27}{41.3}}\right|\le 1.0$$

Solving the previous equation, $P_r = 62.6$ kips.

Apply Equation H2-1 at point B:

$$\left|\frac{f_{ra}}{F_{ca}}+\frac{f_{rbz(B)}}{F_{cbz(B)}}\right|=\left|\frac{P_r/2.86}{20.7}+\frac{\left(\dfrac{76.7\tau_b(e_zP_r)}{76.7\tau_b-P_r}\right)\Big/1.09}{48.6}\right|\le 1.0$$

Solving the previous equation, $P_r = 33.5$ kips.

Apply Equation H2-1 at point C:

$$\left|\frac{f_{ra}}{F_{ca}}-\frac{f_{rbw(A)}}{F_{cbw(A)}}-\frac{f_{rbz(A)}}{F_{cbz(A)}}\right|=$$

$$\left|\frac{\dfrac{P_r/2.86}{20.66}-\dfrac{\left(\dfrac{305\tau_b(e_wP_r)}{305\tau_b-P_r}\right)\Big/2.56}{44.4}}{-\dfrac{\left(\dfrac{76.7\tau_b(e_zP_r)}{76.7\tau_b-P_r}\right)\Big/1.27}{41.3}}\right|\le 1.0$$

Solving the previous equation, $P_r = 56.2$ kips.

Determine the design compressive strength, $\phi_c P_n$, and the allowable compressive strength, P_n/Ω_c:

$$\phi_c P_n = P_r = \min [62.6, 33.5, 56.2] = 33.5 \text{ kips (LRFD)}$$

$$P_n/\Omega_c = (P_r/\phi_c)/\Omega_c = (33.5/0.9)/1.67 = 22.3 \text{ kips (ASD)}$$

Method 4

L4×4×⅜, connected to one leg, axial load is applied at geometric axis *y-y*, and mid-thickness of gusset plate. Angle is designed on the basis of principal axes (*w-w, z-z*) bending. See Figure 7.

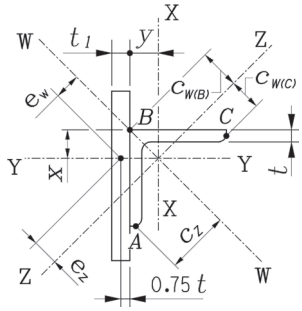

Fig. 7. Method 4.

e_w = 0.998 in.
e_z = 0.998 in.

See Method 3 for additional information.

Solution

All calculations are the same as Method 3, except for replacing values of e_z and e_w in Method 3 with the values provided in this method.

Apply Equation H2-1 at point A, solve for $P_r = 46.7$ kips
Apply Equation H2-1 at point B, solve for $P_r = 22.8$ kips
Apply Equation H2-1 at point C, solve for $P_r = 39.0$ kips

Determine the design compressive strength, $\phi_c P_n$ and the allowable compressive strength, P_n/Ω_c:

$$\phi_c P_n = P_r = \min [46.7, 22.8, 39.0] = 22.8 \text{ kips (LRFD)}$$
$$P_n/\Omega_c = (P_r/\phi_c)/\Omega_c = (22.8/0.9)/1.67 = 15.2 \text{ kips (ASD)}$$

DISCUSSION

Axial capacities of an L4×4×⅜ from the design examples are summarized in Table 1. The axial capacities based on Methods 2 and 4 (highlighted) are similar, while Method 1 gives the largest axial capacity and Method 2 yields the smallest capacity. It is further noted that the axial capacities based on Method 3 are slightly smaller than the values from Table 4-12 in the 14th edition AISC *Manual* when the direct analysis method and the flexural rigidity $EI^* = 0.8\tau_b EI$ were used (2010 AISC *Specification* Appendix 8). Further investigation reveals that the axial capacities based on Method 3 match the values from Table 4-12 in the 14th edition AISC *Manual* when $EI^* = EI$ was used in the analysis (example not shown).

Because the axial compressive design strength of the same angle with the same connection and the same unbraced length varies significantly with the different design methods, it should be interesting to see the variability among the different angles with different unbraced lengths. Figures 8a through 8d graphically illustrate the differences in the axial compressive design strength of the largest equal-leg angle

Table 1. Available Compressive Strength of L4×4×3/8, L = 72 in.		
	$\phi_c P_n$	P_n/Ω
Method 1	45.69	30.40
Method 2	22.54	15.00
Method 3[a]	33.49	22.28
Method 3[b]	35.17	23.40
AISC Table 4-12	35.2	23.2
Method 4	22.76	15.14

[a] $EI^* = 0.8\tau_b EI$
[b] $EI^* = EI$

(L8×8) and one of the smallest equal-leg angles (L3×3) with the thickest and thinnest angle legs. The available axial compressive strength from Table 4-12 of both the 13th and 14th edition AISC *Manuals* are also included for the purpose of comparison. The following can be observed:

1. The axial compressive design strengths of single angles are the greatest based on Method 1 and the smallest based on Method 2 or 4. The magnitude of difference varies with the thickness of angle leg, a heavier section results in a greater difference. The ratios of the design strengths based on Method 1 to the design strengths based on Method 2 or 4 are in the range of 1.5 to 2.0.

2. The axial compressive design strengths of single angles based on Method 2 and Method 4 are similar. For angles with smaller unbraced lengths, the design strengths based on Method 4 are slightly larger than that based on Method 2; however, for angles with larger unbraced lengths, the design strengths based on Method 2 are slightly larger than that predicted based on Method 4.

3. When the axial compressive force is applied at the geometric axis *y*-*y*, the axial compressive design strengths of single angles based on Method 4 are smaller than those from Table 4-12 of the 13th edition AISC *Manual*, but they are close and almost parallel.

4. When the axial compressive force is applied at mid-point of the connected leg (*b*/2), the axial compressive design strength of single angles based on Method 3 considering the flexural rigidity $EI^* = 0.8\tau_b EI$ ($0.8\tau_b EI$ is shown in Figure 8) is slightly smaller than that from Table 4-12 of the 14th edition AISC *Manual*. However, when $EI^* = EI$ is used instead, the design strengths based on Method 3 are identical to that from Table 4-12 of the 14th edition AISC *Manual*.

5. As discussed in the design consideration section, because the slight eccentricity between the neutral axis of the single angle and the center of gravity of the weld group has negligible effect on the static strength of the member, the angle should be designed assuming the static axial compressive force is applied at the mid-point of the connected leg (Method 3). However, for angles subject to cyclic force, one could choose to design the angle assuming the axial compressive force is applied at the neutral axis of the single angle, as it is required that the center of gravity of the weld group coincides with the neutral axis of the member.

On the other hand, single angles subject to cyclic loads can be designed assuming that the axial compressive force is applied at the mid-point of the connected leg (Method 3) per 2010 AISC *Specification* Section J1.7, as long as the requirement of center of gravity of the weld group coinciding with the neutral axis of the member is satisfied.

6. While the larger capacities predicted by Method 1 based on Section E5 of the 2010 AISC *Specification* are welcomed by the engineering community, the design engineer may wish to choose the values from Table 4-12 in the 14th edition AISC *Manual* or Design Table 2 presented at end of this paper, as the available strengths from these tables are conservative.

7. The 2005 and 2010 AISC *Specifications* do not address how to determine the eccentricity of applied axial force relative to the connected leg. However, a distance of 0.75*t* (*t* is the angle thickness) from the back face of the connected leg is used by Table 4-12 of the 13th and 14th edition AISC *Manauls*. As discussed in the design consideration section, this distance can be taken as small as –0.50*t*, instead of 0.75*t*. The design strengths based on Method 4 using different eccentricities are presented in Design Tables 3 and 4.

8. It is beneficial to point out that the larger available axial compressive strength of the single angles determined based on the specified effective slenderness ratio, *KL*/*r*

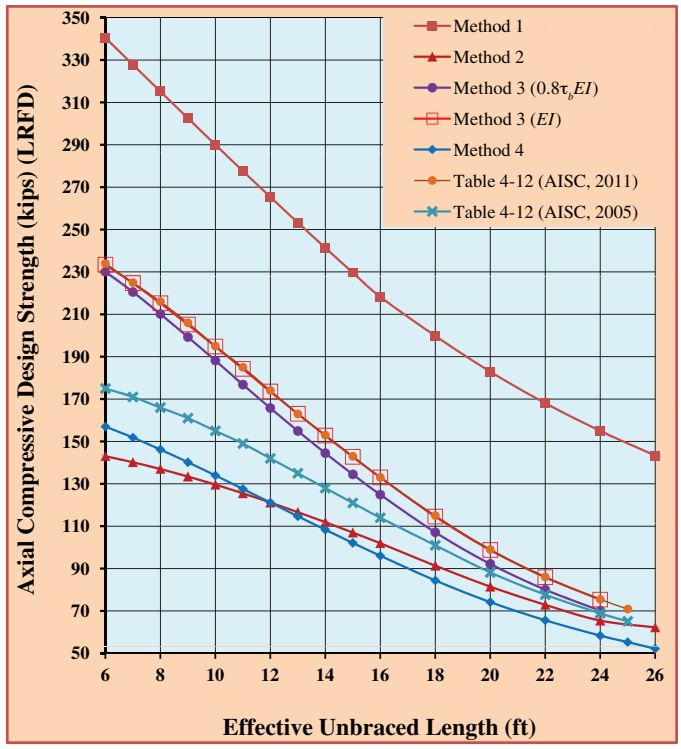

Fig. 8a. Axial compressive design strength (L8×8×1⅛).

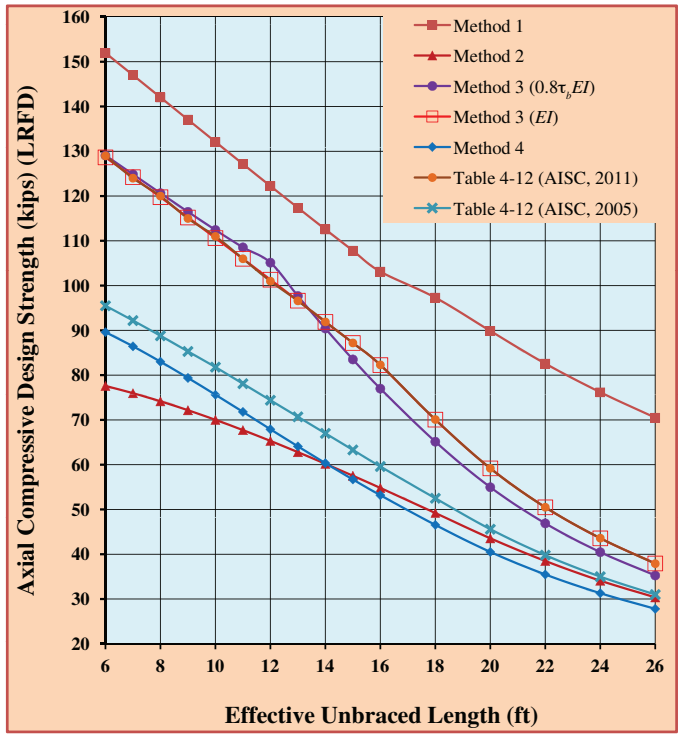

Fig. 8b. Axial compressive design strength (L8×8×½).

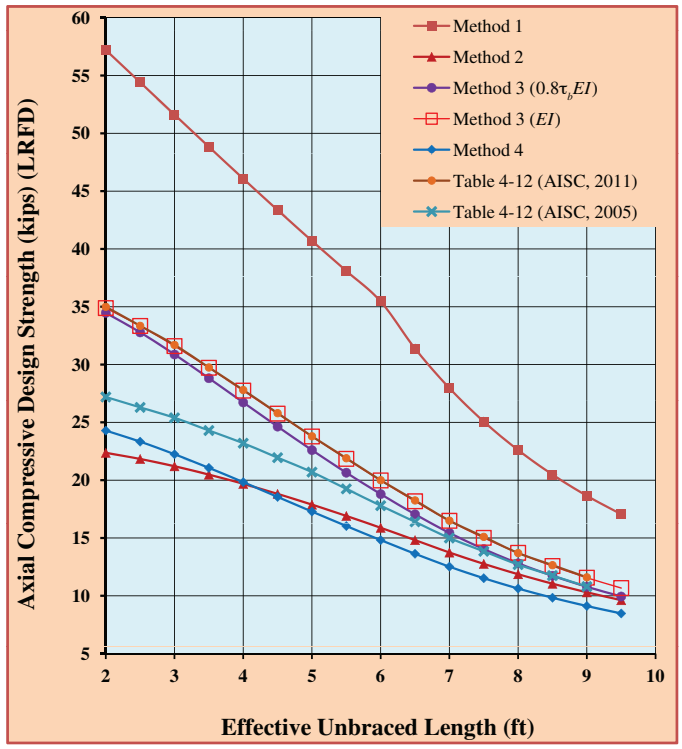

Fig. 8c. Axial compressive design strength (L3×3×½).

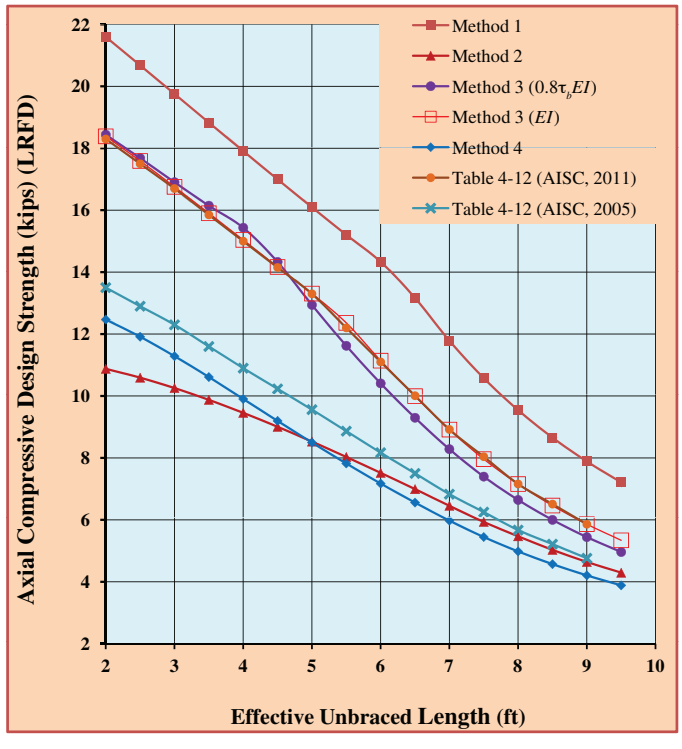

Fig. 8d. Axial compressive design strength (L3×3×13⁄16).

(Method 1) are due to the presumptions that the significant bending and rotational restraints are provided by the end connections; in other words, if another method (Method 2, 3 or 4) is used to evaluate the available compressive strength of the single angles, the reduced unbraced lengths (effective length factor, *K*) and eccentricities due to the end restraints should be considered to avoid overly conservative results, as described in Commentary section E5 of the 2010 AISC *Specification*. However, this could pose some challenges when the design is based on a particular code, where the unbraced length reduction factor is limited to 1.0, as discussed in design considerations of single angles in compression.

DESIGN TABLES

Design tables for the axial compressive design strength of eccentrically loaded equal-leg single angles (grades 36 and 50) are prepared based on previously discussed Methods 1, 3 and 4. The format of the tables follows the format of Table 4-12 of the 14th edition AISC *Manual*.

Design Table 1: Axial compressive design strength of equal-leg angles based on Method 1, see Method 1.

Design Table 2: Axial compressive design strength of equal-leg angles based on Method 3, assuming the axial load is applied at mid-point of the connected leg and mid-thickness of the gusset plate. Angles are designed on the basis of principal axes *(w-w, z-z)* bending. See Method 3.

Design Table 3: Axial compressive design strength of equal-leg angles based on Method 4, assuming the axial load is applied at geometric axis *y-y* and mid-thickness of the gusset plate. Angles are designed on the basis of principal axes (*w-w, z-z*) bending. See Method 4.

Design Table 4: Axial compressive design strength of equal-leg angles based on Method 4, assuming the axial load is applied at geometric axis *y-y*, and mid-thickness of the connected leg. Angles are designed on the basis of principal axes (*w-w, z-z*) bending.

Design Tables 3 and 4 are integrated such that identical angle sizes appear in adjacent tables for ease of comparison.

REFERENCES

AASHTO (2004), *LRFD Bridge Design Specifications,* 3rd Edition, American Association of State Highway and Transportation Offices, Washington, D.C.

AASHTO (2007), *LRFD Bridge Design Specifications,* 4th Edition, American Association of State Highway and Transportation Offices, Washington, D.C.

AISC (1986), *Manual of Steel Construction, Load and Resistance Factor Design,* 1st Edition, American Institute of Steel Construction, Chicago, IL.

AISC (1989), *Steel Construction Manual, Allowable Stress Design,* 9th Edition, American Institute of Steel Construction, Chicago, IL.

AISC (1993), *Specification for Load and Resistance Factor Design of Single Angle Members*, American Institute of Steel Construction, Chicago, IL.

AISC (1994), *Manual of Steel Construction, Load and Resistance Factor Design,* 2nd Edition, American Institute of Steel Construction, Chicago, IL.

AISC (2001), *Manual of Steel Construction, Load and Resistance Factor Design,* 3rd Edition, American Institute of Steel Construction, Chicago, IL.

AISC (2005a), *Specification for Structural Steel Buildings,* American Institute of Steel Construction, Chicago, IL.

AISC (2005b), *Steel Construction Manual,* 13th Edition, American Institute of Steel Construction, Chicago, IL.

AISC (2010), *Specification for Structural Steel Buildings,* American Institute of Steel Construction, Chicago, IL.

AISC (2011), *Steel Construction Manual,* 14th Edition, American Institute of Steel Construction, Chicago, IL.

Blodgett, O.W. (1966), *Design of Welded Structures,* The James F. Lincoln Arc Welding Foundation, Cleveland, OH.

Lutz, L.A. (2006), "Evaluating Single-Angle Compression Struts Using an Effective Slenderness Approach," *Engineering Journal*, AISC, Fourth Quarter, 2006, pp. 241–246.

Sakla, S.S. (2001), "Tables for the Design Strength of Eccentrically-Loaded Single Angle Struts," *Engineering Journal*, AISC, Third Quarter, 2001, pp. 127–136.

Walker, W.W. (1991), "Table for Equal Single Angles in Compression," *Engineering Journal*, AISC, Second Quarter, 1991, pp. 65–68.

Woolcock, S.T. and Kitipornchai, S. (1986), "Design of Single-Angle Web Struts in Trusses," *Journal of Structural Engineering*, ASCE, Vol. 112, No. 6, pp. 1327–1345.

Zureick, A. (1993), "Design Strength of Concentrically Loaded Single Angle Struts," *Engineering Journal*, AISC, First Quarter, 1993, pp. 17–30.

Design Table 1. Available Strength in Axial Compression, kips* Eccentrically Loaded Single Angles

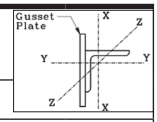

Shape		L8×8×													
		1 1/8		1		7/8		3/4		5/8[c]		9/16[c]		1/2[c, f]	
lb/ft		56.9		51.0		45.0		38.9		32.7		29.6		26.4	
Design		P_n/Ω_c ASD	$\phi_c P_n$ LRFD	P_n/Ω_c ASD	$\phi_c P_n$ LRFD	P_n/Ω_c ASD	$\phi_c P_n$ LRFD	P_n/Ω_c ASD	$\phi_c P_n$ LRFD	P_n/Ω_c ASD	$\phi_c P_n$ LRFD	P_n/Ω_c ASD	$\phi_c P_n$ LRFD	P_n/Ω_c ASD	$\phi_c P_n$ LRFD
		F_y = 36 ksi													
Unbraced Length between Work Points, L (ft)	6	227	340	204	307	180	271	156	234	131	197	116	175	101	152
	7	218	328	196	295	173	261	150	226	127	190	112	169	97.8	147
	8	210	315	189	284	167	251	144	217	122	183	108	163	94.5	142
	9	201	303	182	273	160	241	139	209	117	176	104	157	91.2	137
	10	193	290	174	262	154	231	133	200	113	169	100	151	87.9	132
	11	185	278	167	251	147	222	128	192	108	162	96.5	145	84.6	127
	12	177	265	159	240	141	212	122	184	103	155	92.6	139	81.3	122
	13	169	253	152	229	135	203	117	176	98.8	149	88.7	133	78.1	117
	14	161	241	145	218	129	193	111	168	94.4	142	84.9	128	74.9	113
	15	153	230	138	208	122	184	106	160	90.0	135	81.1	122	71.7	108
	16	145	218	131	198	117	175	101	152	85.7	129	77.4	116	68.6	103
	18	133	200	121	182	108	162	93.9	141	80.1	120	72.8	109	64.7	97.3
	20	122	183	111	167	98.9	149	86.0	129	73.4	110	66.8	100	59.8	89.9
	22	112	168	102	153	90.9	137	79.1	119	67.5	101	61.5	92.4	54.9	82.6
	24	103	155	93.9	141	83.8	126	72.9	110	62.2	94	56.7	85.2	50.7	76.2
	26	95.4	143	86.9	131	77.5	117	67.5	101	57.6	86.6	52.5	78.9	46.9	70.5
Design		F_y = 50 ksi													
		1 1/8		1		7/8		3/4		5/8[c]		9/16[c, f]		1/2[c, f]	
Unbraced Length between Work Points, L (ft)	6	262	394	236	355	209	314	181	271	149	224	132	199	115	172
	7	249	374	224	337	198	298	172	258	142	213	126	190	110	165
	8	236	354	212	319	188	282	163	244	135	203	121	181	105	158
	9	223	334	201	302	178	267	154	231	128	193	115	173	101	151
	10	210	315	190	285	168	252	145	219	122	183	109	164	96.0	144
	11	197	297	178	268	158	238	137	206	115	173	104	156	91.4	137
	12	185	278	167	252	148	223	129	193	109	164	98.3	148	87.0	131
	13	174	261	157	236	139	210	121	182	103	154	93.0	140	82.6	124
	14	163	246	148	222	131	197	114	171	96.6	145	87.7	132	78.3	118
	15	154	232	139	210	124	186	107	161	91.1	137	82.7	124	74.0	111
	16	145	219	132	198	117	176	101	152	86.1	129	78.2	118	69.9	105
	18	133	200	121	182	108	162	93.9	141	80.1	120	73.0	110	65.2	98.0
	20	122	183	111	167	98.9	149	86.0	129	73.4	110	66.8	100	59.8	89.8
	22	112	168	102	153	90.9	137	79.1	119	67.5	101	61.5	92.4	54.9	82.6
	24	103	155	93.9	141	83.8	126	72.9	110	62.2	93.6	56.7	85.2	50.7	76.2
	26	95.4	143	86.9	131	77.5	117	67.5	101	57.6	86.6	52.5	78.9	46.9	70.5
Properties															
A_g (in.^{2})		16.8		15.1		13.3		11.5		9.69		8.77		7.84	
γ_z (in.)		1.56		1.56		1.57		1.57		1.58		1.58		1.59	
ASD	LRFD	[c] Shape is slender for compression. [f] Shape exceeds compact limit for flexure.													
Ω_c = 1.67	ϕ_c = 0.9	Notes: Heavy lines indicate L/r_z equal to or greater than 120, 140 and 200, respectively. *Method 1.													

Design Table 1. Available Strength in Axial Compression, kips* Eccentrically Loaded Single Angles

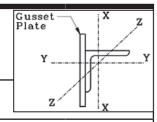

Shape		L6×6×													
		1		7/8		3/4		5/8		9/16		1/2		7/16[c]	
lb/ft		37.4		33.1		28.7		24.2		21.9		19.6		17.3	
Design		P_n/Ω_c ASD	$\phi_c P_n$ LRFD	P_n/Ω_c ASD	$\phi_c P_n$ LRFD	P_n/Ω_c ASD	$\phi_c P_n$ LRFD	P_n/Ω_c ASD	$\phi_c P_n$ LRFD	P_n/Ω_c ASD	$\phi_c P_n$ LRFD	P_n/Ω_c ASD	$\phi_c P_n$ LRFD	P_n/Ω_c ASD	$\phi_c P_n$ LRFD
		F_y = 36 ksi													
Unbraced Length between Work Points, L (ft)	4	152	228	135	203	117	176	98.9	149	89.5	135	80.2	120	69.5	104
	5	144	217	128	193	111	167	94.2	142	85.3	128	76.4	115	66.3	99.7
	6	137	206	122	183	106	159	89.5	135	81.1	122	72.7	109	63.2	94.9
	7	129	195	115	173	100	151	84.8	128	76.9	116	68.9	104	60.0	90.2
	8	122	184	109	164	94.7	142	80.2	121	72.8	109	65.2	98.1	56.9	85.5
	9	115	173	103	154	89.3	134	75.7	114	68.7	103	61.6	92.6	53.8	80.8
	10	108	162	96.3	145	83.9	126	71.2	107	64.6	97.1	58.0	87.2	50.7	76.2
	11	101	152	90.3	136	78.6	118	66.8	100	60.7	91.2	54.5	81.9	47.7	71.7
	12	94.0	141	84.4	127	73.5	111	62.5	94.0	56.8	85.4	51.0	76.7	44.8	67.3
	13	83.2	125	75.1	113	65.7	98.7	56.3	84.6	51.3	77.2	46.3	69.6	40.8	61.3
	14	74.2	111	66.9	101	58.5	88.0	50.2	75.4	45.8	68.8	41.3	62.1	36.4	54.7
	15	66.5	99.9	60.0	90.2	52.5	78.9	45.0	67.7	41.1	61.7	37.1	55.7	32.6	49.0
	16	59.9	90.1	54.1	81.3	47.4	71.2	40.6	61.0	37.1	55.7	33.4	50.3	29.4	44.3
	17	54.3	81.6	49.0	73.7	42.9	64.5	36.8	55.4	33.6	50.5	30.3	45.6	26.7	40.1
	18	49.5	74.3	44.6	67.1	39.1	58.8	33.5	50.4	30.6	46.0	27.6	41.5	24.3	36.6
	19	45.2	68.0	40.8	61.4	35.8	53.7	30.7	46.1	28.0	42.1	25.3	38.0	22.3	33.5
Design		F_y = 50 ksi													
		1		7/8		3/4		5/8		9/16		1/2[c]		7/16[c, f]	
Unbraced Length between Work Points, L (ft)	4	177	266	157	237	137	206	116	174	105	157	92.4	139	79.3	119
	5	165	248	147	221	128	192	108	163	98.0	147	86.7	130	74.7	112
	6	154	231	137	206	119	179	101	151	91.3	137	81.0	122	70.1	105
	7	142	214	127	191	110	166	93.5	141	84.9	128	75.5	114	65.6	98.6
	8	131	197	117	176	102	153	86.5	130	78.5	118	70.2	105	61.2	92.0
	9	120	181	108	162	93.7	141	79.6	120	72.3	109	65.0	97.7	56.9	85.5
	10	111	166	98.9	149	86.2	130	73.3	110	66.6	100	59.8	89.9	52.7	79.2
	11	102	153	91.3	137	79.6	120	67.7	102	61.5	92.5	55.3	83.1	48.7	73.2
	12	94.1	141	84.5	127	73.7	111	62.7	94.3	57.0	85.7	51.3	77.1	45.1	67.8
	13	83.2	125	75.1	113	65.7	98.7	56.3	84.6	51.3	77.2	46.3	69.6	40.8	61.3
	14	74.2	111	66.9	101	58.5	88.0	50.2	75.4	45.8	68.8	41.3	62.1	36.4	54.7
	15	66.5	99.9	60.0	90.2	52.5	78.9	45.0	67.7	41.1	61.7	37.1	55.7	32.6	49.0
	16	59.9	90.1	54.1	81.3	47.4	71.2	40.6	61.0	37.1	55.7	33.4	50.3	29.4	44.3
	17	54.3	81.6	49.0	73.7	42.9	64.5	36.8	55.4	33.6	50.5	30.3	45.6	26.7	40.1
	18	49.5	74.3	44.6	67.1	39.1	58.8	33.5	50.4	30.6	46.0	27.6	41.5	24.3	36.6
	19	45.2	68.0	40.8	61.4	35.8	53.7	30.7	46.1	28.0	42.1	25.3	38.0	22.3	33.5
Properties															
A_g (in.^{2})		11.0		9.75		8.46		7.13		6.45		5.77		5.08	
γ_z (in.)		1.17		1.17		1.17		1.17		1.18		1.18		1.18	
ASD	LRFD	[c] Shape is slender for compression. [f] Shape exceeds compact limit for flexure.													
Ω_c = 1.67	ϕ_c = 0.9	Notes: Heavy lines indicate L/r_z equal to or greater than 120, 140 and 200, respectively. *Method 1.													

Design Table 1. Available Strength in Axial Compression, kips* Eccentrically Loaded Single Angles

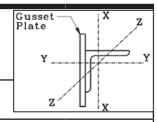

Shape		L5×5×													
		7/8		3/4		5/8		1/2		7/16		3/8[c]		5/16[c, f]	
lb/ft		27.2		23.6		20.0		16.2		14.3		12.3		10.4	
Design		P_n/Ω_c ASD	$\phi_c P_n$ LRFD	P_n/Ω_c ASD	$\phi_c P_n$ LRFD	P_n/Ω_c ASD	$\phi_c P_n$ LRFD	P_n/Ω_c ASD	$\phi_c P_n$ LRFD	P_n/Ω_c ASD	$\phi_c P_n$ LRFD	P_n/Ω_c ASD	$\phi_c P_n$ LRFD	P_n/Ω_c ASD	$\phi_c P_n$ LRFD
		F_y = 36 ksi													
Unbraced Length between Work Points, L (ft)	1	125	188	109	164	92.4	139	75.0	113	66.1	99.4	56.5	85.0	45.2	67.9
	2	119	179	104	156	87.8	132	71.4	107	62.9	94.6	53.9	81.0	43.2	64.9
	3	112	169	98.2	148	83.2	125	67.6	102	59.7	89.7	51.1	76.9	41.2	61.9
	4	106	159	92.6	139	78.5	118	63.9	96.0	56.4	84.7	48.4	72.7	39.1	58.8
	5	99.5	150	87.0	131	73.9	111	60.1	90.3	53.0	79.7	45.6	68.5	37.0	55.7
	6	93.1	140	81.4	122	69.2	104	56.3	84.7	49.8	74.8	42.8	64.4	35.0	52.6
	7	86.7	130	75.9	114	64.6	97.1	52.6	79.1	46.5	69.9	40.1	60.3	32.9	49.5
	8	80.5	121	70.5	106	60.1	90.3	49.0	73.6	43.3	65.1	37.4	56.2	30.9	46.4
	9	74.4	112	65.2	98.0	55.7	83.7	45.4	68.2	40.2	60.4	34.8	52.3	28.9	43.4
	10	68.3	103	60.1	90.4	51.4	77.2	41.9	63.0	37.1	55.8	32.2	48.4	26.9	40.5
	11	59.0	88.7	52.0	78.2	44.9	67.5	36.8	55.3	32.8	49.2	28.6	43.0	24.3	36.5
	12	51.5	77.4	45.4	68.3	39.2	58.9	32.1	48.3	28.6	43.0	25.0	37.6	21.2	31.9
	13	45.3	68.1	40.0	60.1	34.5	51.9	28.3	42.6	25.2	37.9	22.0	33.1	18.7	28.1
	14	40.2	60.4	35.5	53.3	30.6	46.0	25.1	37.8	22.4	33.6	19.6	29.4	16.6	25.0
	15	35.9	54.0	31.7	47.6	27.4	41.1	22.5	33.8	20.0	30.1	17.5	26.3	14.9	22.3
	16	32.3	48.5	28.5	42.8	24.6	37.0	20.2	30.3	18.0	27.0	15.7	23.6	13.4	20.1
Design		F_y = 50 ksi													
		7/8		3/4		5/8		1/2		7/16[c]		3/8[c, f]		5/16[c, f]	
Unbraced Length between Work Points, L (ft)	1	153	231	134	201	113	170	92.0	138	80.2	121	66.9	101	53.1	79.8
	2	143	215	125	188	106	159	85.9	129	75.0	113	62.8	94.4	50.2	75.4
	3	132	199	116	174	98.0	147	79.7	120	69.7	105	58.7	88.2	47.2	70.9
	4	122	183	107	160	90.4	136	73.6	111	64.5	97.0	54.6	82.1	44.2	66.5
	5	112	168	97.7	147	83.0	125	67.6	102	59.4	89.3	50.6	76.0	41.3	62.0
	6	102	153	89.1	134	75.9	114	61.8	92.9	54.5	81.8	46.6	70.1	38.4	57.6
	7	92.1	138	80.7	121	68.9	104	56.2	84.5	49.7	74.6	42.8	64.3	35.5	53.4
	8	83.1	125	72.9	110	62.2	93.5	50.8	76.3	45.0	67.6	39.1	58.8	32.7	49.2
	9	75.3	113	66.1	99.3	56.5	84.9	46.1	69.3	40.9	61.4	35.5	53.4	30.1	45.2
	10	68.3	103	60.2	90.5	51.5	77.4	42.1	63.2	37.3	56.0	32.4	48.7	27.4	41.2
	11	59.0	88.7	52.0	78.2	44.9	67.5	36.8	55.3	32.8	49.2	28.6	43.0	24.3	36.5
	12	51.5	77.4	45.4	68.3	39.2	58.9	32.1	48.3	28.6	43.0	25.0	37.6	21.2	31.9
	13	45.3	68.1	40.0	60.1	34.5	51.9	28.3	42.6	25.2	37.9	22.0	33.1	18.7	28.1
	14	40.2	60.4	35.5	53.3	30.6	46.0	25.1	37.8	22.4	33.6	19.6	29.4	16.6	25.0
	15	35.9	54.0	31.7	47.6	27.4	41.1	22.5	33.8	20.0	30.1	17.5	26.3	14.9	22.3
	16	32.3	48.5	28.5	42.8	24.6	37.0	20.2	30.3	18.0	27.0	15.7	23.6	13.4	20.1
Properties															
A_g (in.^{2})		8.00		6.98		5.90		4.79		4.22		3.65		3.07	
γ_z (in.)		0.971		0.972		0.975		0.980		0.983		0.986		0.990	
ASD	LRFD	[c] Shape is slender for compression. [f] Shape exceeds compact limit for flexure.													
Ω_c = 1.67	ϕ_c = 0.9	Notes: Heavy lines indicate L/r_z equal to or greater than 120, 140 and 200, respectively. *Method 1.													

Design Table 1. Available Strength in Axial Compression, kips* Eccentrically Loaded Single Angles

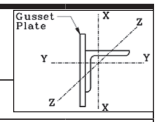

Shape		L4×4×													
		3/4		5/8		1/2		7/16		3/8		5/16[c]		1/4[c, f]	
lb/ft		18.5		15.7		12.8		11.3		9.8		8.2		6.6	
Design		P_n/Ω_c ASD	$\phi_c P_n$ LRFD	P_n/Ω_c ASD	$\phi_c P_n$ LRFD	P_n/Ω_c ASD	$\phi_c P_n$ LRFD	P_n/Ω_c ASD	$\phi_c P_n$ LRFD	P_n/Ω_c ASD	$\phi_c P_n$ LRFD	P_n/Ω_c ASD	$\phi_c P_n$ LRFD	P_n/Ω_c ASD	$\phi_c P_n$ LRFD
		F_y = 36 ksi													
Unbraced Length between Work Points, L (ft)	2	78.5	118	66.7	100	54.3	81.7	47.9	71.9	41.5	62.4	34.8	52.3	26.5	39.8
	2.5	75.8	114	64.4	96.8	52.5	78.9	46.2	69.5	40.1	60.3	33.7	50.6	25.7	38.6
	3	73.0	110	62.1	93.3	50.6	76.1	44.6	67.1	38.7	58.2	32.5	48.9	24.9	37.4
	3.5	70.2	106	59.8	89.9	48.7	73.3	43.0	64.6	37.3	56.1	31.4	47.1	24.1	36.2
	4	67.4	101	57.5	86.4	46.9	70.4	41.4	62.2	35.9	54.0	30.2	45.4	23.3	35.0
	4.5	64.7	97.2	55.2	82.9	45.0	67.6	39.7	59.7	34.5	51.9	29.0	43.6	22.5	33.8
	5	61.9	93.1	52.9	79.5	43.2	64.9	38.1	57.3	33.1	49.8	27.9	41.9	21.7	32.6
	5.5	59.2	89.0	50.6	76.0	41.3	62.1	36.5	54.9	31.8	47.7	26.7	40.2	20.9	31.4
	6	56.5	84.9	48.3	72.7	39.5	59.4	34.9	52.5	30.4	45.7	25.6	38.5	20.1	30.2
	7	51.3	77.0	43.9	66.0	35.9	54.0	31.8	47.8	27.7	41.7	23.4	35.1	18.5	27.8
	8	45.8	68.8	39.7	59.7	32.5	48.9	28.8	43.3	25.1	37.8	21.2	31.9	16.9	25.5
	9	38.1	57.3	33.2	49.9	27.3	41.1	24.4	36.6	21.4	32.2	18.2	27.3	14.8	22.3
	10	32.3	48.5	28.1	42.3	23.2	34.8	20.7	31.1	18.1	27.3	15.4	23.2	12.6	18.9
	11	27.7	41.6	24.1	36.2	19.9	29.9	17.7	26.7	15.6	23.4	13.2	19.9	10.8	16.2
	12	24.0	36.1	20.9	31.4	17.3	25.9	15.4	23.1	13.5	20.3	11.5	17.3	9.4	14.1
	13											10.0	15.1	8.1	12.2
Design		F_y = 50 ksi													
		3/4		5/8		1/2		7/16		3/8		5/16[c]		1/4[c, f]	
Unbraced Length between Work Points, L (ft)	2	93.3	140	79.4	119	64.7	97.2	57.0	85.7	49.5	74.3	40.3	60.6	30.6	46.0
	2.5	88.8	133	75.6	114	61.6	92.6	54.3	81.7	47.2	70.9	38.6	58.0	29.4	44.2
	3	84.3	127	71.8	108	58.6	88.1	51.7	77.7	44.9	67.5	36.8	55.4	28.3	42.5
	3.5	79.9	120	68.1	102	55.6	83.6	49.1	73.8	42.7	64.1	35.1	52.8	27.1	40.7
	4	75.5	114	64.5	96.9	52.7	79.2	46.5	69.9	40.5	60.8	33.4	50.3	25.9	39.0
	4.5	71.3	107	60.9	91.6	49.8	74.8	44.0	66.1	38.3	57.5	31.8	47.8	24.8	37.3
	5	67.1	101	57.4	86.3	47.0	70.6	41.5	62.4	36.2	54.3	30.1	45.3	23.7	35.6
	5.5	63.0	94.6	54.0	81.2	44.2	66.4	39.1	58.8	34.1	51.2	28.5	42.9	22.6	33.9
	6	59.0	88.6	50.6	76.1	41.4	62.3	36.7	55.2	32.0	48.1	27.0	40.5	21.5	32.3
	7	52.0	78.2	44.7	67.2	36.6	55.0	32.4	48.8	28.3	42.6	23.9	36.0	19.3	29.1
	8	45.7	68.8	39.8	59.8	32.6	49.0	28.9	43.4	25.2	37.9	21.3	32.1	17.3	26.0
	9	38.1	57.3	33.2	49.9	27.3	41.1	24.4	36.6	21.4	32.2	18.2	27.3	14.8	22.2
	10	32.3	48.5	28.1	42.3	23.2	34.8	20.7	31.1	18.1	27.3	15.4	23.2	12.6	18.9
	11	27.7	41.6	24.1	36.2	19.9	29.9	17.7	26.7	15.6	23.4	13.2	19.9	10.8	16.2
	12	24.0	36.1	20.9	31.4	17.3	25.9	15.4	23.1	13.5	20.3	11.5	17.3	9.4	14.1
	13											10.0	15.1	8.1	12.2
Properties															
A_g (in.^{2})		5.43		4.61		3.75		3.30		2.86		2.40		1.93	
γ_z (in.)		0.774		0.774		0.776		0.777		0.779		0.781		0.783	
ASD	LRFD	[c] Shape is slender for compression. [f] Shape exceeds compact limit for flexure.													
Ω_c = 1.67	ϕ_c = 0.9	Notes: Heavy lines indicate L/r_z equal to or greater than 120, 140 and 200, respectively. *Method 1.													

Design Table 1. Available Strength in Axial Compression, kips* Eccentrically Loaded Single Angles

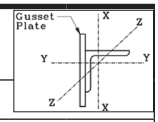

Shape		L3½×3½×									
		½		7/16		3/8		5/16		1/4[c]	
lb/ft		11.1		9.80		8.50		7.20		5.80	
Design		P_n/Ω_c ASD	$\phi_c P_n$ LRFD	P_n/Ω_c ASD	$\phi_c P_n$ LRFD	P_n/Ω_c ASD	$\phi_c P_n$ LRFD	P_n/Ω_c ASD	$\phi_c P_n$ LRFD	P_n/Ω_c ASD	$\phi_c P_n$ LRFD
		F_y = 36 ksi									
Unbraced Length between Work Points, L (ft)	2	46.1	69.3	41.1	61.7	35.6	53.5	29.9	45.0	23.8	35.7
	2.5	44.2	66.5	39.4	59.3	34.2	51.4	28.8	43.2	22.9	34.4
	3	42.4	63.7	37.8	56.8	32.8	49.2	27.6	41.5	22.0	33.0
	3.5	40.5	60.9	36.1	54.3	31.4	47.1	26.4	39.7	21.1	31.7
	4	38.7	58.1	34.5	51.8	29.9	45.0	25.2	37.9	20.2	30.4
	4.5	36.8	55.3	32.9	49.4	28.6	42.9	24.1	36.2	19.3	29.0
	5	35.0	52.6	31.3	47.0	27.2	40.8	22.9	34.5	18.4	27.7
	5.5	33.2	49.9	29.7	44.6	25.8	38.8	21.8	32.8	17.6	26.4
	6	31.4	47.2	28.1	42.3	24.5	36.8	20.7	31.1	16.7	25.1
	6.5	29.7	44.6	26.6	40.0	23.2	34.8	19.6	29.4	15.9	23.8
	7	28.0	42.1	25.1	37.7	21.9	32.9	18.5	27.8	15.0	22.6
	7.5	25.2	37.9	22.8	34.2	20.0	30.0	17.0	25.6	14.0	21.0
	8	22.8	34.3	20.6	31.0	18.1	27.2	15.4	23.2	12.7	19.0
	9	18.9	28.5	17.1	25.7	15.0	22.6	12.8	19.2	10.5	15.8
	10	16.0	24.0	14.4	21.7	12.7	19.0	10.8	16.2	8.9	13.3
	11	13.7	20.5	12.3	18.5	10.8	16.3	9.2	13.9	7.6	11.4
Design		F_y = 50 ksi									
		½		7/16		3/8		5/16		1/4[c]	
Unbraced Length between Work Points, L (ft)	2	54.4	81.8	48.5	72.9	42.0	63.2	35.2	52.9	27.3	41.1
	2.5	51.4	77.3	45.8	68.9	39.8	59.8	33.3	50.1	26.0	39.1
	3	48.4	72.8	43.2	64.9	37.5	56.4	31.5	47.3	24.7	37.1
	3.5	45.5	68.3	40.6	61.0	35.3	53.0	29.6	44.6	23.4	35.2
	4	42.6	64.0	38.1	57.2	33.1	49.7	27.9	41.9	22.2	33.3
	4.5	39.8	59.8	35.6	53.5	31.0	46.6	26.1	39.3	20.9	31.4
	5	37.0	55.7	33.2	49.8	28.9	43.5	24.4	36.7	19.7	29.6
	5.5	34.4	51.7	30.8	46.3	26.9	40.4	22.7	34.2	18.5	27.8
	6	32.1	48.2	28.7	43.2	25.1	37.7	21.2	31.9	17.3	26.0
	6.5	29.9	45.0	26.9	40.4	23.4	35.2	19.8	29.8	16.2	24.3
	7	28.0	42.1	25.1	37.8	21.9	33.0	18.6	27.9	15.2	22.8
	7.5	25.2	37.9	22.8	34.2	20.0	30.0	17.0	25.6	14.0	21.0
	8	22.8	34.3	20.6	31.0	18.1	27.2	15.4	23.2	12.7	19.0
	9	18.9	28.5	17.1	25.7	15.0	22.6	12.8	19.2	10.5	15.8
	10	16.0	24.0	14.4	21.7	12.7	19.0	10.8	16.2	8.9	13.3
	11	13.7	20.5	12.3	18.5	10.8	16.3	9.2	13.9	7.6	11.4
Properties											
A_g (in.^{2})		3.25		2.89		2.50		2.10		1.70	
γ_z (in.)		0.679		0.681		0.683		0.685		0.688	
ASD	LRFD	[c] Shape is slender for compression.									
Ω_c = 1.67	ϕ_c = 0.9	[f] Shape exceeds compact limit for flexure.									
		Notes: Heavy lines indicate L/r_z equal to or greater than 120, 140 and 200, respectively.									
		*Method 1.									

Design Table 1. Available Strength in Axial Compression, kips*
Eccentrically Loaded Single Angles

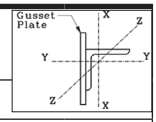

Shape		L3×3×											
		1/2		7/16		3/8		5/16		1/4		3/16[c, f]	
lb/ft		9.40		8.30		7.20		6.10		4.90		3.71	
Design		P_n/Ω_c ASD	$\phi_c P_n$ LRFD	P_n/Ω_c ASD	$\phi_c P_n$ LRFD	P_n/Ω_c ASD	$\phi_c P_n$ LRFD	P_n/Ω_c ASD	$\phi_c P_n$ LRFD	P_n/Ω_c ASD	$\phi_c P_n$ LRFD	P_n/Ω_c ASD	$\phi_c P_n$ LRFD
		F_y = 36 ksi											
Unbraced Length between Work Points, L (ft)	2	38.1	57.2	33.6	50.5	29.2	43.9	24.7	37.1	20.0	30.0	14.4	21.6
	2.5	36.2	54.4	31.9	48.0	27.8	41.8	23.5	35.3	19.1	28.6	13.8	20.7
	3	34.3	51.6	30.3	45.6	26.4	39.7	22.3	33.6	18.1	27.2	13.1	19.8
	3.5	32.5	48.8	28.7	43.1	25.0	37.6	21.2	31.8	17.2	25.8	12.5	18.8
	4	30.7	46.1	27.1	40.7	23.6	35.5	20.0	30.1	16.3	24.4	11.9	17.9
	4.5	28.9	43.4	25.5	38.4	22.3	33.5	18.9	28.4	15.3	23.0	11.3	17.0
	5	27.1	40.7	24.0	36.0	20.9	31.4	17.7	26.7	14.4	21.7	10.7	16.1
	5.5	25.3	38.1	22.5	33.8	19.6	29.5	16.7	25.0	13.6	20.4	10.1	15.2
	6	23.6	35.5	21.0	31.5	18.3	27.6	15.6	23.4	12.7	19.1	9.5	14.3
	6.5	20.9	31.4	18.6	28.0	16.4	24.6	14.0	21.1	11.5	17.3	8.8	13.2
	7	18.6	28.0	16.6	25.0	14.6	21.9	12.5	18.8	10.2	15.4	7.8	11.8
	7.5	16.7	25.1	14.9	22.4	13.1	19.7	11.2	16.8	9.2	13.8	7.0	10.6
	8	15.0	22.6	13.4	20.2	11.8	17.8	10.1	15.2	8.3	12.5	6.4	9.5
	8.5	13.6	20.5	12.2	18.3	10.7	16.1	9.2	13.8	7.5	11.3	5.8	8.7
	9	12.4	18.7	11.1	16.7	9.8	14.7	8.3	12.5	6.8	10.3	5.2	7.9
	9.5	11.3	17.1	10.1	15.2	8.9	13.4	7.6	11.5	6.3	9.4	4.8	7.2
Design		F_y = 50 ksi											
		1/2		7/16		3/8		5/16		1/4		3/16[c]	
Unbraced Length between Work Points, L (ft)	2	44.4	66.8	39.2	58.9	34.1	51.3	28.9	43.4	23.0	34.6	16.4	24.6
	2.5	41.4	62.3	36.6	55.0	31.9	47.9	27.0	40.5	21.6	32.5	15.5	23.3
	3	38.5	57.9	34.1	51.2	29.7	44.6	25.1	37.8	20.2	30.3	14.6	22.0
	3.5	35.7	53.6	31.6	47.4	27.5	41.4	23.3	35.1	18.8	28.3	13.8	20.7
	4	32.9	49.5	29.1	43.8	25.4	38.2	21.6	32.4	17.5	26.3	12.9	19.4
	4.5	30.2	45.4	26.8	40.2	23.4	35.1	19.8	29.8	16.2	24.3	12.1	18.2
	5	27.7	41.7	24.6	37.0	21.5	32.3	18.3	27.5	14.9	22.4	11.3	16.9
	5.5	25.6	38.5	22.7	34.1	19.9	29.8	16.9	25.4	13.8	20.7	10.5	15.7
	6	23.6	35.5	21.0	31.6	18.4	27.6	15.6	23.5	12.7	19.2	9.7	14.6
	6.5	20.9	31.4	18.6	28.0	16.4	24.6	14.0	21.1	11.5	17.3	8.8	13.2
	7	18.6	28.0	16.6	25.0	14.6	21.9	12.5	18.8	10.2	15.4	7.8	11.8
	7.5	16.7	25.1	14.9	22.4	13.1	19.7	11.2	16.8	9.2	13.8	7.0	10.6
	8	15.0	22.6	13.4	20.2	11.8	17.8	10.1	15.2	8.3	12.5	6.4	9.5
	8.5	13.6	20.5	12.2	18.3	10.7	16.1	9.2	13.8	7.5	11.3	5.8	8.7
	9	12.4	18.7	11.1	16.7	9.8	14.7	8.3	12.5	6.8	10.3	5.2	7.9
	9.5	11.3	17.1	10.1	15.2	8.9	13.4	7.6	11.5	6.3	9.4	4.8	7.2
Properties													
A_g (in.^{2})		2.76		2.43		2.11		1.78		1.44		1.09	
γ_z (in.)		0.580		0.580		0.581		0.583		0.585		0.586	
ASD	LRFD	[c] Shape is slender for compression. [f] Shape exceeds compact limit for flexure.											
Ω_c = 1.67	ϕ_c = 0.9	Notes: Heavy lines indicate L/r_z equal to or greater than 120, 140 and 200, respectively. *Method 1.											

Design Table 2. Available Strength in Axial Compression, kips* Eccentrically Loaded Single Angles

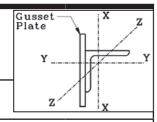

Shape		L8×8×													
		1 1/8		1		7/8		3/4		5/8[c]		9/16[c]		1/2[c, f]	
lb/ft		56.9		51.0		45.0		38.9		32.7		29.6		26.4	
Design		P_n/Ω_c ASD	$\phi_c P_n$ LRFD	P_n/Ω_c ASD	$\phi_c P_n$ LRFD	P_n/Ω_c ASD	$\phi_c P_n$ LRFD	P_n/Ω_c ASD	$\phi_c P_n$ LRFD	P_n/Ω_c ASD	$\phi_c P_n$ LRFD	P_n/Ω_c ASD	$\phi_c P_n$ LRFD	P_n/Ω_c ASD	$\phi_c P_n$ LRFD
		F_y = 36 ksi													
Effective Length, *KL* (ft)	6	153	230	147	220	139.7	210	131	196	119	180	103	155	85.9	129
	7	147	221	140	211	133.5	201	125	187	114	171	99.9	150	83.1	125
	8	140	210	133	201	126.8	191	118	178	108	162	96.9	146	80.3	121
	9	133	199	126	190	119.9	180	112	168	102	153	93.7	141	77.5	116
	10	125	188	119	179	112.7	169	105	157	95.3	143	87.9	132	74.8	112
	11	118	177	112	168	105.5	159	97.7	147	88.9	134	82.1	123	72.2	109
	12	110	166	104	157	98.5	148	91.0	137	82.6	124	76.3	115	69.9	105
	13	103	155	97.4	146	91.7	138	84.4	127	76.5	115	70.7	106	65.0	97.7
	14	96.1	144	90.6	136	85.1	128	78.2	117	70.6	106	65.4	98.2	60.2	90.4
	15	89.5	134	84.1	126	78.9	119	72.2	109	65.1	97.9	60.3	90.6	55.6	83.5
	16	83.1	125	78.0	117	73.0	110	66.6	100	60.0	90.1	55.5	83.4	51.2	77.0
	18	71.3	107	66.6	100	62.1	93.3	56.4	84.8	50.5	75.9	46.8	70.4	43.3	65.1
	20	61.3	92.2	57.1	85.8	53.0	79.7	47.9	72.1	42.7	64.2	39.5	59.4	36.6	55.0
	22	53.3	80.1	49.5	74.3	45.8	68.8	41.2	61.9	36.6	55.0	33.8	50.8	31.2	46.9
	24	46.7	70.1	43.2	65.0	39.9	59.9	35.8	53.8	31.7	47.6	29.2	43.9	26.9	40.5
	26	41.2	61.9	38.1	57.2	35.0	52.7	31.4	47.1	27.7	41.6	25.5	38.3	23.5	35.3
Design		F_y = 50 ksi													
		1 1/8		1		7/8		3/4		5/8[c]		9/16[c, f]		1/2[c, f]	
Effective Length, *KL* (ft)	6	203	305	194	292	185	277	172	259	153	230	130	195	104	157
	7	192	288	183	275	174	261	162	243	144	216	125	188	102	154
	8	180	270	171	257	162	244	151	227	134	201	120	181	98.6	148
	9	167	252	159	239	150	226	139	210	124	187	114	172	94.3	142
	10	155	234	147	221	139	209	128	193	114	172	105	158	90.2	136
	11	144	216	136	204	128	192	118	177	105	158	96.7	145	86.3	130
	12	132	199	125	187	117	176	107	161	95.9	144	88.5	133	81.0	122
	13	121	182	114	171	107	161	97.8	147	87.4	131	80.7	121	74.1	111
	14	111	167	104	157	97.4	146	88.8	133	79.4	119	73.3	110	67.5	101
	15	102	153	95.0	143	88.5	133	80.5	121	72.0	108	66.6	100	61.4	92.3
	16	92.7	139	86.5	130	80.5	121	72.9	110	65.2	98.0	60.4	90.7	55.8	83.9
	18	78.2	117	72.6	109	67.2	101	60.6	91.1	54.0	81.1	49.8	74.9	46.1	69.2
	20	66.7	100	61.8	92.8	57.0	85.6	51.2	76.9	45.4	68.2	41.8	62.8	38.6	58.0
	22	57.5	86.4	53.1	79.9	48.9	73.5	43.8	65.8	38.6	58.1	35.6	53.4	32.8	49.2
	24	50.1	75.2	46.2	69.4	42.4	63.7	37.8	56.8	33.3	50.1	30.6	46.0	28.2	42.3
	26	44.0	66.1	40.5	60.8	37.1	55.7	33.0	49.6	29.0	43.6	26.6	40.0	24.5	36.8
Properties															
A_g (in.^{2})		16.8		15.1		13.3		11.5		9.69		8.77		7.84	
γ_z (in.)		1.56		1.56		1.57		1.57		1.58		1.58		1.59	
ASD	LRFD	[c] Shape is slender for compression. [f] Shape exceeds compact limit for flexure.													
Ω_c = 1.67	ϕ_c = 0.9	Notes: Heavy lines indicate KL/r_z equal to or greater than 120, 140 and 200, respectively. *Method 3 (flexural rigidity $EI^* = 0.8\tau_b EI$).													

Design Table 2. Available Strength in Axial Compression, kips* Eccentrically Loaded Single Angles

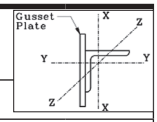

Shape		L6×6×													
		1		7/8		3/4		5/8		9/16		1/2		7/16[c]	
lb/ft		37.4		33.1		28.7		24.2		21.9		19.6		17.3	
Design		P_n/Ω_c ASD	$\phi_c P_n$ LRFD	P_n/Ω_c ASD	$\phi_c P_n$ LRFD	P_n/Ω_c ASD	$\phi_c P_n$ LRFD	P_n/Ω_c ASD	$\phi_c P_n$ LRFD	P_n/Ω_c ASD	$\phi_c P_n$ LRFD	P_n/Ω_c ASD	$\phi_c P_n$ LRFD	P_n/Ω_c ASD	$\phi_c P_n$ LRFD
		F_y = 36 ksi													
Effective Length, *KL* (ft)	4	92.1	138	89.5	135	84.4	127	78.6	118	74.6	112	71.1	107	62.7	94.3
	5	87.5	132	84.9	128	79.9	120	74.2	112	70.4	106	67.1	101	60.4	90.7
	6	82.5	124	79.8	120	74.9	113	69.3	104	65.8	98.8	62.5	93.9	56.8	85.4
	7	77.1	116	74.2	112	69.4	104	64.0	96.3	60.7	91.3	57.6	86.6	52.4	78.7
	8	71.5	108	68.6	103	64.0	96.1	58.7	88.3	55.7	83.7	52.7	79.2	47.9	72.0
	9	66.0	99.2	63.1	94.8	58.6	88.0	53.5	80.4	50.7	76.2	47.8	71.9	43.5	65.4
	10	60.6	91.1	57.7	86.7	53.3	80.1	48.5	72.9	45.9	69.0	43.2	64.9	39.2	59.0
	11	55.4	83.3	52.5	78.9	48.4	72.7	43.8	65.8	41.4	62.2	38.8	58.3	35.2	53.0
	12	50.5	75.9	47.6	71.6	43.7	65.7	39.4	59.2	37.2	55.9	34.8	52.3	31.5	47.4
	13	45.9	68.9	43.1	64.8	39.4	59.2	35.4	53.1	33.3	50.1	31.1	46.7	28.2	42.4
	14	41.5	62.4	38.9	58.4	35.4	53.2	31.7	47.6	29.8	44.8	27.7	41.7	25.1	37.7
	15	37.8	56.8	35.2	53.0	32.0	48.1	28.5	42.8	26.8	40.3	24.9	37.4	22.5	33.8
	16	34.5	51.8	32.1	48.2	29.0	43.7	25.8	38.7	24.2	36.4	22.4	33.7	20.2	30.4
	17	31.6	47.5	29.3	44.0	26.5	39.8	23.4	35.2	22.0	33.0	20.3	30.5	18.3	27.5
	18	29.0	43.6	26.9	40.4	24.2	36.4	21.4	32.1	20.0	30.1	18.5	27.8	16.6	25.0
	19	26.8	40.2	24.7	37.1	22.2	33.4	19.6	29.4	18.3	27.6	16.9	25.4	15.2	22.8
Design		F_y = 50 ksi													
		1		7/8		3/4		5/8		9/16		1/2[c]		7/16[c, f]	
Effective Length, *KL* (ft)	4	123	186	120	180	113	170	105	158	99.5	150	92.9	140	79.8	120
	5	115	173	112	168	105	157	96.9	146	92.0	138	85.9	129	76.0	114
	6	107	160	103	154	95.9	144	88.4	133	83.9	126	78.4	118	70.3	106
	7	97.4	146	93.4	140	87.0	131	79.8	120	75.6	114	70.6	106	63.5	95.5
	8	88.4	133	84.3	127	78.2	118	71.3	107	67.5	101	63.0	94.8	56.8	85.4
	9	79.8	120	75.7	114	69.9	105	63.3	95.2	59.9	90.0	55.9	83.9	50.4	75.8
	10	71.6	108	67.6	102	62.1	93.3	56.0	84.1	52.9	79.5	49.3	74.0	44.5	66.9
	11	64.0	96.1	60.1	90.3	54.9	82.6	49.3	74.1	46.5	69.9	43.3	65.1	39.2	58.8
	12	56.9	85.5	53.2	80.0	48.5	72.9	43.3	65.1	40.8	61.3	37.9	57.0	34.3	51.6
	13	50.9	76.5	47.5	71.3	43.1	64.7	38.3	57.6	36.0	54.1	33.4	50.2	30.2	45.3
	14	45.8	68.8	42.5	63.9	38.5	57.9	34.1	51.3	32.0	48.1	29.6	44.5	26.7	40.1
	15	41.4	62.2	38.3	57.6	34.6	52.0	30.6	45.9	28.7	43.1	26.4	39.7	23.8	35.8
	16	37.6	56.5	34.7	52.2	31.3	47.0	27.5	41.4	25.8	38.8	23.7	35.7	21.4	32.1
	17	34.3	51.5	31.6	47.5	28.4	42.6	24.9	37.5	23.3	35.1	21.4	32.2	19.3	29.0
	18	31.4	47.1	28.8	43.3	25.9	38.9	22.7	34.1	21.2	31.9	19.5	29.2	17.5	26.2
	19	28.8	43.3	26.4	39.7	23.7	35.6	20.7	31.1	19.3	29.1	17.7	26.6	15.9	23.9
Properties															
A_g (in.^{2})		11.0		9.75		8.46		7.13		6.45		5.77		5.08	
γ_z (in.)		1.17		1.17		1.17		1.17		1.18		1.18		1.18	
ASD	LRFD	[c] Shape is slender for compression. [f] Shape exceeds compact limit for flexure.													
Ω_c = 1.67	ϕ_c = 0.9	Notes: Heavy lines indicate KL/r_z equal to or greater than 120, 140 and 200, respectively. *Method 3 (flexural rigidity $EI^* = 0.8\tau_b EI$).													

Design Table 2. Available Strength in Axial Compression, kips*
Eccentrically Loaded Single Angles

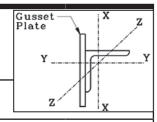

Shape		L5×5×													
		7/8		3/4		5/8		1/2		7/16		3/8[c]		5/16[c, f]	
lb/ft		27.2		23.6		20.0		16.2		14.3		12.3		10.4	
Design		P_n/Ω_c ASD	$\phi_c P_n$ LRFD	P_n/Ω_c ASD	$\phi_c P_n$ LRFD	P_n/Ω_c ASD	$\phi_c P_n$ LRFD	P_n/Ω_c ASD	$\phi_c P_n$ LRFD	P_n/Ω_c ASD	$\phi_c P_n$ LRFD	P_n/Ω_c ASD	$\phi_c P_n$ LRFD	P_n/Ω_c ASD	$\phi_c P_n$ LRFD
		F_y = 36 ksi													
Effective Length, *KL* (ft)	1	71.3	107.2	68.2	102.5	65.1	97.9	60.2	90.5	55.9	84.0	46.3	69.6	35.3	53.1
	2	69.5	104.4	66.3	99.7	63.3	95.1	58.5	87.9	54.2	81.5	45.9	69.0	35.0	52.6
	3	66.7	100.2	63.5	95.4	60.4	90.8	55.7	83.8	51.7	77.7	45.3	68.0	34.4	51.7
	4	63.0	94.7	59.8	89.9	56.8	85.3	52.2	78.5	48.4	72.8	43.7	65.7	33.0	49.6
	5	58.8	88.3	55.6	83.6	52.5	78.9	48.1	72.3	44.5	66.9	41.3	62.0	31.2	46.9
	6	54.1	81.3	51.0	76.7	48.0	72.1	43.7	65.7	40.4	60.8	37.4	56.2	29.5	44.3
	7	49.4	74.3	46.4	69.7	43.3	65.1	39.3	59.1	36.3	54.5	33.5	50.3	27.8	41.8
	8	44.7	67.3	41.8	62.8	38.8	58.4	35.0	52.6	32.2	48.4	29.7	44.6	25.9	38.9
	9	40.3	60.5	37.5	56.3	34.6	52.0	31.0	46.5	28.4	42.7	26.1	39.2	22.8	34.3
	10	36.1	54.2	33.4	50.2	30.6	46.0	27.2	41.0	25.0	37.5	22.9	34.4	20.0	30.1
	11	32.1	48.2	29.6	44.5	27.0	40.6	23.9	35.9	21.8	32.8	20.0	30.0	17.5	26.4
	12	28.6	42.9	26.2	39.4	23.8	35.8	20.9	31.5	19.1	28.7	17.4	26.1	15.3	23.0
	13	25.5	38.4	23.4	35.1	21.1	31.8	18.5	27.8	16.8	25.3	15.3	22.9	13.4	20.1
	14	23.0	34.5	21.0	31.5	18.9	28.4	16.4	24.7	14.9	22.4	13.5	20.3	11.8	17.8
	15	20.8	31.2	18.9	28.4	16.9	25.5	14.7	22.1	13.3	20.0	12.0	18.1	10.5	15.8
	16	18.9	28.3	17.1	25.7	15.3	23.0	13.2	19.9	12.0	18.0	10.8	16.2	9.4	14.1
Design		F_y = 50 ksi													
		7/8		3/4		5/8		1/2		7/16[c]		3/8[c, f]		5/16[c, f]	
Effective Length, *KL* (ft)	1	98.7	148.4	94.3	141.7	90.1	135.4	83.3	125.2	76.4	114.8	61.1	91.9	43.1	64.8
	2	95.3	143.2	90.9	136.6	86.6	130.2	80.0	120.3	73.4	110.2	60.4	90.7	42.5	63.9
	3	90.0	135.2	85.6	128.6	81.3	122.3	74.9	112.6	68.7	103.3	58.6	88.1	41.6	62.5
	4	83.4	125.3	79.0	118.8	74.7	112.2	68.5	103.0	62.9	94.5	55.2	83.0	40.3	60.6
	5	75.9	114.0	71.6	107.6	67.3	101.1	61.4	92.3	56.3	84.7	51.1	76.8	38.4	57.7
	6	68.2	102.4	64.0	96.1	59.7	89.8	54.2	81.4	49.7	74.7	45.2	67.9	35.7	53.7
	7	60.6	91.0	56.5	85.0	52.4	78.8	47.2	70.9	43.2	64.9	39.3	59.1	33.2	50.0
	8	53.4	80.3	49.5	74.4	45.6	68.5	40.7	61.2	37.3	56.0	33.9	51.0	29.5	44.4
	9	46.7	70.2	43.1	64.8	39.4	59.3	35.0	52.6	32.0	48.0	29.1	43.8	25.5	38.3
	10	40.6	61.1	37.4	56.1	33.9	51.0	29.9	44.9	27.3	41.0	24.9	37.4	21.8	32.8
	11	35.6	53.5	32.6	49.0	29.5	44.3	25.8	38.8	23.5	35.3	21.3	32.0	18.7	28.1
	12	31.5	47.3	28.7	43.1	25.8	38.8	22.5	33.8	20.4	30.7	18.5	27.7	16.1	24.3
	13	28.0	42.0	25.4	38.2	22.8	34.2	19.7	29.7	17.9	26.9	16.1	24.2	14.1	21.2
	14	25.0	37.6	22.7	34.1	20.2	30.4	17.5	26.3	15.8	23.8	14.2	21.4	12.4	18.6
	15	22.5	33.8	20.3	30.5	18.1	27.2	15.6	23.4	14.1	21.2	12.6	19.0	11.0	16.5
	16	20.3	30.5	18.3	27.5	16.3	24.4	14.0	21.0	12.6	18.9	11.3	17.0	9.8	14.7
Properties															
A_g (in.^{2})		8.00		6.98		5.90		4.79		4.22		3.65		3.07	
γ_z (in.)		0.971		0.972		0.975		0.980		0.983		0.986		0.990	

ASD	LRFD
Ω_c = 1.67	ϕ_c = 0.9

[c] Shape is slender for compression. [f] Shape exceeds compact limit for flexure.
Notes: Heavy lines indicate KL/r_z equal to or greater than 120, 140 and 200, respectively.
*Method 3 (flexural rigidity $EI^* = 0.8\tau_b EI$).

Design Table 2. Available Strength in Axial Compression, kips*
Eccentrically Loaded Single Angles

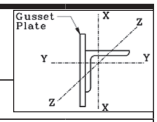

Shape		L4×4×													
		3/4		5/8		1/2		7/16		3/8		5/16[c]		1/4[c, f]	
lb/ft		18.5		15.7		12.8		11.3		9.8		8.2		6.6	
Design		P_n/Ω_c ASD	$\phi_c P_n$ LRFD	P_n/Ω_c ASD	$\phi_c P_n$ LRFD	P_n/Ω_c ASD	$\phi_c P_n$ LRFD	P_n/Ω_c ASD	$\phi_c P_n$ LRFD	P_n/Ω_c ASD	$\phi_c P_n$ LRFD	P_n/Ω_c ASD	$\phi_c P_n$ LRFD	P_n/Ω_c ASD	$\phi_c P_n$ LRFD
		F_y = 36 ksi													
Effective Length, *KL* (ft)	2	43.5	65.4	42.1	63.2	38.9	58.4	37.2	55.9	34.6	52.0	31.3	47.0	22.0	33.0
	2.5	42.3	63.5	40.8	61.4	37.6	56.5	36.0	54.0	33.4	50.3	30.2	45.4	21.7	32.6
	3	40.9	61.4	39.4	59.2	36.2	54.4	34.5	51.9	32.1	48.3	29.0	43.6	21.2	31.9
	3.5	39.3	59.1	37.7	56.7	34.6	52.0	33.0	49.6	30.6	46.0	27.6	41.5	20.5	30.8
	4	37.6	56.6	36.0	54.1	32.9	49.5	31.3	47.1	29.0	43.6	26.1	39.3	19.8	29.8
	4.5	35.9	53.9	34.2	51.4	31.1	46.8	29.6	44.4	27.4	41.1	24.6	37.0	19.1	28.8
	5	34.1	51.2	32.3	48.6	29.3	44.1	27.8	41.7	25.6	38.5	23.0	34.6	18.5	27.8
	5.5	32.2	48.4	30.4	45.7	27.5	41.3	26.0	39.0	23.9	36.0	21.5	32.3	17.9	26.8
	6	30.4	45.6	28.6	42.9	25.7	38.6	24.2	36.4	22.3	33.5	19.9	30.0	17.0	25.6
	7	26.8	40.3	25.0	37.5	22.3	33.5	20.9	31.4	19.1	28.7	17.0	25.6	14.6	21.9
	8	23.4	35.2	21.6	32.5	19.2	28.8	17.9	26.8	16.3	24.5	14.4	21.7	12.4	18.6
	9	20.3	30.5	18.6	28.0	16.4	24.6	15.2	22.8	13.8	20.7	12.1	18.3	10.4	15.7
	10	17.6	26.5	16.1	24.1	14.0	21.1	12.9	19.5	11.7	17.6	10.3	15.5	8.8	13.2
	11	15.5	23.2	14.0	21.0	12.2	18.3	11.2	16.8	10.1	15.1	8.8	13.2	7.5	11.3
	12	13.6	20.5	12.3	18.5	10.6	16.0	9.7	14.6	8.7	13.1	7.6	11.5	6.5	9.7
	13											6.7	10.0	5.6	8.5
Design		F_y = 50 ksi													
		3/4		5/8		1/2		7/16		3/8		5/16[c]		1/4[c, f]	
Effective Length, *KL* (ft)	2	59.2	89.0	57.2	86.0	52.8	79.3	50.4	75.8	46.9	70.5	40.9	61.4	26.6	40.0
	2.5	57.0	85.7	54.9	82.5	50.5	75.9	48.2	72.5	44.8	67.3	39.1	58.8	26.2	39.4
	3	54.4	81.8	52.3	78.5	47.9	72.0	45.7	68.6	42.4	63.7	37.1	55.7	25.7	38.7
	3.5	51.7	77.7	49.4	74.2	45.1	67.8	42.9	64.5	39.7	59.7	34.8	52.3	25.2	37.9
	4	48.8	73.3	46.4	69.7	42.2	63.4	40.0	60.1	37.0	55.6	32.4	48.8	24.3	36.6
	4.5	45.7	68.7	43.3	65.0	39.2	58.9	37.0	55.7	34.2	51.4	30.0	45.2	23.3	35.0
	5	42.7	64.2	40.2	60.4	36.2	54.5	34.2	51.3	31.4	47.3	27.7	41.6	22.3	33.5
	5.5	39.7	59.7	37.2	55.9	33.4	50.2	31.4	47.1	28.8	43.3	25.3	38.1	21.4	32.2
	6	36.8	55.4	34.3	51.6	30.6	46.1	28.7	43.1	26.3	39.5	23.1	34.8	19.7	29.6
	7	31.4	47.2	29.0	43.5	25.6	38.5	23.8	35.8	21.7	32.6	19.1	28.7	16.3	24.5
	8	26.5	39.9	24.2	36.4	21.3	31.9	19.7	29.5	17.8	26.8	15.7	23.6	13.5	20.2
	9	22.6	34.0	20.5	30.8	17.8	26.8	16.4	24.7	14.8	22.3	13.0	19.5	11.1	16.6
	10	19.5	29.2	17.5	26.4	15.2	22.8	13.9	20.9	12.5	18.8	10.9	16.4	9.3	13.9
	11	16.9	25.4	15.2	22.8	13.1	19.6	11.9	17.9	10.7	16.1	9.3	14.0	7.9	11.8
	12	14.8	22.3	13.2	19.9	11.3	17.1	10.3	15.5	9.2	13.9	8.0	12.1	6.8	10.2
	13											7.0	10.5	5.9	8.8
Properties															
A_g (in.^{2})		5.44		4.61		3.75		3.30		2.86		2.40		1.93	
γ_z (in.)		0.774		0.774		0.776		0.777		0.779		0.781		0.783	
ASD	LRFD	[c] Shape is slender for compression. [f] Shape exceeds compact limit for flexure.													
Ω_c = 1.67	ϕ_c = 0.9	Notes: Heavy lines indicate KL/r_z equal to or greater than 120, 140 and 200, respectively. *Method 3 (flexural rigidity $EI^* = 0.8\tau_b EI$).													

Design Table 2. Available Strength in Axial Compression, kips* Eccentrically Loaded Single Angles

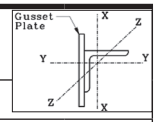

Shape		L3½×3½×									
		½		7/16		3/8		5/16		1/4[c]	
lb/ft		11.1		9.80		8.50		7.20		5.80	
Design		P_n/Ω_c ASD	$\phi_c P_n$ LRFD	P_n/Ω_c ASD	$\phi_c P_n$ LRFD	P_n/Ω_c ASD	$\phi_c P_n$ LRFD	P_n/Ω_c ASD	$\phi_c P_n$ LRFD	P_n/Ω_c ASD	$\phi_c P_n$ LRFD
		F_y = 36 ksi									
Effective Length, *KL* (ft)	2	31.1	46.8	29.6	44.4	28.4	42.6	25.9	38.9	20.7	31.0
	2.5	29.9	45.0	28.4	42.6	27.2	40.8	24.7	37.2	20.2	30.3
	3	28.5	42.8	27.0	40.6	25.8	38.8	23.5	35.3	19.5	29.3
	3.5	27.0	40.5	25.5	38.3	24.3	36.5	22.1	33.2	18.8	28.3
	4	25.4	38.1	23.9	36.0	22.7	34.2	20.6	31.0	18.0	27.1
	4.5	23.7	35.6	22.3	33.6	21.1	31.8	19.1	28.7	16.7	25.1
	5	22.0	33.1	20.7	31.2	19.6	29.4	17.6	26.5	15.4	23.2
	5.5	20.4	30.7	19.2	28.8	18.0	27.1	16.2	24.4	14.1	21.3
	6	18.9	28.4	17.7	26.5	16.5	24.9	14.8	22.3	12.9	19.4
	6.5	17.4	26.1	16.2	24.4	15.1	22.8	13.5	20.4	11.8	17.7
	7	16.0	24.0	14.9	22.4	13.8	20.8	12.3	18.5	10.7	16.1
	7.5	14.6	22.0	13.6	20.5	12.6	19.0	11.2	16.8	9.7	14.6
	8	13.4	20.1	12.4	18.7	11.5	17.2	10.2	15.3	8.8	13.2
	9	11.3	17.0	10.4	15.7	9.6	14.4	8.4	12.7	7.3	10.9
	10	9.7	14.5	8.9	13.4	8.1	12.2	7.1	10.7	6.1	9.2
	11	8.3	12.5	7.7	11.5	7.0	10.5	6.1	9.2	5.2	7.8
Design		F_y = 50 ksi									
		½		7/16		3/8		5/16		1/4[c]	
Effective Length, *KL* (ft)	2	42.0	63.2	39.9	59.9	38.2	57.4	34.6	52.0	26.4	39.7
	2.5	39.8	59.8	37.7	56.7	36.0	54.2	32.6	49.0	25.6	38.4
	3	37.3	56.1	35.3	53.0	33.6	50.5	30.4	45.7	24.5	36.8
	3.5	34.6	52.1	32.7	49.1	31.0	46.6	28.0	42.1	23.4	35.2
	4	31.9	48.0	30.1	45.2	28.4	42.7	25.6	38.4	21.9	32.9
	4.5	29.3	44.0	27.5	41.3	25.9	38.9	23.2	34.9	19.9	30.0
	5	26.7	40.1	25.0	37.5	23.4	35.2	21.0	31.5	18.0	27.1
	5.5	24.2	36.4	22.6	34.0	21.1	31.7	18.8	28.3	16.2	24.4
	6	21.9	32.9	20.4	30.7	19.0	28.5	16.9	25.4	14.6	21.9
	6.5	19.8	29.7	18.4	27.6	17.0	25.5	15.1	22.7	13.0	19.6
	7	17.8	26.7	16.5	24.8	15.2	22.9	13.5	20.2	11.6	17.5
	7.5	16.1	24.2	14.9	22.4	13.7	20.6	12.1	18.1	10.4	15.6
	8	14.6	22.0	13.5	20.3	12.4	18.6	10.9	16.4	9.3	14.0
	9	12.2	18.4	11.3	16.9	10.3	15.4	9.0	13.5	7.7	11.5
	10	10.4	15.6	9.5	14.3	8.6	13.0	7.5	11.3	6.4	9.6
	11	8.9	13.4	8.2	12.3	7.4	11.1	6.4	9.6	5.4	8.2
Properties											
A_g (in.^{2})		3.25		2.89		2.50		2.10		1.70	
γ_z (in.)		0.679		0.681		0.683		0.685		0.688	
ASD	LRFD	[c] Shape is slender for compression.									
Ω_c = 1.67	ϕ_c = 0.9	[f] Shape exceeds compact limit for flexure.									
		Notes: Heavy lines indicate KL/r_z equal to or greater than 120, 140 and 200, respectively.									
		*Method 3 (flexural rigidity $EI^* = 0.8\tau_b EI$).									

Design Table 2. Available Strength in Axial Compression, kips* Eccentrically Loaded Single Angles

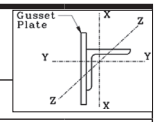

Shape		L3×3×											
		1/2		7/16		3/8		5/16		1/4		3/16[c, f]	
lb/ft		9.40		8.30		7.20		6.10		4.90		3.71	
		P_n/Ω_c	$\phi_c P_n$	P_n/Ω_c	$\phi_c P_n$	P_n/Ω_c	$\phi_c P_n$	P_n/Ω_c	$\phi_c P_n$	P_n/Ω_c	$\phi_c P_n$	P_n/Ω_c	$\phi_c P_n$
Design		ASD	LRFD	ASD	LRFD	ASD	LRFD	ASD	LRFD	ASD	LRFD	ASD	LRFD
		F_y = 36 ksi											
Effective Length, *KL* (ft)	2	22.9	34.5	22.0	33.1	21.0	31.5	19.5	29.3	17.5	26.3	12.3	18.4
	2.5	21.8	32.8	20.9	31.4	19.9	29.8	18.4	27.7	16.5	24.8	11.8	17.7
	3	20.5	30.9	19.6	29.4	18.6	27.9	17.2	25.9	15.4	23.1	11.2	16.9
	3.5	19.2	28.8	18.2	27.4	17.2	25.9	15.9	23.9	14.1	21.3	10.7	16.1
	4	17.8	26.7	16.8	25.3	15.9	23.8	14.6	21.9	12.9	19.4	10.3	15.4
	4.5	16.4	24.6	15.5	23.2	14.5	21.8	13.3	20.0	11.7	17.6	9.5	14.3
	5	15.0	22.6	14.1	21.2	13.2	19.8	12.0	18.1	10.6	15.9	8.6	12.9
	5.5	13.7	20.6	12.9	19.3	12.0	18.0	10.9	16.3	9.5	14.3	7.7	11.6
	6	12.5	18.8	11.7	17.5	10.8	16.2	9.8	14.7	8.5	12.8	6.9	10.4
	6.5	11.3	17.1	10.5	15.8	9.7	14.6	8.8	13.2	7.6	11.4	6.2	9.3
	7	10.3	15.4	9.5	14.3	8.7	13.1	7.8	11.8	6.8	10.2	5.5	8.3
	7.5	9.3	14.0	8.6	12.9	7.9	11.9	7.1	10.6	6.1	9.1	4.9	7.4
	8	8.5	12.8	7.8	11.8	7.2	10.8	6.4	9.6	5.5	8.2	4.4	6.6
	8.5	7.8	11.7	7.2	10.8	6.5	9.8	5.8	8.7	5.0	7.5	4.0	6.0
	9	7.2	10.8	6.6	9.9	6.0	9.0	5.3	8.0	4.5	6.8	3.6	5.4
	9.5	6.6	9.9	6.0	9.1	5.5	8.2	4.9	7.3	4.1	6.2	3.3	5.0
Design		F_y = 50 ksi											
		1/2		7/16		3/8		5/16		1/4		3/16[c]	
Effective Length, *KL* (ft)	2	30.8	46.2	29.4	44.3	28.0	42.1	26.0	39.1	22.9	34.4	14.8	22.2
	2.5	28.7	43.2	27.4	41.2	26.0	39.1	24.1	36.2	21.1	31.8	14.4	21.7
	3	26.5	39.8	25.2	37.8	23.8	35.8	21.9	33.0	19.2	28.9	13.8	20.8
	3.5	24.2	36.4	22.9	34.4	21.5	32.4	19.8	29.7	17.3	26.0	13.0	19.6
	4	22.0	33.0	20.7	31.1	19.4	29.1	17.7	26.6	15.5	23.2	12.4	18.6
	4.5	19.8	29.7	18.5	27.9	17.3	26.0	15.7	23.6	13.7	20.6	11.0	16.5
	5	17.7	26.7	16.5	24.9	15.3	23.0	13.9	20.9	12.1	18.1	9.7	14.6
	5.5	15.8	23.8	14.7	22.1	13.6	20.4	12.2	18.4	10.6	15.9	8.6	12.9
	6	14.1	21.1	13.0	19.6	12.0	18.0	10.7	16.1	9.3	13.9	7.5	11.3
	6.5	12.6	18.9	11.6	17.4	10.6	16.0	9.5	14.3	8.2	12.3	6.6	9.9
	7	11.3	17.0	10.4	15.6	9.5	14.3	8.5	12.7	7.2	10.9	5.8	8.8
	7.5	10.2	15.4	9.4	14.1	8.5	12.8	7.6	11.4	6.5	9.7	5.2	7.8
	8	9.3	14.0	8.5	12.8	7.7	11.6	6.8	10.3	5.8	8.7	4.6	7.0
	8.5	8.5	12.7	7.7	11.6	7.0	10.5	6.2	9.3	5.2	7.9	4.2	6.3
	9	7.7	11.6	7.1	10.6	6.4	9.6	5.6	8.4	4.8	7.2	3.8	5.7
	9.5	7.1	10.7	6.5	9.7	5.8	8.8	5.1	7.7	4.3	6.5	3.4	5.2
Properties													
A_g (in.^{2})		2.76		2.43		2.11		1.78		1.44		1.09	
γ_z (in.)		0.580		0.580		0.581		0.583		0.585		0.586	
ASD	LRFD	[c] Shape is slender for compression.											
		[f] Shape exceeds compact limit for flexure.											
Ω_c = 1.67	ϕ_c = 0.9	Notes: Heavy lines indicate KL/r_z equal to or greater than 120, 140 and 200, respectively.											
		*Method 3 (flexural rigidity $EI^* = 0.8\tau_b EI$).											

Design Table 3. Available Strength in Axial Compression, kips* Eccentrically Loaded Single Angles

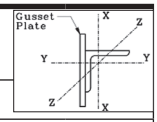

Shape		L8×8×													
		1 1/8		1		7/8		3/4		5/8[c]		9/16[c]		1/2[c, f]	
lb/ft		56.9		51.0		45.0		38.9		32.7		29.6		26.4	
Design		P_n/Ω_c ASD	$\phi_c P_n$ LRFD	P_n/Ω_c ASD	$\phi_c P_n$ LRFD	P_n/Ω_c ASD	$\phi_c P_n$ LRFD	P_n/Ω_c ASD	$\phi_c P_n$ LRFD	P_n/Ω_c ASD	$\phi_c P_n$ LRFD	P_n/Ω_c ASD	$\phi_c P_n$ LRFD	P_n/Ω_c ASD	$\phi_c P_n$ LRFD
		F_y = 36 ksi													
Effective Length, *KL* (ft)	6	104	157	97.7	147	90.4	136	82.1	123	72.5	109	66.1	99.3	59.6	89.6
	7	101	152	94.4	142	87.3	131	79.1	119	69.9	105	63.7	95.8	57.5	86.4
	8	97.3	146	90.8	136	83.9	126	75.9	114	67.0	101	61.1	91.9	55.2	83.0
	9	93.3	140	86.9	131	80.3	121	72.6	109	64.0	96.2	58.4	87.8	52.8	79.4
	10	89.1	134	83.0	125	76.6	115	69.1	104	60.9	91.5	55.6	83.5	50.3	75.6
	11	84.9	128	78.9	119	72.8	109	65.6	98.6	57.7	86.8	52.7	79.2	47.8	71.8
	12	80.6	121	74.9	113	68.9	104	62.0	93.2	54.5	81.9	49.8	74.8	45.2	67.9
	13	76.3	115	70.8	106	65.1	97.8	58.5	87.9	51.4	77.2	46.9	70.5	42.6	64.1
	14	72.1	108	66.8	100	61.3	92.2	55.0	82.7	48.3	72.6	44.1	66.3	40.2	60.4
	15	67.9	102	62.9	94.5	57.7	86.7	51.7	77.6	45.3	68.1	41.4	62.3	37.7	56.7
	16	63.9	96.1	59.0	88.8	54.1	81.4	48.4	72.8	42.4	63.8	38.8	58.3	35.4	53.2
	18	56.2	84.4	51.8	77.8	47.4	71.2	42.2	63.5	37.0	55.6	33.9	50.9	31.0	46.6
	20	49.4	74.2	45.4	68.2	41.5	62.3	36.9	55.4	32.2	48.4	29.5	44.3	27.0	40.5
	22	43.6	65.6	40.1	60.2	36.5	54.9	32.4	48.7	28.2	42.4	25.8	38.8	23.6	35.5
	24	38.8	58.4	35.6	53.5	32.4	48.7	28.7	43.1	25.0	37.5	22.8	34.3	20.8	31.3
	26	34.7	52.2	31.8	47.8	28.9	43.4	25.5	38.4	22.2	33.4	20.3	30.5	18.5	27.8
Design		F_y = 50 ksi													
		1 1/8		1		7/8		3/4		5/8[c]		9/16[c, f]		1/2[c, f]	
Effective Length, *KL* (ft)	6	140	210	131	196	121	182	110	165	94.9	143	86.1	129	77.2	116
	7	134	201	125	188	115	173	104	157	90.5	136	82.1	123	73.8	111
	8	127	191	118	178	109	164	98.8	148	85.7	129	77.9	117	70.1	105
	9	120	181	112	168	103	155	93.0	140	80.8	121	73.5	110	66.2	99.5
	10	113	170	105	158	96.8	146	87.1	131	75.7	114	68.9	104	62.3	93.6
	11	106	160	98.5	148	90.6	136	81.4	122	70.8	106	64.5	96.9	58.4	87.7
	12	99.3	149	92.0	138	84.5	127	75.7	114	65.9	99.1	60.1	90.4	54.5	81.9
	13	92.6	139	85.6	129	78.5	118	70.3	106	61.3	92.1	55.9	84.0	50.8	76.3
	14	86.0	129	79.4	119	72.8	109	65.0	97.8	56.8	85.3	51.8	77.9	47.2	70.9
	15	79.7	120	73.5	110	67.3	101	60.0	90.2	52.5	78.8	48.0	72.1	43.7	65.7
	16	73.8	111	67.9	102	62.1	93.3	55.3	83.1	48.3	72.7	44.3	66.5	40.5	60.8
	18	63.6	95.6	58.4	87.8	53.3	80.1	47.3	71.1	41.3	62.0	37.7	56.7	34.5	51.9
	20	55.3	83.1	50.7	76.2	46.1	69.4	40.9	61.4	35.6	53.5	32.5	48.9	29.7	44.6
	22	48.4	72.8	44.3	66.6	40.3	60.6	35.6	53.5	31.0	46.5	28.3	42.5	25.8	38.8
	24	42.8	64.3	39.1	58.7	35.5	53.3	31.3	47.0	27.2	40.8	24.8	37.2	22.6	34.0
	26	38.0	57.1	34.7	52.1	31.4	47.2	27.7	41.6	24.0	36.1	21.9	32.9	20.0	30.0
Properties															
A_g (in.^{2})		16.8		15.1		13.3		11.5		9.69		8.77		7.84	
γ_z (in.)		1.56		1.56		1.57		1.57		1.58		1.58		1.59	
ASD	LRFD	[c] Shape is slender for compression. [f] Shape exceeds compact limit for flexure.													
Ω_c = 1.67	ϕ_c = 0.9	Notes: Heavy lines indicate L/r_z equal to or greater than 120, 140 and 200, respectively. *Method 4 (flexural rigidity $EI^* = 0.8\tau_b EI$).													

Design Table 3. Available Strength in Axial Compression, kips*
Eccentrically Loaded Single Angles

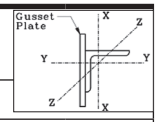

Shape		L6×6×													
		1		7/8		3/4		5/8		9/16		1/2		7/16[c]	
lb/ft		37.4		33.1		28.7		24.2		21.9		19.6		17.3	
Design		P_n/Ω_c ASD	$\phi_c P_n$ LRFD	P_n/Ω_c ASD	$\phi_c P_n$ LRFD	P_n/Ω_c ASD	$\phi_c P_n$ LRFD	P_n/Ω_c ASD	$\phi_c P_n$ LRFD	P_n/Ω_c ASD	$\phi_c P_n$ LRFD	P_n/Ω_c ASD	$\phi_c P_n$ LRFD	P_n/Ω_c ASD	$\phi_c P_n$ LRFD
		F_y = 36 ksi													
Effective Length, *KL* (ft)	4	64.9	97.6	61.2	92.0	55.9	84.1	50.0	75.2	46.6	70.0	43.4	65.2	38.7	58.2
	5	62.4	93.8	58.7	88.2	53.6	80.5	47.8	71.9	44.6	67.0	41.4	62.3	37.0	55.6
	6	59.5	89.5	55.9	84.0	50.9	76.5	45.4	68.2	42.2	63.5	39.2	58.9	35.0	52.6
	7	56.4	84.8	52.8	79.4	48.0	72.2	42.7	64.2	39.8	59.8	36.9	55.4	32.9	49.4
	8	53.1	79.9	49.6	74.6	45.0	67.6	39.9	60.0	37.1	55.8	34.4	51.7	30.7	46.1
	9	49.7	74.8	46.3	69.7	42.0	63.1	37.1	55.8	34.5	51.9	31.9	48.0	28.5	42.8
	10	46.4	69.7	43.1	64.8	38.9	58.5	34.3	51.6	32.0	48.0	29.5	44.3	26.3	39.5
	11	43.1	64.7	39.9	60.0	36.0	54.1	31.7	47.6	29.4	44.3	27.1	40.7	24.2	36.4
	12	39.8	59.8	36.8	55.3	33.1	49.8	29.1	43.7	27.0	40.6	24.8	37.3	22.2	33.3
	13	36.7	55.1	33.8	50.9	30.4	45.6	26.6	40.0	24.7	37.2	22.7	34.1	20.3	30.4
	14	33.7	50.6	31.0	46.6	27.8	41.7	24.3	36.5	22.6	33.9	20.7	31.1	18.4	27.7
	15	31.0	46.6	28.5	42.8	25.5	38.3	22.2	33.4	20.6	31.0	18.9	28.4	16.8	25.3
	16	28.6	43.0	26.2	39.4	23.4	35.2	20.4	30.6	18.9	28.4	17.3	26.0	15.4	23.2
	17	26.5	39.8	24.2	36.4	21.6	32.4	18.7	28.2	17.4	26.2	15.9	23.9	14.1	21.3
	18	24.5	36.9	22.4	33.7	20.0	30.0	17.3	26.0	16.1	24.1	14.6	22.0	13.0	19.6
	19	22.8	34.3	20.8	31.3	18.5	27.8	16.0	24.1	14.9	22.3	13.5	20.3	12.0	18.1
Design		F_y = 50 ksi													
		1		7/8		3/4		5/8		9/16		1/2[c]		7/16[c, f]	
Effective Length, *KL* (ft)	4	87.7	132	82.5	124	75.4	113	67.3	101	62.8	94.4	57.6	86.6	50.9	76.5
	5	83.1	125	78.0	117	71.1	107	63.4	95.3	59.0	88.7	54.2	81.5	47.9	72.0
	6	78.1	117	73.1	110	66.4	99.9	59.1	88.8	54.9	82.6	50.4	75.8	44.7	67.1
	7	72.6	109	67.8	102	61.5	92.4	54.5	81.9	50.7	76.2	46.5	69.9	41.2	61.9
	8	67.1	101	62.4	93.8	56.5	84.9	49.9	75.0	46.4	69.8	42.6	64.0	37.8	56.8
	9	61.6	92.6	57.2	85.9	51.6	77.5	45.4	68.3	42.3	63.5	38.7	58.2	34.4	51.7
	10	56.3	84.6	52.0	78.2	46.8	70.4	41.1	61.8	38.3	57.5	35.1	52.7	31.2	46.9
	11	51.1	76.8	47.1	70.9	42.3	63.6	37.1	55.7	34.5	51.8	31.6	47.5	28.1	42.3
	12	46.2	69.5	42.5	63.9	38.1	57.2	33.3	50.0	30.9	46.5	28.3	42.6	25.3	38.0
	13	42.0	63.1	38.5	57.9	34.4	51.7	30.0	45.1	27.9	41.9	25.5	38.3	22.7	34.1
	14	38.2	57.4	35.0	52.6	31.2	46.9	27.1	40.8	25.2	37.9	23.0	34.6	20.5	30.8
	15	34.9	52.5	31.9	48.0	28.4	42.7	24.7	37.1	22.9	34.4	20.9	31.4	18.6	27.9
	16	32.0	48.1	29.2	43.9	26.0	39.0	22.5	33.8	20.9	31.4	19.0	28.6	16.9	25.4
	17	29.4	44.3	26.8	40.3	23.8	35.8	20.6	31.0	19.1	28.7	17.4	26.1	15.5	23.2
	18	27.2	40.8	24.7	37.1	21.9	32.9	18.9	28.5	17.5	26.4	16.0	24.0	14.2	21.3
	19	25.1	37.8	22.8	34.3	20.2	30.4	17.4	26.2	16.2	24.3	14.7	22.1	13.0	19.6
Properties															
A_g (in.^{2})		11.0		9.75		8.46		7.13		6.45		5.77		5.08	
γ_z (in.)		1.17		1.17		1.17		1.17		1.18		1.18		1.18	
ASD	LRFD	[c] Shape is slender for compression. [f] Shape exceeds compact limit for flexure.													
Ω_c = 1.67	ϕ_c = 0.9	Notes: Heavy lines indicate L/r_z equal to or greater than 120, 140 and 200, respectively. *Method 4 (flexural rigidity $EI^* = 0.8\tau_b EI$).													

Design Table 3. Available Strength in Axial Compression, kips*
Eccentrically Loaded Single Angles

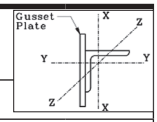

Shape		L5×5×													
		7/8		3/4		5/8		1/2		7/16		3/8[c]		5/16[c, f]	
lb/ft		27.2		23.6		20.0		16.2		14.3		12.3		10.4	
Design		P_n/Ω_c ASD	$\phi_c P_n$ LRFD	P_n/Ω_c ASD	$\phi_c P_n$ LRFD	P_n/Ω_c ASD	$\phi_c P_n$ LRFD	P_n/Ω_c ASD	$\phi_c P_n$ LRFD	P_n/Ω_c ASD	$\phi_c P_n$ LRFD	P_n/Ω_c ASD	$\phi_c P_n$ LRFD	P_n/Ω_c ASD	$\phi_c P_n$ LRFD
		F_y = 36 ksi													
Effective Length, *KL* (ft)	1	50.0	75.1	46.0	69.2	42.1	63.3	37.2	55.9	33.6	50.5	30.4	45.7	25.7	38.6
	2	48.9	73.6	45.1	67.7	41.2	61.9	36.3	54.6	32.8	49.4	29.7	44.6	25.1	37.7
	3	47.4	71.2	43.5	65.5	39.8	59.7	35.0	52.6	31.6	47.5	28.5	42.9	24.2	36.4
	4	45.3	68.0	41.6	62.5	37.9	56.9	33.3	50.0	30.0	45.1	27.1	40.7	23.0	34.6
	5	42.8	64.4	39.2	59.0	35.6	53.6	31.2	46.9	28.2	42.3	25.4	38.2	21.6	32.5
	6	40.1	60.3	36.7	55.1	33.2	49.9	29.0	43.6	26.1	39.3	23.5	35.4	20.0	30.1
	7	37.2	56.0	34.0	51.0	30.6	46.0	26.7	40.1	24.0	36.1	21.6	32.5	18.4	27.7
	8	34.3	51.6	31.2	46.9	28.1	42.2	24.4	36.6	21.9	32.9	19.7	29.6	16.8	25.3
	9	31.4	47.2	28.5	42.9	25.6	38.4	22.1	33.2	19.9	29.9	17.8	26.8	15.3	23.0
	10	28.6	43.0	25.9	39.0	23.2	34.8	20.0	30.0	17.9	26.9	16.1	24.1	13.8	20.7
	11	25.9	39.0	23.4	35.2	20.8	31.3	17.9	26.9	16.1	24.2	14.4	21.6	12.4	18.6
	12	23.4	35.2	21.1	31.7	18.7	28.2	16.1	24.1	14.4	21.6	12.9	19.3	11.1	16.7
	13	21.2	31.9	19.1	28.7	16.9	25.4	14.4	21.7	12.9	19.5	11.5	17.3	9.9	14.9
	14	19.3	29.1	17.4	26.1	15.3	23.0	13.1	19.6	11.7	17.6	10.4	15.6	9.0	13.5
	15	17.7	26.5	15.8	23.8	13.9	21.0	11.9	17.8	10.6	15.9	9.4	14.2	8.1	12.2
	16	16.2	24.3	14.5	21.8	12.7	19.1	10.8	16.2	9.7	14.5	8.6	12.9	7.4	11.1
Design		F_y = 50 ksi													
		7/8		3/4		5/8		1/2		7/16[c]		3/8[c, f]		5/16[c, f]	
Effective Length, *KL* (ft)	1	69.2	104	63.8	95.9	58.3	87.7	51.5	77.4	46.2	69.4	41.0	61.6	34.2	51.5
	2	67.3	101	61.9	93.1	56.6	85.1	49.9	75.0	44.7	67.3	39.7	59.7	33.2	50.0
	3	64.3	96.6	59.1	88.8	53.9	81.0	47.4	71.2	42.5	63.9	37.7	56.7	31.7	47.6
	4	60.5	90.9	55.5	83.4	50.4	75.8	44.2	66.5	39.7	59.6	35.2	53.0	29.7	44.6
	5	56.1	84.4	51.3	77.1	46.5	69.8	40.6	61.0	36.4	54.7	32.4	48.7	27.4	41.1
	6	51.4	77.3	46.9	70.5	42.3	63.6	36.8	55.3	33.0	49.6	29.4	44.2	24.9	37.5
	7	46.7	70.1	42.4	63.8	38.1	57.3	33.0	49.7	29.6	44.6	26.4	39.7	22.5	33.8
	8	42.0	63.1	38.1	57.2	34.1	51.2	29.4	44.2	26.4	39.7	23.5	35.3	20.1	30.2
	9	37.5	56.3	33.9	50.9	30.2	45.4	26.0	39.1	23.3	35.1	20.8	31.3	17.9	26.8
	10	33.3	50.0	30.0	45.1	26.6	40.0	22.8	34.3	20.5	30.8	18.3	27.5	15.8	23.7
	11	29.6	44.5	26.6	40.0	23.6	35.4	20.1	30.2	18.0	27.1	16.1	24.2	13.9	20.8
	12	26.5	39.9	23.8	35.8	21.0	31.5	17.9	26.9	16.0	24.1	14.2	21.4	12.3	18.4
	13	23.9	35.8	21.4	32.1	18.8	28.3	16.0	24.0	14.3	21.5	12.7	19.1	10.9	16.4
	14	21.5	32.4	19.3	29.0	16.9	25.4	14.3	21.5	12.8	19.3	11.4	17.1	9.8	14.7
	15	19.6	29.4	17.5	26.2	15.3	23.0	12.9	19.4	11.6	17.4	10.2	15.4	8.8	13.2
	16	17.8	26.8	15.9	23.9	13.9	20.9	11.7	17.6	10.5	15.8	9.3	13.9	8.0	12.0
Properties															
A_g (in.^{2})		8.00		6.98		5.90		4.79		4.22		3.65		3.07	
γ_z (in.)		0.971		0.972		0.975		0.980		0.983		0.986		0.990	
ASD	LRFD	[c] Shape is slender for compression. [f] Shape exceeds compact limit for flexure.													
Ω_c = 1.67	ϕ_c = 0.9	Notes: Heavy lines indicate L/r_z equal to or greater than 120, 140 and 200, respectively. *Method 4 (flexural rigidity $EI^* = 0.8\tau_b EI$).													

Design Table 3. Available Strength in Axial Compression, kips*
Eccentrically Loaded Single Angles

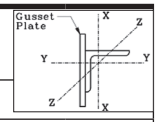

Shape		L4×4×													
		3/4		5/8		1/2		7/16		3/8		5/16[c]		1/4[c, f]	
lb/ft		18.5		15.7		12.8		11.3		9.8		8.2		6.6	
Design		P_n/Ω_c ASD	$\phi_c P_n$ LRFD	P_n/Ω_c ASD	$\phi_c P_n$ LRFD	P_n/Ω_c ASD	$\phi_c P_n$ LRFD	P_n/Ω_c ASD	$\phi_c P_n$ LRFD	P_n/Ω_c ASD	$\phi_c P_n$ LRFD	P_n/Ω_c ASD	$\phi_c P_n$ LRFD	P_n/Ω_c ASD	$\phi_c P_n$ LRFD
		F_y = 36 ksi													
Effective Length, *KL* (ft)	2	31.3	47.0	28.9	43.4	25.4	38.2	23.5	35.3	21.3	32.0	18.7	28.1	15.4	23.1
	2.5	30.6	46.0	28.2	42.4	24.8	37.3	22.9	34.4	20.7	31.1	18.2	27.3	15.0	22.5
	3	29.8	44.8	27.4	41.2	24.1	36.2	22.2	33.4	20.1	30.2	17.6	26.4	14.5	21.8
	3.5	28.9	43.4	26.5	39.9	23.2	34.9	21.4	32.2	19.3	29.1	16.9	25.5	14.0	21.0
	4	27.9	41.9	25.5	38.4	22.3	33.6	20.6	30.9	18.6	27.9	16.2	24.4	13.4	20.2
	4.5	26.8	40.3	24.5	36.8	21.4	32.2	19.7	29.6	17.7	26.7	15.5	23.3	12.8	19.3
	5	25.7	38.6	23.4	35.2	20.4	30.7	18.8	28.2	16.9	25.4	14.7	22.1	12.2	18.3
	5.5	24.6	36.9	22.3	33.6	19.4	29.2	17.8	26.8	16.0	24.1	14.0	21.0	11.6	17.4
	6	23.4	35.2	21.2	31.9	18.4	27.7	16.9	25.4	15.1	22.8	13.2	19.8	10.9	16.4
	7	21.1	31.7	19.0	28.6	16.4	24.7	15.0	22.5	13.4	20.2	11.7	17.5	9.7	14.6
	8	18.8	28.3	16.9	25.4	14.5	21.8	13.2	19.9	11.8	17.8	10.2	15.4	8.5	12.8
	9	16.6	25.0	14.9	22.3	12.7	19.1	11.5	17.4	10.3	15.5	8.9	13.4	7.4	11.2
	10	14.7	22.1	13.1	19.7	11.2	16.8	10.1	15.2	9.0	13.5	7.8	11.7	6.5	9.7
	11	13.1	19.7	11.6	17.4	9.8	14.8	8.9	13.4	7.9	11.9	6.8	10.2	5.7	8.5
	12	11.7	17.6	10.3	15.5	8.7	13.1	7.9	11.9	7.0	10.5	6.0	9.0	5.0	7.5
	13											5.4	8.1	4.4	6.7
Design		F_y = 50 ksi													
		3/4		5/8		1/2		7/16		3/8		5/16[c]		1/4[c, f]	
Effective Length, *KL* (ft)	2	42.8	64.3	39.5	59.3	34.7	52.2	32.1	48.2	29.0	43.6	24.9	37.4	20.3	30.5
	2.5	41.5	62.4	38.2	57.4	33.5	50.4	31.0	46.5	28.0	42.0	24.0	36.1	19.6	29.4
	3	40.0	60.1	36.7	55.2	32.2	48.4	29.7	44.6	26.8	40.3	23.0	34.6	18.8	28.3
	3.5	38.4	57.7	35.1	52.8	30.7	46.2	28.3	42.5	25.5	38.3	21.9	32.9	17.9	27.0
	4	36.6	55.0	33.4	50.2	29.2	43.8	26.8	40.3	24.1	36.3	20.7	31.2	17.0	25.6
	4.5	34.7	52.2	31.6	47.6	27.5	41.4	25.3	38.0	22.7	34.2	19.5	29.4	16.1	24.1
	5	32.9	49.4	29.8	44.8	25.9	38.9	23.7	35.6	21.3	32.0	18.3	27.5	15.1	22.7
	5.5	30.9	46.5	28.0	42.1	24.2	36.4	22.2	33.3	19.9	29.9	17.1	25.7	14.1	21.2
	6	29.0	43.6	26.2	39.4	22.6	34.0	20.6	31.0	18.5	27.8	15.9	24.0	13.2	19.8
	7	25.4	38.1	22.7	34.2	19.5	29.3	17.8	26.7	15.9	23.9	13.7	20.6	11.4	17.1
	8	21.9	32.9	19.5	29.3	16.7	25.1	15.1	22.7	13.5	20.3	11.7	17.5	9.7	14.6
	9	19.0	28.6	16.9	25.3	14.4	21.6	13.0	19.5	11.5	17.4	10.0	15.0	8.3	12.4
	10	16.6	25.0	14.7	22.1	12.5	18.7	11.2	16.9	10.0	15.0	8.6	12.9	7.1	10.7
	11	14.6	22.0	12.9	19.4	10.9	16.4	9.8	14.8	8.7	13.1	7.5	11.2	6.2	9.3
	12	13.0	19.5	11.4	17.1	9.6	14.4	8.6	13.0	7.6	11.5	6.6	9.9	5.4	8.1
	13											5.8	8.7	4.8	7.2
Properties															
A_g (in.^{2})		5.43		4.61		3.75		3.30		2.86		2.40		1.93	
γ_z (in.)		0.774		0.774		0.776		0.777		0.779		0.781		0.783	
ASD	LRFD	[c] Shape is slender for compression. [f] Shape exceeds compact limit for flexure.													
Ω_c = 1.67	ϕ_c = 0.9	Notes: Heavy lines indicate L/r_z equal to or greater than 120, 140 and 200, respectively. *Method 4 (flexural rigidity $EI^* = 0.8\tau_b EI$).													

Design Table 3. Available Strength in Axial Compression, kips* Eccentrically Loaded Single Angles

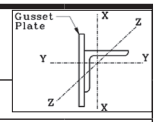

Shape		L3½×3½×									
		½		7/16		3/8		5/16		1/4[c]	
lb/ft		11.1		9.80		8.50		7.20		5.80	
Design		P_n/Ω_c ASD	$\phi_c P_n$ LRFD	P_n/Ω_c ASD	$\phi_c P_n$ LRFD	P_n/Ω_c ASD	$\phi_c P_n$ LRFD	P_n/Ω_c ASD	$\phi_c P_n$ LRFD	P_n/Ω_c ASD	$\phi_c P_n$ LRFD
		F_y = 36 ksi									
Effective Length, *KL* (ft)	2	21.0	31.6	19.4	29.1	17.9	26.9	15.8	23.7	13.3	20.1
	2.5	20.4	30.6	18.8	28.2	17.3	26.1	15.3	22.9	12.9	19.4
	3	19.6	29.5	18.1	27.2	16.7	25.0	14.6	22.0	12.4	18.6
	3.5	18.8	28.3	17.3	26.0	15.9	23.9	14.0	21.0	11.8	17.7
	4	17.9	26.9	16.5	24.7	15.1	22.7	13.3	19.9	11.2	16.8
	4.5	17.0	25.5	15.6	23.4	14.3	21.5	12.5	18.8	10.6	15.9
	5	16.0	24.1	14.7	22.1	13.4	20.2	11.8	17.7	9.9	14.9
	5.5	15.1	22.7	13.8	20.7	12.6	18.9	11.0	16.5	9.3	13.9
	6	14.1	21.2	12.9	19.4	11.8	17.7	10.3	15.4	8.7	13.0
	6.5	13.2	19.8	12.1	18.1	11.0	16.5	9.6	14.4	8.0	12.1
	7	12.3	18.5	11.2	16.9	10.2	15.3	8.9	13.3	7.5	11.2
	7.5	11.4	17.2	10.4	15.7	9.5	14.2	8.2	12.3	6.9	10.4
	8	10.6	15.9	9.7	14.5	8.7	13.1	7.6	11.4	6.4	9.6
	9	9.2	13.8	8.3	12.5	7.5	11.3	6.5	9.8	5.4	8.2
	10	8.0	12.0	7.2	10.9	6.5	9.8	5.6	8.4	4.7	7.1
	11	7.0	10.5	6.3	9.5	5.7	8.5	4.9	7.4	4.1	6.1
Design		F_y = 50 ksi									
		½		7/16		3/8		5/16		1/4[c]	
Effective Length, *KL* (ft)	2	28.6	43.0	26.3	39.6	24.3	36.6	21.3	32.1	17.6	26.5
	2.5	27.4	41.2	25.2	37.9	23.2	34.9	20.4	30.6	16.9	25.3
	3	26.0	39.1	23.9	36.0	22.0	33.1	19.3	29.0	16.0	24.0
	3.5	24.6	36.9	22.6	33.9	20.7	31.1	18.1	27.2	15.0	22.6
	4	23.0	34.6	21.1	31.7	19.3	29.1	16.9	25.4	14.0	21.1
	4.5	21.5	32.2	19.7	29.5	18.0	27.0	15.7	23.5	13.0	19.6
	5	19.9	29.9	18.2	27.4	16.6	24.9	14.5	21.7	12.1	18.1
	5.5	18.4	27.6	16.8	25.3	15.3	23.0	13.3	20.0	11.1	16.7
	6	16.9	25.4	15.5	23.2	14.0	21.1	12.2	18.3	10.2	15.3
	6.5	15.5	23.3	14.1	21.3	12.8	19.2	11.1	16.7	9.3	14.0
	7	14.2	21.3	12.9	19.4	11.7	17.5	10.1	15.2	8.5	12.8
	7.5	13.0	19.6	11.8	17.8	10.7	16.0	9.2	13.9	7.8	11.7
	8	12.0	18.0	10.9	16.4	9.8	14.7	8.5	12.7	7.1	10.7
	9	10.2	15.4	9.3	14.0	8.3	12.5	7.2	10.8	6.0	9.0
	10	8.8	13.2	8.0	12.0	7.1	10.7	6.1	9.2	5.1	7.7
	11	7.7	11.5	6.9	10.4	6.2	9.3	5.3	8.0	4.4	6.7
Properties											
A_g (in.^{2})		3.25		2.89		2.50		2.10		1.70	
γ_z (in.)		0.679		0.681		0.683		0.685		0.688	
ASD	LRFD	[c] Shape is slender for compression.									
Ω_c = 1.67	ϕ_c = 0.9	[f] Shape exceeds compact limit for flexure.									
		Notes: Heavy lines indicate L/r_z equal to or greater than 120, 140 and 200, respectively.									
		*Method 4 (flexural rigidity $EI^* = 0.8\tau_b EI$).									

Design Table 3. Available Strength in Axial Compression, kips* Eccentrically Loaded Single Angles

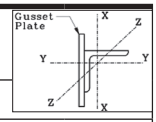

Shape		L3×3×											
		1/2		7/16		3/8		5/16		1/4		3/16[c, f]	
lb/ft		9.40		8.30		7.20		6.10		4.90		3.71	
Design		P_n/Ω_c ASD	$\phi_c P_n$ LRFD	P_n/Ω_c ASD	$\phi_c P_n$ LRFD	P_n/Ω_c ASD	$\phi_c P_n$ LRFD	P_n/Ω_c ASD	$\phi_c P_n$ LRFD	P_n/Ω_c ASD	$\phi_c P_n$ LRFD	P_n/Ω_c ASD	$\phi_c P_n$ LRFD
		F_y = 36 ksi											
Effective Length, *KL* (ft)	2	16.2	24.3	15.0	22.6	13.9	20.9	12.4	18.6	10.6	16.0	8.3	12.5
	2.5	15.5	23.3	14.4	21.7	13.3	20.0	11.9	17.8	10.1	15.3	7.9	11.9
	3	14.8	22.2	13.7	20.6	12.6	19.0	11.2	16.9	9.6	14.4	7.5	11.3
	3.5	14.0	21.1	13.0	19.5	11.9	17.9	10.6	15.9	9.0	13.6	7.1	10.6
	4	13.2	19.8	12.2	18.3	11.1	16.7	9.9	14.9	8.4	12.7	6.6	9.9
	4.5	12.3	18.6	11.4	17.1	10.4	15.6	9.2	13.8	7.8	11.7	6.1	9.2
	5	11.5	17.3	10.6	15.9	9.6	14.5	8.5	12.8	7.2	10.8	5.7	8.5
	5.5	10.7	16.0	9.8	14.7	8.9	13.4	7.8	11.8	6.6	10.0	5.2	7.8
	6	9.9	14.8	9.0	13.6	8.2	12.3	7.2	10.8	6.1	9.1	4.8	7.2
	6.5	9.1	13.6	8.3	12.4	7.5	11.3	6.6	9.9	5.5	8.3	4.4	6.6
	7	8.3	12.5	7.6	11.4	6.8	10.3	6.0	9.0	5.0	7.6	4.0	6.0
	7.5	7.7	11.5	7.0	10.5	6.3	9.4	5.5	8.3	4.6	6.9	3.6	5.4
	8	7.1	10.6	6.4	9.6	5.8	8.7	5.0	7.6	4.2	6.4	3.3	5.0
	8.5	6.5	9.8	5.9	8.9	5.3	8.0	4.6	7.0	3.9	5.8	3.0	4.6
	9	6.1	9.1	5.5	8.3	4.9	7.4	4.3	6.4	3.6	5.4	2.8	4.2
	9.5	5.6	8.5	5.1	7.7	4.6	6.9	4.0	6.0	3.3	5.0	2.6	3.9
Design		F_y = 50 ksi											
		1/2		7/16		3/8		5/16		1/4		3/16[c]	
Effective Length, *KL* (ft)	2	21.8	32.8	20.3	30.5	18.7	28.1	16.7	25.1	14.1	21.2	10.8	16.3
	2.5	20.7	31.1	19.2	28.8	17.6	26.5	15.7	23.6	13.3	20.0	10.2	15.3
	3	19.4	29.1	17.9	27.0	16.5	24.7	14.6	22.0	12.4	18.6	9.5	14.3
	3.5	18.0	27.1	16.6	25.0	15.2	22.9	13.5	20.3	11.4	17.1	8.8	13.2
	4	16.6	25.0	15.3	23.0	14.0	21.0	12.4	18.6	10.4	15.7	8.1	12.1
	4.5	15.3	23.0	14.0	21.1	12.7	19.2	11.3	16.9	9.5	14.2	7.4	11.1
	5	13.9	20.9	12.8	19.2	11.6	17.4	10.2	15.3	8.6	12.9	6.7	10.1
	5.5	12.6	19.0	11.5	17.4	10.4	15.7	9.2	13.8	7.7	11.6	6.0	9.1
	6	11.4	17.2	10.4	15.6	9.4	14.1	8.2	12.4	6.9	10.4	5.4	8.2
	6.5	10.4	15.6	9.4	14.2	8.5	12.8	7.4	11.2	6.2	9.4	4.9	7.3
	7	9.4	14.2	8.6	12.9	7.7	11.6	6.7	10.1	5.6	8.5	4.4	6.6
	7.5	8.6	13.0	7.8	11.7	7.0	10.5	6.1	9.2	5.1	7.7	4.0	6.0
	8	7.9	11.9	7.2	10.8	6.4	9.6	5.6	8.4	4.7	7.0	3.6	5.5
	8.5	7.3	10.9	6.6	9.9	5.9	8.8	5.1	7.7	4.3	6.4	3.3	5.0
	9	6.7	10.1	6.0	9.1	5.4	8.1	4.7	7.0	3.9	5.9	3.0	4.6
	9.5	6.2	9.3	5.6	8.4	5.0	7.5	4.3	6.5	3.6	5.4	2.8	4.2
Properties													
A_g (in.^{2})		2.76		2.43		2.11		1.78		1.44		1.09	
γ_z (in.)		0.580		0.580		0.581		0.583		0.585		0.586	
ASD	LRFD	[c] Shape is slender for compression.											
		[f] Shape exceeds compact limit for flexure.											
Ω_c = 1.67	ϕ_c = 0.9	Notes: Heavy lines indicate L/r_z equal to or greater than 120, 140 and 200, respectively.											
		*Method 4 (flexural rigidity $EI^* = 0.8\tau_b EI$).											

Design Table 4. Available Strength in Axial Compression, kips* Eccentrically Loaded Single Angles

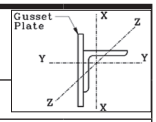

Shape		L8×8×													
		1 1/8		1		7/8		3/4		5/8 [c]		9/16 [c]		1/2 [c, f]	
lb/ft		56.9		51.0		45.0		38.9		32.7		29.6		26.4	
Design		P_n/Ω_c ASD	$\phi_c P_n$ LRFD	P_n/Ω_c ASD	$\phi_c P_n$ LRFD	P_n/Ω_c ASD	$\phi_c P_n$ LRFD	P_n/Ω_c ASD	$\phi_c P_n$ LRFD	P_n/Ω_c ASD	$\phi_c P_n$ LRFD	P_n/Ω_c ASD	$\phi_c P_n$ LRFD	P_n/Ω_c ASD	$\phi_c P_n$ LRFD
		F_y = 36 ksi													
Effective Length, *KL* (ft)	6	145	218	131	197	117	176	102	154	87.2	131	77.9	117	68.7	103
	7	139	209	125	189	112	169	98.1	147	83.7	126	74.8	112	66.1	99.4
	8	133	200	120	180	107	161	93.6	141	79.9	120	71.5	107	63.3	95.1
	9	126	190	114	171	102	153	88.9	134	75.9	114	68.0	102	60.3	90.7
	10	119	179	108	162	96.1	145	84.1	126	71.8	108	64.3	96.7	57.2	86.0
	11	112	169	101	152	90.5	136	79.1	119	67.6	102	60.7	91.2	54.1	81.3
	12	106	159	95.1	143	85.0	128	74.3	112	63.4	95.4	57.0	85.7	50.9	76.6
	13	98.8	149	89.0	134	79.6	120	69.5	105	59.4	89.3	53.5	80.4	47.9	71.9
	14	92.3	139	83.2	125	74.4	112	64.9	97.6	55.5	83.4	50.0	75.2	44.8	67.4
	15	86.1	129	77.5	117	69.4	104	60.5	91.0	51.8	77.8	46.7	70.2	41.9	63.0
	16	80.1	120	72.1	108	64.6	97.1	56.3	84.6	48.2	72.4	43.5	65.4	39.2	58.9
	18	68.9	104	62.1	93.3	55.6	83.6	48.4	72.8	41.5	62.3	37.6	56.5	34.0	51.1
	20	59.5	89.4	53.6	80.5	48.0	72.1	41.8	62.8	35.7	53.7	32.4	48.7	29.3	44.1
	22	51.8	77.9	46.6	70.1	41.7	62.7	36.3	54.6	31.1	46.7	28.2	42.3	25.5	38.3
	24	45.5	68.4	41.0	61.6	36.6	55.1	31.9	47.9	27.3	41.0	24.7	37.1	22.4	33.6
	26	40.2	60.5	36.2	54.4	32.4	48.7	28.2	42.3	24.1	36.2	21.8	32.8	19.8	29.7
Design		F_y = 50 ksi													
		1 1/8		1		7/8		3/4		5/8 [c]		9/16 [c, f]		1/2 [c, f]	
Effective Length, *KL* (ft)	6	193	290	174	261	155	233	136	204	113	170	101	151	88.4	133
	7	182	274	164	247	147	221	128	193	107	161	95.6	144	84.2	127
	8	171	257	154	232	138	207	121	181	101	152	90.2	136	79.6	120
	9	160	240	144	216	129	194	113	169	94.5	142	84.6	127	74.9	113
	10	149	223	134	201	120	180	105	157	88.1	132	78.9	119	70.1	105
	11	138	207	124	186	111	167	96.8	146	81.8	123	73.4	110	65.4	98.3
	12	127	191	114	172	102	154	89.3	134	75.6	114	68.0	102	60.8	91.3
	13	117	176	105	158	94.2	142	82.2	123	69.8	105	62.8	94.5	56.3	84.6
	14	107	161	96.6	145	86.5	130	75.4	113	64.2	96.5	57.9	87.1	52.1	78.2
	15	98.2	148	88.4	133	79.2	119	69.0	104	59.0	88.6	53.3	80.1	48.0	72.2
	16	89.8	135	80.9	122	72.4	109	63.1	94.8	54.0	81.2	48.9	73.5	44.2	66.5
	18	75.9	114	68.4	103	61.2	92.0	53.3	80.1	45.6	68.5	41.3	62.1	37.4	56.2
	20	65.0	97.6	58.5	87.9	52.3	78.6	45.5	68.4	38.9	58.5	35.3	53.0	31.9	48.0
	22	56.1	84.4	50.5	75.9	45.2	67.9	39.3	59.1	33.6	50.5	30.4	45.8	27.6	41.4
	24	49.0	73.6	44.1	66.3	39.4	59.3	34.3	51.5	29.3	44.0	26.5	39.9	24.0	36.1
	26	43.1	64.8	38.8	58.3	34.7	52.1	30.1	45.3	25.8	38.7	23.3	35.1	21.1	31.7
Properties															
A_g (in.^{2})		16.8		15.1		13.3		11.5		9.69		8.77		7.84	
γ_z (in.)		1.56		1.56		1.57		1.57		1.58		1.58		1.59	
ASD	LRFD	[c] Shape is slender for compression. [f] Shape exceeds compact limit for flexure.													
Ω_c = 1.67	ϕ_c = 0.9	Notes: Heavy lines indicate L/r_z equal to or greater than 120, 140 and 200, respectively. *Method 4, except the axial load is applied at mid-thickness of connected leg.													

Design Table 4. Available Strength in Axial Compression, kips* Eccentrically Loaded Single Angles

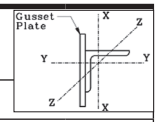

Shape		L6×6×													
		1		7/8		3/4		5/8		9/16		1/2		7/16[c]	
lb/ft		37.4		33.1		28.7		24.2		21.9		19.6		17.3	
Design		P_n/Ω_c ASD	$\phi_c P_n$ LRFD	P_n/Ω_c ASD	$\phi_c P_n$ LRFD	P_n/Ω_c ASD	$\phi_c P_n$ LRFD	P_n/Ω_c ASD	$\phi_c P_n$ LRFD	P_n/Ω_c ASD	$\phi_c P_n$ LRFD	P_n/Ω_c ASD	$\phi_c P_n$ LRFD	P_n/Ω_c ASD	$\phi_c P_n$ LRFD
		F_y = 36 ksi													
Effective Length, KL (ft)	4	95.9	144	86.2	130	75.2	113	64.1	96.4	58.3	87.6	52.9	79.6	46.1	69.2
	5	91.1	137	81.9	123	71.4	107	60.9	91.5	55.4	83.3	50.3	75.6	43.8	65.8
	6	85.8	129	77.0	116	67.1	101	57.2	86.0	52.1	78.3	47.3	71.0	41.2	61.9
	7	80.0	120	71.8	108	62.6	94.1	53.3	80.1	48.6	73.0	44.0	66.2	38.4	57.8
	8	74.1	111	66.5	99.9	57.9	87.1	49.3	74.1	45.0	67.6	40.8	61.3	35.6	53.5
	9	68.3	103	61.2	92.0	53.3	80.1	45.4	68.2	41.4	62.3	37.5	56.4	32.8	49.3
	10	62.6	94.0	56.0	84.2	48.8	73.4	41.5	62.4	37.9	57.0	34.3	51.6	30.1	45.2
	11	57.1	85.8	51.1	76.8	44.5	66.9	37.8	56.9	34.6	52.0	31.3	47.0	27.4	41.3
	12	51.9	78.1	46.5	69.8	40.5	60.8	34.4	51.7	31.5	47.3	28.4	42.7	25.0	37.5
	13	47.1	70.8	42.1	63.3	36.6	55.1	31.1	46.8	28.5	42.9	25.8	38.7	22.6	34.0
	14	42.6	64.0	38.1	57.2	33.1	49.8	28.1	42.2	25.8	38.8	23.3	35.0	20.5	30.8
	15	38.7	58.1	34.5	51.9	30.0	45.2	25.5	38.3	23.4	35.2	21.1	31.7	18.6	27.9
	16	35.2	53.0	31.5	47.3	27.4	41.1	23.2	34.9	21.3	32.0	19.2	28.8	16.9	25.4
	17	32.2	48.5	28.8	43.2	25.0	37.6	21.2	31.9	19.5	29.3	17.5	26.4	15.4	23.2
	18	29.6	44.5	26.4	39.7	23.0	34.5	19.5	29.3	17.9	26.9	16.1	24.2	14.2	21.3
	19	27.3	41.0	24.3	36.5	21.1	31.8	17.9	26.9	16.4	24.7	14.8	22.3	13.0	19.6
Design		F_y = 50 ksi													
		1		7/8		3/4		5/8		9/16		1/2[c]		7/16[c, f]	
Effective Length, KL (ft)	4	129	193	116	174	101	151	85.9	129	78.1	117	69.9	105	60.1	90.3
	5	120	180	108	162	93.9	141	80.1	120	72.9	110	65.3	98.1	56.3	84.6
	6	111	166	99.2	149	86.5	130	73.7	111	67.1	101	60.2	90.4	52.0	78.2
	7	101	152	90.5	136	78.8	119	67.1	101	61.3	92.1	55.0	82.6	47.7	71.6
	8	91.4	137	81.9	123	71.3	107	60.7	91.2	55.5	83.3	49.8	74.9	43.3	65.1
	9	82.2	124	73.6	111	64.1	96.4	54.5	82.0	49.9	75.0	44.9	67.4	39.1	58.8
	10	73.6	111	65.9	99.0	57.4	86.2	48.8	73.3	44.6	67.1	40.2	60.4	35.2	52.8
	11	65.6	98.6	58.7	88.2	51.1	76.7	43.4	65.2	39.8	59.8	35.8	53.9	31.4	47.3
	12	58.3	87.6	52.1	78.3	45.3	68.1	38.5	57.8	35.3	53.0	31.8	47.9	28.0	42.1
	13	52.1	78.3	46.5	69.9	40.5	60.8	34.3	51.6	31.5	47.3	28.4	42.7	25.0	37.6
	14	46.8	70.3	41.7	62.7	36.3	54.6	30.8	46.3	28.3	42.5	25.5	38.3	22.4	33.7
	15	42.2	63.5	37.7	56.6	32.8	49.2	27.8	41.7	25.5	38.3	23.0	34.5	20.2	30.4
	16	38.3	57.5	34.1	51.3	29.7	44.6	25.2	37.8	23.1	34.7	20.8	31.3	18.3	27.5
	17	34.9	52.4	31.1	46.7	27.0	40.6	22.9	34.4	21.0	31.6	18.9	28.4	16.7	25.0
	18	31.9	47.9	28.4	42.7	24.7	37.1	20.9	31.4	19.2	28.9	17.3	26.0	15.2	22.9
	19	29.2	44.0	26.1	39.2	22.7	34.1	19.2	28.8	17.6	26.5	15.8	23.8	13.9	21.0
Properties															
A_g (in.^{2})		11.0		9.75		8.46		7.13		6.45		5.77		5.08	
γ_z (in.)		1.17		1.17		1.17		1.17		1.18		1.18		1.18	
ASD	LRFD	[c] Shape is slender for compression. [f] Shape exceeds compact limit for flexure.													
Ω_c = 1.67	ϕ_c = 0.9	Notes: Heavy lines indicate L/r_z equal to or greater than 120, 140 and 200, respectively. *Method 4, except the axial load is applied at mid-thickness of connected leg.													

Design Table 4. Available Strength in Axial Compression, kips* Eccentrically Loaded Single Angles

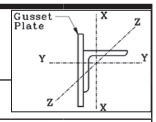

Shape		L5×5×													
		7/8		3/4		5/8		1/2		7/16		3/8[c]		5/16[c, f]	
lb/ft		27.2		23.6		20.0		16.2		14.3		12.3		10.4	
		P_n/Ω_c	$\phi_c P_n$	P_n/Ω_c	$\phi_c P_n$	P_n/Ω_c	$\phi_c P_n$	P_n/Ω_c	$\phi_c P_n$	P_n/Ω_c	$\phi_c P_n$	P_n/Ω_c	$\phi_c P_n$	P_n/Ω_c	$\phi_c P_n$
Design		ASD	LRFD	ASD	LRFD	ASD	LRFD	ASD	LRFD	ASD	LRFD	ASD	LRFD	ASD	LRFD
		F_y = 36 ksi													
Effective Length, *KL* (ft)	1	76.6	115	66.8	100	57.5	86.5	47.8	71.8	41.9	63.0	36.7	55.1	29.9	44.9
	2	74.6	112	65.0	97.7	56.0	84.2	46.5	69.9	40.8	61.3	35.7	53.6	29.2	43.8
	3	71.5	107	62.2	93.5	53.6	80.6	44.5	66.9	39.1	58.8	34.2	51.4	28.0	42.1
	4	67.4	101	58.7	88.2	50.6	76.0	42.0	63.1	36.9	55.4	32.3	48.5	26.5	39.9
	5	62.7	94.2	54.6	82.1	47.0	70.7	39.0	58.6	34.3	51.6	30.0	45.1	24.8	37.2
	6	57.5	86.5	50.1	75.4	43.1	64.9	35.8	53.8	31.5	47.3	27.6	41.5	22.8	34.3
	7	52.3	78.6	45.6	68.6	39.2	59.0	32.5	48.9	28.6	43.1	25.1	37.7	20.9	31.4
	8	47.2	71.0	41.2	61.9	35.4	53.2	29.3	44.1	25.8	38.8	22.7	34.1	18.9	28.4
	9	42.3	63.6	36.9	55.5	31.7	47.7	26.3	39.5	23.2	34.8	20.3	30.5	17.0	25.6
	10	37.8	56.8	32.9	49.5	28.3	42.5	23.4	35.2	20.7	31.1	18.1	27.3	15.3	23.0
	11	33.5	50.3	29.2	43.9	25.1	37.7	20.8	31.2	18.4	27.6	16.1	24.2	13.6	20.5
	12	29.7	44.6	25.9	39.0	22.2	33.4	18.4	27.7	16.3	24.4	14.3	21.4	12.1	18.2
	13	26.5	39.8	23.1	34.8	19.8	29.8	16.4	24.7	14.5	21.8	12.7	19.1	10.8	16.2
	14	23.8	35.7	20.8	31.2	17.8	26.7	14.7	22.1	13.0	19.5	11.4	17.1	9.7	14.5
	15	21.4	32.2	18.7	28.1	16.0	24.1	13.3	19.9	11.7	17.6	10.3	15.4	8.7	13.1
	16	19.4	29.2	17.0	25.5	14.5	21.8	12.0	18.0	10.6	15.9	9.3	14.0	7.9	11.8
Design		F_y = 50 ksi													
		7/8		3/4		5/8		1/2		7/16[c]		3/8[c, f]		5/16[c, f]	
Effective Length, *KL* (ft)	1	106	159	92.3	139	79.6	120	66.1	99.3	57.5	86.4	49.1	73.8	39.6	59.5
	2	102	154	89.0	134	76.7	115	63.7	95.7	55.4	83.3	47.5	71.3	38.4	57.7
	3	96.4	145	83.9	126	72.3	109	60.0	90.2	52.3	78.6	44.9	67.4	36.4	54.8
	4	89.0	134	77.5	117	66.8	100	55.4	83.3	48.4	72.7	41.6	62.6	34.0	51.0
	5	80.7	121	70.3	106	60.5	90.9	50.2	75.5	43.9	66.0	37.9	57.0	31.1	46.8
	6	72.2	108	62.9	94.6	54.1	81.3	44.9	67.5	39.3	59.1	34.1	51.2	28.1	42.3
	7	63.9	96.0	55.7	83.7	47.9	71.9	39.7	59.6	34.8	52.4	30.3	45.5	25.2	37.8
	8	56.0	84.2	48.8	73.4	42.0	63.1	34.8	52.3	30.6	46.0	26.7	40.1	22.3	33.5
	9	48.8	73.3	42.6	64.0	36.6	54.9	30.3	45.5	26.7	40.1	23.4	35.1	19.7	29.5
	10	42.3	63.6	36.9	55.5	31.7	47.6	26.2	39.4	23.2	34.8	20.3	30.6	17.2	25.9
	11	37.0	55.6	32.3	48.5	27.7	41.6	22.9	34.4	20.2	30.4	17.7	26.6	15.0	22.6
	12	32.5	48.9	28.4	42.7	24.3	36.6	20.1	30.2	17.8	26.7	15.6	23.4	13.2	19.9
	13	28.8	43.4	25.2	37.9	21.6	32.4	17.8	26.8	15.7	23.7	13.8	20.7	11.7	17.6
	14	25.7	38.7	22.5	33.8	19.2	28.9	15.9	23.9	14.0	21.1	12.3	18.5	10.4	15.7
	15	23.1	34.7	20.2	30.3	17.3	25.9	14.2	21.4	12.6	18.9	11.0	16.6	9.4	14.1
	16	20.8	31.3	18.2	27.3	15.6	23.4	12.8	19.3	11.4	17.1	9.9	14.9	8.4	12.7
Properties															
A_g (in.^{2})		8.00		6.98		5.90		4.79		4.22		3.65		3.07	
γ_z (in.)		0.971		0.972		0.975		0.980		0.983		0.986		0.990	
ASD	LRFD	[c] Shape is slender for compression. [f] Shape exceeds compact limit for flexure.													
Ω_c = 1.67	ϕ_c = 0.9	Notes: Heavy lines indicate KL/r_z equal to or greater than 120, 140 and 200, respectively. *Method 4, except that the axial load is applied at mid-thickness of connected leg.													

Design Table 4. Available Strength in Axial Compression, kips* Eccentrically Loaded Single Angles

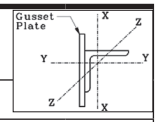

Shape		L4×4×													
		3/4		5/8		1/2		7/16		3/8		5/16[c]		1/4[c, f]	
lb/ft		18.5		15.7		12.8		11.3		9.8		8.2		6.6	
Design		P_n/Ω_c ASD	$\phi_c P_n$ LRFD	P_n/Ω_c ASD	$\phi_c P_n$ LRFD	P_n/Ω_c ASD	$\phi_c P_n$ LRFD	P_n/Ω_c ASD	$\phi_c P_n$ LRFD	P_n/Ω_c ASD	$\phi_c P_n$ LRFD	P_n/Ω_c ASD	$\phi_c P_n$ LRFD	P_n/Ω_c ASD	$\phi_c P_n$ LRFD
		F_y = 36 ksi													
Effective Length, *KL* (ft)	2	48.9	73.6	42.1	63.3	34.5	51.8	30.8	46.3	26.8	40.3	22.6	34.0	17.9	26.8
	2.5	47.5	71.4	40.8	61.4	33.5	50.3	29.8	44.8	26.0	39.1	22.0	33.0	17.3	26.1
	3	45.8	68.8	39.4	59.2	32.3	48.5	28.8	43.2	25.1	37.7	21.2	31.8	16.8	25.2
	3.5	43.9	66.0	37.8	56.8	30.9	46.5	27.6	41.4	24.0	36.1	20.3	30.5	16.1	24.2
	4	41.9	63.0	36.0	54.1	29.5	44.3	26.3	39.5	22.9	34.4	19.4	29.1	15.4	23.1
	4.5	39.8	59.8	34.2	51.4	28.0	42.1	25.0	37.5	21.8	32.7	18.4	27.6	14.7	22.0
	5	37.7	56.6	32.3	48.6	26.5	39.8	23.6	35.5	20.6	30.9	17.4	26.1	13.9	20.9
	5.5	35.5	53.3	30.4	45.7	24.9	37.5	22.2	33.4	19.3	29.1	16.4	24.6	13.1	19.7
	6	33.3	50.1	28.6	42.9	23.4	35.2	20.8	31.3	18.2	27.3	15.4	23.1	12.3	18.5
	7	29.1	43.8	25.0	37.5	20.5	30.7	18.2	27.4	15.9	23.9	13.4	20.2	10.8	16.3
	8	25.3	38.0	21.6	32.5	17.7	26.7	15.8	23.7	13.8	20.7	11.6	17.5	9.4	14.2
	9	21.8	32.7	18.6	28.0	15.3	22.9	13.6	20.4	11.8	17.8	10.0	15.0	8.2	12.3
	10	18.8	28.3	16.1	24.1	13.2	19.8	11.7	17.6	10.2	15.3	8.6	13.0	7.0	10.6
	11	16.4	24.6	14.0	21.0	11.5	17.2	10.2	15.3	8.9	13.3	7.5	11.3	6.1	9.2
	12	14.4	21.6	12.3	18.5	10.1	15.1	8.9	13.4	7.8	11.7	6.6	9.9	5.4	8.1
	13											5.8	8.7	4.7	7.1
Design		F_y = 50 ksi													
		3/4		5/8		1/2		7/16		3/8		5/16[c]		1/4[c, f]	
Effective Length, *KL* (ft)	2	66.5	100	57.3	86.1	46.9	70.5	41.8	62.9	36.4	54.8	30.0	45.1	23.4	35.1
	2.5	63.9	96.0	54.9	82.6	45.0	67.6	40.1	60.3	35.0	52.5	28.8	43.3	22.5	33.8
	3	60.8	91.4	52.3	78.6	42.8	64.4	38.2	57.4	33.3	50.0	27.5	41.3	21.5	32.4
	3.5	57.5	86.4	49.4	74.3	40.5	60.8	36.1	54.2	31.4	47.2	26.0	39.1	20.5	30.8
	4	54.0	81.2	46.4	69.7	38.0	57.1	33.9	50.9	29.5	44.4	24.5	36.8	19.3	29.1
	4.5	50.4	75.8	43.3	65.1	35.5	53.3	31.6	47.5	27.5	41.4	22.9	34.4	18.2	27.3
	5	46.9	70.5	40.2	60.5	33.0	49.5	29.3	44.1	25.6	38.4	21.3	32.1	17.0	25.5
	5.5	43.4	65.3	37.2	56.0	30.5	45.8	27.1	40.8	23.7	35.6	19.8	29.7	15.8	23.8
	6	40.1	60.3	34.3	51.6	28.1	42.3	25.0	37.6	21.8	32.8	18.3	27.5	14.7	22.1
	7	33.9	50.9	29.0	43.6	23.7	35.7	21.1	31.7	18.4	27.7	15.5	23.3	12.5	18.8
	8	28.4	42.6	24.3	36.5	19.9	29.9	17.7	26.5	15.4	23.1	13.0	19.6	10.6	16.0
	9	24.0	36.1	20.5	30.8	16.8	25.2	14.9	22.4	13.0	19.5	11.0	16.5	9.0	13.5
	10	20.6	30.9	17.5	26.4	14.4	21.6	12.7	19.2	11.1	16.7	9.4	14.1	7.7	11.5
	11	17.8	26.7	15.2	22.8	12.4	18.7	11.0	16.5	9.6	14.4	8.1	12.2	6.6	9.9
	12	15.5	23.3	13.2	19.9	10.8	16.3	9.6	14.4	8.4	12.6	7.1	10.6	5.8	8.7
	13											6.2	9.3	5.1	7.6
Properties															
A_g (in.^{2})		5.44		4.61		3.75		3.30		2.86		2.40		1.93	
γ_z (in.)		0.774		0.774		0.776		0.777		0.779		0.781		0.783	
ASD	LRFD	[c] Shape is slender for compression. [f] Shape exceeds compact limit for flexure.													
Ω_c = 1.67	ϕ_c = 0.9	Notes: Heavy lines indicate KL/r_z equal to or greater than 120, 140 and 200, respectively. *Method 4, except that the axial load is applied at mid-thickness of connected leg.													

Design Table 4. Available Strength in Axial Compression, kips* Eccentrically Loaded Single Angles

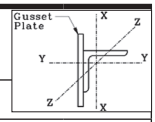

Shape		L3½×3½×									
		1/2		7/16		3/8		5/16		1/4[c]	
lb/ft		11.1		9.80		8.50		7.20		5.80	
Design		P_n/Ω_c ASD	$\phi_c P_n$ LRFD	P_n/Ω_c ASD	$\phi_c P_n$ LRFD	P_n/Ω_c ASD	$\phi_c P_n$ LRFD	P_n/Ω_c ASD	$\phi_c P_n$ LRFD	P_n/Ω_c ASD	$\phi_c P_n$ LRFD
		F_y = 36 ksi									
Effective Length, *KL* (ft)	2	29.6	44.5	26.2	39.4	23.2	34.9	19.6	29.5	15.9	23.8
	2.5	28.5	42.8	25.2	37.9	22.3	33.6	18.9	28.4	15.3	22.9
	3	27.2	40.8	24.1	36.2	21.3	32.0	18.0	27.1	14.6	21.9
	3.5	25.7	38.7	22.8	34.3	20.2	30.4	17.1	25.7	13.8	20.8
	4	24.2	36.4	21.5	32.3	19.0	28.6	16.1	24.2	13.1	19.6
	4.5	22.7	34.1	20.2	30.3	17.8	26.8	15.1	22.6	12.2	18.4
	5	21.2	31.8	18.8	28.2	16.6	25.0	14.0	21.1	11.4	17.2
	5.5	19.6	29.5	17.5	26.2	15.4	23.2	13.0	19.6	10.6	16.0
	6	18.2	27.3	16.2	24.3	14.3	21.4	12.1	18.1	9.8	14.8
	6.5	16.8	25.2	14.9	22.4	13.2	19.8	11.1	16.7	9.1	13.7
	7	15.4	23.2	13.7	20.7	12.1	18.2	10.3	15.4	8.4	12.6
	7.5	14.2	21.3	12.6	19.0	11.1	16.7	9.4	14.2	7.7	11.6
	8	13.0	19.5	11.6	17.4	10.2	15.3	8.6	13.0	7.1	10.6
	9	11.0	16.5	9.8	14.7	8.6	13.0	7.3	11.0	6.0	9.0
	10	9.4	14.2	8.4	12.6	7.4	11.1	6.2	9.4	5.1	7.7
	11	8.1	12.2	7.3	10.9	6.4	9.6	5.4	8.1	4.4	6.6
Design		F_y = 50 ksi									
		1/2		7/16		3/8		5/16		1/4[c]	
Effective Length, *KL* (ft)	2	40.0	60.1	35.5	53.3	31.4	47.2	26.4	39.7	20.8	31.3
	2.5	37.9	57.0	33.6	50.6	29.8	44.7	25.0	37.6	19.8	29.8
	3	35.6	53.5	31.6	47.5	28.0	42.0	23.5	35.4	18.7	28.1
	3.5	33.1	49.8	29.4	44.2	26.0	39.1	21.9	32.9	17.5	26.3
	4	30.6	46.0	27.2	40.9	24.0	36.1	20.2	30.4	16.2	24.4
	4.5	28.1	42.2	25.0	37.5	22.1	33.1	18.6	28.0	15.0	22.5
	5	25.7	38.6	22.8	34.3	20.2	30.3	17.0	25.6	13.7	20.6
	5.5	23.4	35.1	20.8	31.3	18.3	27.6	15.5	23.3	12.6	18.9
	6	21.2	31.9	18.9	28.4	16.6	25.0	14.1	21.1	11.4	17.2
	6.5	19.2	28.8	17.1	25.6	15.0	22.6	12.7	19.1	10.4	15.6
	7	17.3	26.0	15.4	23.2	13.6	20.4	11.5	17.2	9.4	14.2
	7.5	15.7	23.6	14.0	21.0	12.3	18.5	10.4	15.6	8.5	12.8
	8	14.3	21.5	12.7	19.1	11.2	16.8	9.5	14.2	7.8	11.7
	9	12.0	18.0	10.7	16.0	9.4	14.1	7.9	11.9	6.5	9.8
	10	10.2	15.3	9.1	13.6	8.0	12.0	6.7	10.1	5.5	8.3
	11	8.7	13.1	7.8	11.7	6.8	10.3	5.8	8.7	4.7	7.1
Properties											
A_g (in.^{2})		3.25		2.89		2.50		2.10		1.70	
γ_z (in.)		0.679		0.681		0.683		0.685		0.688	
ASD	LRFD	[c] Shape is slender for compression. [f] Shape exceeds compact limit for flexure.									
Ω_c = 1.67	ϕ_c = 0.9	Notes: Heavy lines indicate L/r_z equal to or greater than 120, 140 and 200, respectively. *Method 4, except that the axial load is applied at mid-thickness of connected leg.									

Design Table 4. Available Strength in Axial Compression, kips* Eccentrically Loaded Single Angles

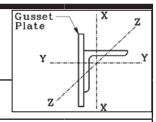

Shape		L3×3×											
		1/2		7/16		3/8		5/16		1/4		3/16[c, f]	
lb/ft		9.40		8.30		7.20		6.10		4.90		3.71	
Design		P_n/Ω_c ASD	$\phi_c P_n$ LRFD	P_n/Ω_c ASD	$\phi_c P_n$ LRFD	P_n/Ω_c ASD	$\phi_c P_n$ LRFD	P_n/Ω_c ASD	$\phi_c P_n$ LRFD	P_n/Ω_c ASD	$\phi_c P_n$ LRFD	P_n/Ω_c ASD	$\phi_c P_n$ LRFD
		F_y = 36 ksi											
Effective Length, *KL* (ft)	2	23.9	35.9	21.2	31.9	18.7	28.1	15.9	23.9	13.0	19.5	9.6	14.4
	2.5	22.7	34.1	20.2	30.3	17.7	26.6	15.1	22.7	12.3	18.5	9.1	13.7
	3	21.3	32.1	18.9	28.5	16.7	25.0	14.2	21.3	11.6	17.4	8.6	13.0
	3.5	19.9	29.9	17.7	26.5	15.5	23.3	13.2	19.9	10.8	16.2	8.1	12.1
	4	18.4	27.7	16.3	24.5	14.3	21.6	12.2	18.4	10.0	15.0	7.5	11.2
	4.5	16.9	25.5	15.0	22.6	13.2	19.8	11.2	16.9	9.2	13.8	6.9	10.4
	5	15.5	23.3	13.8	20.7	12.1	18.1	10.3	15.5	8.4	12.6	6.3	9.5
	5.5	14.1	21.3	12.5	18.8	11.0	16.5	9.4	14.1	7.7	11.5	5.8	8.7
	6	12.9	19.3	11.4	17.1	10.0	15.0	8.5	12.8	7.0	10.5	5.3	7.9
	6.5	11.6	17.5	10.3	15.5	9.0	13.6	7.7	11.6	6.3	9.5	4.8	7.2
	7	10.5	15.8	9.3	14.0	8.2	12.3	7.0	10.5	5.7	8.5	4.4	6.5
	7.5	9.6	14.4	8.5	12.7	7.4	11.1	6.3	9.5	5.2	7.8	3.9	5.9
	8	8.7	13.1	7.7	11.6	6.7	10.1	5.8	8.6	4.7	7.1	3.6	5.4
	8.5	8.0	12.0	7.0	10.6	6.2	9.3	5.3	7.9	4.3	6.5	3.3	4.9
	9	7.3	11.0	6.5	9.7	5.7	8.5	4.8	7.2	3.9	5.9	3.0	4.5
	9.5	6.7	10.1	6.0	8.9	5.2	7.8	4.4	6.7	3.6	5.4	2.8	4.2
Design		F_y = 50 ksi											
		1/2		7/16		3/8		5/16		1/4		3/16[c]	
Effective Length, *KL* (ft)	2	32.0	48.1	28.4	42.7	25.0	37.6	21.3	32.0	17.1	25.8	12.4	18.7
	2.5	29.9	44.9	26.5	39.8	23.3	35.0	19.9	29.9	16.0	24.1	11.7	17.6
	3	27.5	41.3	24.4	36.7	21.4	32.2	18.3	27.5	14.8	22.2	10.8	16.3
	3.5	25.1	37.7	22.2	33.4	19.5	29.3	16.6	25.0	13.5	20.2	10.0	15.0
	4	22.7	34.1	20.1	30.2	17.6	26.5	15.0	22.6	12.2	18.3	9.1	13.6
	4.5	20.4	30.6	18.1	27.2	15.9	23.8	13.5	20.3	11.0	16.5	8.2	12.4
	5	18.2	27.4	16.2	24.3	14.2	21.3	12.1	18.2	9.8	14.8	7.4	11.1
	5.5	16.2	24.4	14.4	21.6	12.6	18.9	10.7	16.1	8.8	13.2	6.7	10.0
	6	14.4	21.7	12.7	19.2	11.2	16.8	9.5	14.3	7.8	11.7	6.0	8.9
	6.5	12.9	19.3	11.4	17.1	10.0	15.0	8.5	12.8	6.9	10.4	5.3	8.0
	7	11.6	17.4	10.2	15.4	9.0	13.5	7.6	11.5	6.2	9.4	4.8	7.2
	7.5	10.4	15.7	9.2	13.9	8.1	12.1	6.9	10.3	5.6	8.4	4.3	6.4
	8	9.5	14.2	8.4	12.6	7.3	11.0	6.2	9.4	5.1	7.6	3.9	5.8
	8.5	8.6	12.9	7.6	11.4	6.7	10.0	5.7	8.5	4.6	7.0	3.5	5.3
	9	7.9	11.8	7.0	10.5	6.1	9.1	5.2	7.8	4.2	6.4	3.2	4.9
	9.5	7.2	10.9	6.4	9.6	5.6	8.4	4.8	7.1	3.9	5.8	3.0	4.4
Properties													
A_g (in.^{2})		2.76		2.43		2.11		1.78		1.44		1.09	
γ_z (in.)		0.580		0.580		0.581		0.583		0.585		0.586	
ASD	LRFD	[c] Shape is slender for compression. [f] Shape exceeds compact limit for flexure.											
Ω_c = 1.67	ϕ_c = 0.9	Notes: Heavy lines indicate L/r_z equal to or greater than 120, 140 and 200, respectively. *Method 4, except that the axial load is applied at mid-thickness of connected leg.											

Bond Behavior of Concrete-Filled Steel Tube (CFT) Structures

JIE ZHANG, MARK D. DENAVIT, JEROME F. HAJJAR and XILIN LU

ABSTRACT

To achieve internal force transfer while avoiding the use of steel stud anchors or a bearing mechanism within concrete-filled steel tubes (CFTs), an accurate assessment of the bond strength of CFTs is required. However, calculation of the bond within CFTs remains a challenging problem due to lack of a general procedure that can account for the range of connection configurations seen within composite construction. A new approach for assessing the nominal bond strength for both rectangular and circular CFTs is proposed. Based on the results of push-out experiments of CFTs, the nominal bond stress is shown to vary with tube shape and dimensions, and formulas are proposed to capture this behavior. The longitudinal bond transfer length is derived by examining the distribution of bond stress along the height of the column as well as experimental data from CFT connection tests. The circumferential bond transfer width is identified as the entire perimeter of the interface, accounting for the contribution to the bond strength from the interface on the sides that do not have girders or braces framing in. The resulting nominal bond strength is then shown to have a resistance factor of 0.45 for load and resistance factor design (LRFD) and safety factor of 3.33 for allowable strength design (ASD).

Keywords: concrete-filled steel tubes, composite action, connections, bond strength, critical bond stress, slip.

INTRODUCTION

Composite braced or unbraced frame structures that use concrete-filled steel tube (CFT) columns provide superior performance when subjected to nonseismic and seismic lateral loading. This has led to a continued increase in the use of these members in the primary lateral-resistance systems of structures. Steel tubes serve as the formwork for concrete placement, potentially expediting construction and reducing cost (Bridge and Webb, 1993). In addition, the composite action of the steel tube and concrete core can effectively delay the buckling of steel tubes and significantly increase the ductility of the concrete core. To ensure these beneficial effects, it is important to have a comprehensive understanding of the composite action between the constituent materials, particularly in critical connection regions where load is transferred to the CFT column from girders or braces. If the steel tube cannot effectively transfer the axial forces to the concrete, the resulting localized stresses may lead to premature yielding or local buckling of the steel tube. Therefore, the bond transfer mechanisms need to be accurately assessed and incorporated into the design. Transfer of stress through natural bond, without the use of steel stud anchors or a bearing mechanism, is often the most economical connection detail; however, efforts to characterize the bond strength are hindered by varying experimental results, even among like specimens (Roeder et al., 1999).

The design provisions for load transfer in CFTs through direct bond in the AISC *Specification for Structural Steel Buildings* (AISC, 2010) are based predominantly on the results of push-out and push-off tests. Using only these data, there is little quantitative evidence to support the effective transfer area because these experimental configurations do not share the same loading and boundary conditions as typical composite columns. Thus, further investigation into bond behavior is important to ascertain a more accurate prediction on the bond strength of CFTs in the design provisions. In this work, a new formula for nominal bond strength is proposed. Nominal bond strength, longitudinal bond transfer length, circumferential bond transfer width and resistance and safety factors are examined separately.

EXISTING DESIGN PROVISIONS

The nominal bond strength of rectangular (RCFT) and circular concrete filled-steel tubes (CCFT) prescribed in the AISC *Specification* (AISC, 2010) is given as:

(a) For RCFT:

$$R_n = B^2 C_{in} F_{in} \tag{1}$$

Jie Zhang, Ph.D., Assistant Chief Engineer, Jiading MTR Construction and Investment Co. Ltd., Shanghai, China. E-mail: jiezhang000@gmail.com

Mark D. Denavit, Graduate Research Assistant, Department of Civil and Environmental Engineering, University of Illinois at Urbana-Champaign, Urbana, IL. E-mail: denavit2@illinois.edu

Jerome F. Hajjar, Ph.D., P.E., Professor and Chair, Department of Civil and Environmental Engineering, Northeastern University, Boston, MA (corresponding author). E-mail: jf.hajjar@neu.edu

Xilin Lu, Ph.D., Cheung Kong Scholars Professor, Tongji University, Shanghai, China. E-mail: lxlst@tongji.edu.cn

(b) For CCFT:

$$R_n = 0.25\pi D^2 C_{in} F_{in} \quad (2)$$

where

C_{in} = 2 if the CFT extends to one side of the point of force transfer
= 4 if the CFT extends to both sides of the point of force transfer
R_n = nominal bond strength, kips
F_{in} = nominal bond stress = 60 psi
B = overall width of rectangular steel section along face transferring load, in.
D = outside diameter of the round steel section, in.

This formula can be seen as the product of three values: the nominal bond stress, F_{in}; the circumferential bond transfer width, B for RCFT and $0.25\pi D$ for CCFT; and the longitudinal bond transfer length, BC_{in} for RCFT and DC_{in} for CCFT. The nominal bond stress, F_{in}, is taken as 60 psi (0.4 MPa). This value is seen as a reasonable lower bound of bond stresses observed in experimental results, mostly consisting of push-out tests (AISC, 2010). The bond length is dependent on the value of C_{in}, which is equal to 2 if CFT extends to only one side of the point of force transfer (e.g., the top or bottom story) and 4 if the CFT extends both sides. The bond width is computed assuming only the face to which load is applied for RCFT, or one-quarter of the perimeter for CCFT is active in transferring stress. The resistance factor, ϕ, is given as 0.45 and safety factor, Ω, is given as 3.33 based on an examination of push-off test results from Morishita et al. (1979a, 1979b).

The European model building code (CEN, 2004) also provides provisions relating to transfer strength by direct bond. A differentiation is made in the bond stress based on the shape of the steel tube: 60 psi (0.40 MPa) for RCFT and 80 psi (0.55 MPa) for CCFT. The bond transfer length is limited to the lesser of twice the minimum transverse dimension of the column, or one-third the column length. No mention is given to the bond transfer width, so it may be assumed that the full perimeter is engaged in the load transfer. It is noted that for a RCFT column with two girders framing in, the nominal bond strength, as calculated by the AISC *Specification* and Eurocode, is the same.

Tomii (1985) highlights a design procedure from the Japanese code in which a lower bond strength and larger bond transfer area are used. For long-term loading, the bond strength is 14 psi (0.10 MPa) for RCFT and 21 psi (0.15 MPa) for CCFT. The bond length is taken as the distance from the mid-height of the upper column to the mid-height of the lower column, and the bond width is taken as the full perimeter of the steel–concrete interface.

Other procedures have been proposed to characterize bond strength for design. Roeder et al., (1999) examined results from push-out tests on CCFTs and found a correlation between bond strength and the cross-sectional dimensions of the tube. A linear equation was proposed to describe the bond stress as a function of the D/t ratio. The linear equation implied that no reliable bond stress could be obtained for CCFTs with a D/t ratio greater than 80. Two checks are proposed using this bond stress. First, at the ultimate load level, the bond stress is applied around the entire perimeter and along a length equal to the lesser of length of the column, or 3.5 times the diameter of the steel tube. Second,

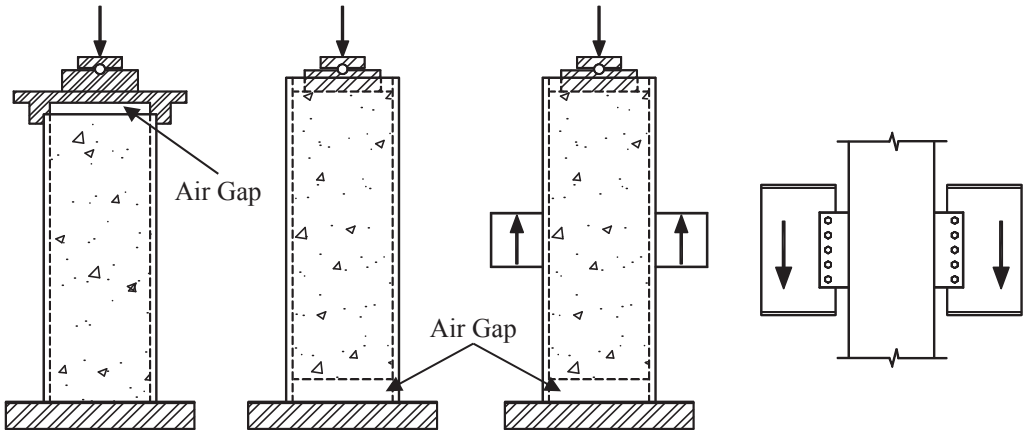

Fig. 1. Typical CFT test configurations to assess bond behavior.

noting evidence of cyclic deterioration of bond strength, at the serviceability level, the bond strength is computed using a triangular stress distribution over a length of one-half the tube diameter.

Variation in the bond stress based on tube dimensions was also observed for RCFTs by Parsley et al. (2000). A formula for bond strength was proposed as a linear function of the slenderness parameter t/H^2.

EXPERIMENTAL STUDIES

Experimental studies on bond behavior of CFT members have most frequently been conducted through the use of push-out tests (Virdi and Dowling, 1980; Shakir-Khalil, 1991, 1993b, 1993c; Roeder et al., 1999; Parsley et al., 2000; Xu et al., 2009; Aly et al., 2010; Yin and Lu, 2010), push-off tests (Morishita et al., 1979a, 1979b; Tomii et al., 1980a, 1980b), or connection tests (Dunberry et al., 1987; Shakir-Khalil, 1993a, 1993d, 1994a, 1994b; Shakir-Khalil and Al-Rawdan, 1995). Each of these types of tests (see Figure 1) has advantages and disadvantages in the assessment of the natural bond strength of CFTs. The boundary conditions of push-out tests (Figures 1b and 1c) induce constant bond stress at the ultimate limit state and thus provide little information as to the distribution of bond stress over the length along the column. However, in push-off and connection tests, where the bond stress is not constant, it is difficult to accurately estimate the magnitude of stress. In typical push-out and push-off tests, the specimen bears directly on a rigid support at the base (Figure 1b), excluding the beneficial effects that a shear connection provides. Push-out tests where force is applied to the concrete core and resisted by shear tabs attached to the steel tube (Figure 1c) and connection tests (Figure 2) include these beneficial effects and thus provide the closest analogs to typical shear connections (or other connection types that feature eccentric introduction of force into the CFT) used in practice.

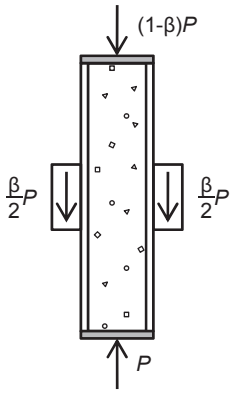

Fig. 2. CFT connection test schematic.

CFT Push-Out Tests without Shear Tabs

Critical bond stresses from push-out test results are computed by dividing the peak load attained during the test by the entire area of the steel–concrete interface. The resistance observed in these tests has been generally attributed to three primary mechanisms: adhesion, friction and wedging (Parsley et al., 2000; Johansson 2003). Adhesion, provided by the chemical bond between the concrete and steel, is a brittle mechanism and is only active at most during the early stages of load. It may not be active at all depending on the relative amplitudes of radial enlargement of the steel tube caused by the wet concrete, shrinkage of the concrete and the roughness of the steel tube (Roeder et al., 1999). Friction is the product of the roughness of the steel–concrete interface and the contact pressure existing at the interface. Wedging occurs as the motion of the concrete core is resisted by geometric irregularities in the steel tube.

Bond stresses obtained from push-out tests are highly variable and found to range over two orders of magnitude. However, some noticeable trends have been identified (Roeder et al., 1999; Parsley et al., 2000). The bond stress for CCFTs is larger than for RCFTs. Tube dimensions have an effect on the results, with lower bond stress obtained for larger and more slender tubes. The surface preparation of the interior of the steel tube and the shrinkage/expansive potential of the concrete have also been shown to have an influence on the bond stress. Concrete and steel material strengths, however, appear to have no consistent effect on the bond stress. Eccentric loading of the column has also been shown to have a beneficial effect on the bond stress. This increase is so significant that it has been suggested that a bond need not be checked in the presence of significant bending moments in the column (Roeder et al., 2009). This paper does not specifically address the effect of eccentrically loaded columns, rather concentrating on the worst-case concentric loading.

Details of push-out tests without shear tabs reported in the literature are presented in Table 1 for RCFTs and Table 2 for CCFTs. All specimens from each reference were included, with the exception of those with shear tabs, those with mechanical shear connecters, those where the steel-concrete interface was manipulated by machining or applying a lubricant, those where the load was applied eccentrically or those with expansive concrete. Specimens that were loaded cyclically were included in the table because they represent loading conditions that typical connections may experience, and they did not significantly skew the results of the analysis.

CFT Push-Out Tests with Shear Tabs

Assessing bond stress based on the results of typical push-out and push-off tests neglects beneficial effects that occur in typical beam-to-column connections due to the rotation

Table 1. RCFT Push-Out Tests without Shear Tabs								
Reference	Number of Specimens	L (in.)	H, B (in.)	t (in.)	H/t, B/t	F_y (ksi)	f'_c (ksi)	F_{in} (psi)
Shakir-Khalil, 1991	6	16	3.1–5.9	0.20	16–30	43.0	5.7–6.3	29–193
Shakir-Khalil, 1993a	6	8–24	5.9	0.20	30	43.0	5.9	48–86
Shakir-Khalil, 1993b	2	16	5.9	0.20	30	43.0	5.7	29
Parsley et al., 2000	4	48–60	8.0–10.0	0.25	32–40	48.0	5.9–6.6	25–42

Table 2. CCFT Push-Out Tests without Shear Tabs								
Reference	Number of Specimens	L (in.)	D (in.)	t (in.)	D/t	F_y (ksi)	f'_c (ksi)	F_{in} (psi)
Virdi and Dowling, 1975	82	6–18	5.7–12.0	0.20–0.40	15–32	mild steel	3.2–6.7	75–431
Shakir-Khalil, 1991	2	16	6.6	0.20	34	43.0	6.5	63–69
Shakir-Khalil, 1993a	6	8–24	6.6	0.20	34	43.0	6.1	95–134
Shakir-Khalil, 1993b	2	16	6.6	0.20	34	43.0	6.5	63–69
Roeder et al., 1999	18	30–76	10.8–24.0	0.22–0.53	20–109	not given	4.0–6.9	1.5–114
Xu et al., 2009	3	20	6.1–6.3	0.11–0.18	35–56	not given	6.8	87–97
Aly et al., 2010	14	16	4.5	0.13	36	50.8	5.9–13.2	51–181

of the shear tabs (or similar eccentricities that may occur for introduction of force between a girder and the steel tube in the connection topology) (Johansson, 2003). The rotation of the shear tab during loading results in pinching of the concrete core where the shear tab rotates inward and constriction of the steel tube where the shear tab rotates outward (Figure 3). Both cases result in increased contact pressure between the steel and concrete and thus greater frictional resistance to slip.

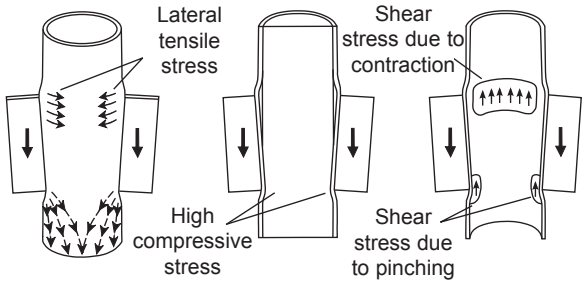

Fig. 3. Increased contact force with shear tab rotation (adapted from Johansson, 2003).

Push-out tests where load was applied to the steel tube through shear tabs have been reported in the literature (Shakir-Khalil, 1993c; Parsley et al., 2000). Details of these experiments are presented in Table 3 for RCFTs and Table 4 for CCFTs.

The failure mode of the all of the RCFT specimens was slip. A typical load-slip relationship shows a high initial stiffness up to the peak load. Many specimens showed a sharp decrease in strength following the peak load, while others maintained a load near the peak load. Two specimens (G2 and G3) displayed a steadily increasing load following a reduction in stiffness near the peak load of other similar specimens. In all cases, $P_{applied}$ was taken as the peak load attained during the test. The average bond stress, F_{in}, for the full set of RCFT tests is 93 psi. The average bond stress for specimens where the shear tabs were located near mid-height of the column is 118 psi, while it is 53 psi for specimens with shear tabs near the column ends.

Only some of the CCFT specimens failed due to slip. Specimens D1a, D1b, F1a and F1b (Shakir-Khalil, 1993c)

Table 3. RCFT Push-Out Tests with Shear Tabs									
Reference	Specimen	L (in.)	$H = B$ (in.)	t (in.)	H/t	F_y (ksi)	f'_c (ksi)	$P_{applied}$ (kip)	F_{in} (psi)
Shakir-Khalil, 1993c	C1a	15.6	5.91	0.197	30.0	39.9	6.2	38.1	110.5
	C1b	15.6	5.91	0.197	30.0	39.9	6.2	51.5	149.5
	C2a	15.7	5.91	0.197	30.0	39.9	6.2	51.5	148.4
	C2b	15.7	5.91	0.197	30.0	39.9	6.2	53.1	153.3
	E1a	15.7	7.87	0.248	31.7	39.9	6.6	37.5	81.0
	E1b	15.7	7.87	0.248	31.7	39.9	6.6	18.0	38.7
	G2	15.8	5.91	0.197	30.0	39.9	6.5	44.7	128.2
	G3	15.9	5.91	0.197	30.0	39.9	6.5	47.0	133.7
	G4	15.8	5.91	0.197	30.0	39.9	6.5	23.4	67.0
Parsley et al., 2000	CFT2	48.0	8.00	0.228	35.1	48.0	6.6	98.0	67.7
	CFT5	48.0	8.00	0.228	35.1	48.0	6.6	101.0	69.7
	CFT8	58.5	10.00	0.232	43.1	48.0	5.9	67.0	30.0
	CFT6	58.5	10.00	0.234	42.7	48.0	5.9	70.0	31.4
								Average:	93.0
								Std. Dev.:	46.4

Table 4. CCFT Push-Out Tests with Shear Tabs									
Reference	Specimen	L (in.)	D (in.)	t (in.)	D/t	F_y (ksi)	f'_c (ksi)	$V_{applied}$ (kip)	F_{in} (psi)
Shakir-Khalil, 1993c	D1a	15.7	6.63	0.197	33.7	39.9	6.2	186.6	605
	D1b	15.7	6.63	0.197	33.7	39.9	6.2	182.1	594
	F1a	15.8	6.63	0.197	33.7	39.9	6.1	212.9	689
	F1b	15.6	6.63	0.197	33.7	39.9	6.6	218.3	715
	H2	15.8	6.63	0.197	33.7	39.9	6.5	172.0	556
	H3	15.9	6.63	0.197	33.7	39.9	6.5	167.0	538
	H4	15.7	6.63	0.197	33.7	39.9	6.5	60.5	196
								Average:	556
								Std. Dev.:	172

achieved higher-than-expected strengths, and the shear tabs failed prior to slip. In an analysis of one of these specimens, Johansson (2003) identified the rotation of the shear tabs and the increased contact forces to be the cause of the unexpectedly high bond strength. The failure mode of specimens H2 and H3 was slip; however, no peak load was observed because the load was seen to steadily increase. One specimen, H4, failed through slip and displayed a peak load. Again, in all cases, $P_{applied}$ was taken as the peak load attained during the test. The bond stress for CCFTs is much larger than for RCFTs, with an average applied bond stress, F_{in}, of 556 psi. However, this value is unreasonably high for design purposes, because it was achieved only for a few similarly proportioned tests and may not be indicative of expected behavior for the variety of configurations expected in practice.

Nominal Bond Stress

Push-out tests, whether with or without shear tabs, provide a direct means of assessing the bond stress. Trends in the push-out test results that have been identified include the dependence of the bond stress on factors not typically known at the time of design (e.g., the condition of the steel–concrete

surface and the shrinkage/expansive potential of the concrete). For a bond stress formula intended for design, these factors should thus be included in an average sense rather than explicitly. Among the strongest trends identified is the dependence of the bond stress on tube dimensions. Roeder et al., (1999) proposed a formula for bond stress of CCFTs based on the D/t ratio. Parsley et al., (2000) proposed a formula for bond stress of RCFTs based on t/H^2. The ratio t/H^2 was selected based on a mechanistic analysis; it is proportional to the radial stiffness of cylindrical, thin-walled pressure vessels.

It is noted that there is insufficient experimental evidence to determine which of the two transverse dimensions of an RCFT cross-sections—i.e., the width or the height—should be used for determining bond stress because most of the RCFT push-out tests (Tables 1 and 3) had square sections. The height, defined here as the longer transverse dimension, was selected as the conservative choice, but further investigation is appropriate for sections with a high aspect ratio (H/B).

The results of push-out tests are plotted in Figure 4 against both of these parameters. All push-out tests from Tables 1 through 4 were included. The bond stress is typically higher for push-out tests with shear tabs, showing the

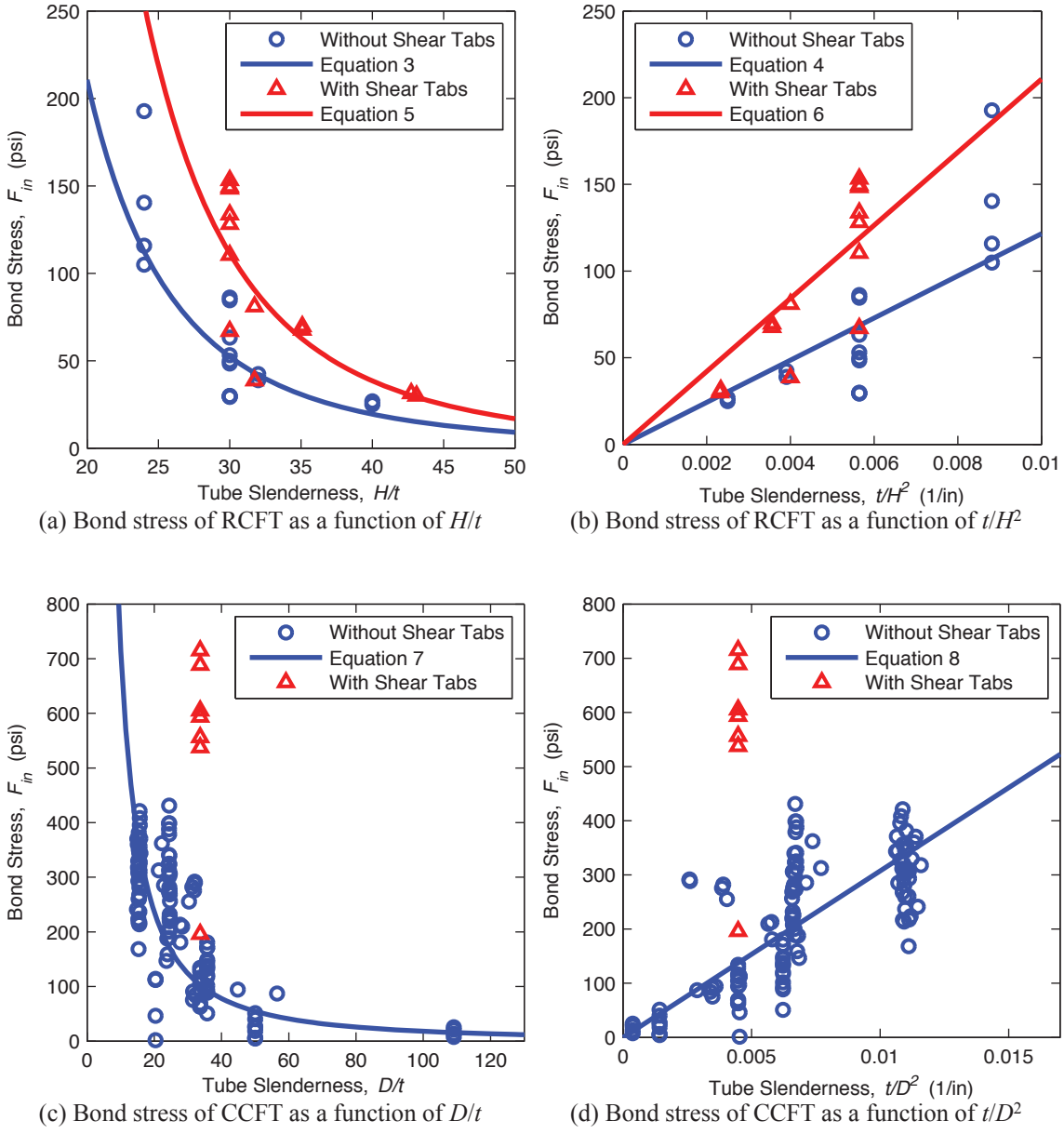

(a) Bond stress of RCFT as a function of H/t

(b) Bond stress of RCFT as a function of t/H^2

(c) Bond stress of CCFT as a function of D/t

(d) Bond stress of CCFT as a function of t/D^2

Fig. 4. Bond stress for CFT as a function of tube slenderness.

beneficial effects rotation of the shear tab has on bond stress. As seen in Figure 4, there is significant variation in the bond stress, indicating that the constant values used in current design methodologies are insufficient, especially for thin tubes and large cross-sections where the bond stress may be overestimated.

To obtain a design formula, a least squares curve fit can be made to these data. The forms of the equations chosen were selected to provide a good fit to the available data, have reasonable bounds, and produce non-negative bond stress values. The results of the regression analysis are as follows:

RCFT push-out tests without shear tabs:

$$F_{in} = 6.23 \times 10^6 \left(H/t\right)^{-3.44} \quad R^2 = 0.68 \tag{3}$$

$$F_{in} = 12{,}100\left(t/H^2\right) \quad R^2 = 0.56 \tag{4}$$

RCFT push-out tests with shear tabs:

$$F_{in} = 3.23 \times 10^7 \left(H/t\right)^{-3.70} \quad R^2 = 0.61 \tag{5}$$

$$F_{in} = 21{,}100\left(t/H^2\right) \quad R^2 = 0.66 \tag{6}$$

CCFT push-out tests without shear tabs:

$$F_{in} = 28{,}500\left(D/t\right)^{-1.59} \quad R^2 = 0.33 \tag{7}$$

$$F_{in} = 30{,}700\left(t/D^2\right) \; R^2 = 0.50 \tag{8}$$

where F_{in} is in psi and t, H, and D are in inches.

A curve fit was not performed for CCFT push-out tests with shear tabs because all the available tests had nearly the same size tube. The two different functions for each case represent the two different parameters (e.g., H/t and t/H^2) chosen to represent the tube dimensions. In addition to accuracy, quantified by the R^2 value associated with each formula, the formulas can be judged by their usability. Based on these criteria, the formulas based on t/D^2 and t/H^2 are recommended for design. Furthermore, the formulas computed with the data from the push-out tests without shear tabs are recommended for design because they provide a lower bound for the behavior expected in typical shear connections and allow for the greatest consistency between tube shapes. Thus Equation 4 is recommended for the nominal bond stress of RCFTs, and Equation 8 is recommended for CCFTs. Both of these formulas have no upper bound on the bond stress, though one could be implemented based on the results of the stockiest tubes for each shape (i.e., 100 to 200 psi for RCFTs and 200 to 400 psi for CCFTs).

CFT Connection Tests

Push-out tests have explicit boundary conditions and paths for load transfer and thus are well suited for an assessment of bond stress; however, they provide little evidence of the bond length or bond width of typical connections. Column connection tests that are instrumented to measure load transfer such as those conducted by Dunberry et al. (1987), Shakir-Khalil (1993a and d, 1994a and b) and Shakir-Khalil and Al-Rawdan (1995) provide a means to quantify the area over which a nominal bond stress acts in typical connections. A schematic of the test specimens and loading is presented in Figure 2. Shear tabs are welded to the outside of the steel tubes to transfer the eccentric shears through the interfaces. Load is applied at both column ends and at the shear connections, in a ratio described by β.

The experimental strength of all of these specimens was near the squash load, indicating that limit states other than cross-sectional strength, including slip, either did not have a significant effect on the strength or did not occur. In the tests performed by Dunberry et al. (1987), local buckling was a typical failure mode. The local buckling occurred near the connection for some specimens, indicating that the loading conditions possibly had an influence on the strength—and away from the connection for other specimens. A strain incompatibility was observed in the connection region, which extended approximately three tube widths below the connection and one to two tube widths above the connection. The concrete load steadily rose in this region, indicating a load was transferred along its length, although the rise was steepest in the bottom half of the connection, indicating that pinching due to rotation of the shear tabs played a significant role in transferring the load. The tests performed by Shakir-Khalil (1993a and d, 1994a and b) and Shakir-Khalil and Al-Rawdan (1995) displayed somewhat similar behavior. The typical failure mode was overall collapse of the column without indication of a detrimental effect on the strength from slip. The observed transfer length was shorter than that observed by Dunberry et al. (1987), as strains equalized within a tube width above and below the connection.

Additional details of the experiments are shown in Table 5 for RCFTs and in Table 6 for CCFTs. The tabulated applied load, $P_{applied}$, is the total load applied to the steel tube in the connection region. This load is not necessarily indicative of the slip strength because many of the specimens failed away from the connection region or the strength was not reached due to test rig limitations. Nonetheless, these specimens were included in the table because they provide a lower

Table 5. RCFT Connection Tests

Reference	Specimen	L (in.)	$H=B$ (in.)	t (in.)	H/t	F_y (ksi)	f'_c (ksi)	β	$P_{applied}$ (kip)	$V'_{applied}$ (kip)	Number of Girders	$R_{n,AISC2010}$ (kip)	Test-to-Predicted	F_{in} (Eq. 6) (psi)	$L_{transfer}$ (in.)	$L_{transfer}/H$
Dunberry et al., 1987	A1	118.1	4.01	0.193	20.8	53.7	3.6	1.00	186.6	38.2	2	7.73	4.9	252.9	10.41	2.6
	A2	118.1	4.99	0.187	26.7	51.3	3.6	1.00	200.8	52.9	2	11.96	4.4	158.3	18.08	3.6
	A3	118.1	5.00	0.189	26.5	51.3	3.6	0.50	130.4	34.1	2	11.98	2.8	159.4	11.59	2.3
	A4	118.1	4.98	0.187	26.7	51.3	3.6	0.30	81.7	21.5	2	11.89	1.8	159.0	7.35	1.5
	B1	118.1	7.02	0.244	28.7	56.3	2.5	0.30	142.7	28.1	2	23.65	1.2	104.7	10.28	1.5
	B2	118.1	7.01	0.189	37.1	51.2	2.5	0.45	172.0	45.3	2	23.60	1.9	81.1	21.05	3.0
	B3	118.1	8.01	0.246	32.5	57.9	2.5	0.30	180.6	38.9	2	30.78	1.3	81.0	15.96	2.0
	C1	59.1	4.01	0.190	21.1	54.2	3.5	1.00	198.1	39.6	2	7.71	5.1	249.3	10.94	2.7
	D1	78.7	6.00	0.190	31.6	64.3	4.3	0.50	201.3	58.1	2	17.28	3.4	111.5	23.20	3.9
	D2	78.7	6.00	0.189	31.8	64.3	4.3	0.50	203.0	59.0	2	17.30	3.4	110.4	23.76	4.0
	D3	78.7	6.00	0.189	31.7	64.3	4.3	0.50	210.8	61.1	2	17.30	3.5	110.8	24.49	4.1
	D4	78.7	6.00	0.189	31.8	64.3	4.3	0.50	199.6	57.9	2	17.30	3.3	110.6	23.28	3.9
Shakir-Khalil, 1993d, 1994a, 1994b	B1	110.2	5.91	0.197	30.0	47.6	5.6	0.20	59.5	23.9	2	16.74	1.4	119.1	9.10	1.5
	B3	110.2	5.91	0.197	30.0	49.3	5.5	0.29	87.0	34.1	2	16.74	2.0	119.1	12.97	2.2
	B5	110.2	5.91	0.197	30.0	47.6	5.9	0.20	57.2	23.9	2	16.74	1.4	119.1	9.08	1.5
	B7	110.2	5.91	0.197	30.0	47.4	5.7	0.29	79.0	32.4	2	16.74	1.9	119.1	12.34	2.1
	D1	110.2	7.87	0.248	31.7	47.4	6.6	0.20	133.5	61.2	2	29.76	2.1	84.4	24.55	3.1
	D2	110.2	7.87	0.248	31.7	60.2	6.5	0.20	130.7	52.2	2	29.76	1.8	84.4	20.96	2.7
	E1	110.2	5.91	0.197	30.0	53.3	6.5	0.20	71.9	29.7	2	16.74	1.8	119.1	11.32	1.9
	E2	110.2	5.91	0.197	30.0	53.5	6.2	0.29	105.6	42.4	2	16.74	2.5	119.1	16.13	2.7
	E3	110.2	5.91	0.197	30.0	53.5	5.7	0.20	68.5	25.9	2	16.74	1.5	119.1	9.88	1.7
	E4	110.2	5.91	0.197	30.0	53.3	5.3	0.29	96.3	34.8	2	16.74	2.1	119.1	13.27	2.2
	E5	110.2	5.91	0.197	30.0	53.3	5.1	0.20	72.1	25.6	2	16.74	1.5	119.1	9.74	1.6
	E6	110.2	5.91	0.197	30.0	52.9	5.5	0.29	97.1	36.4	2	16.74	2.2	119.1	13.86	2.3
	E7	110.2	5.91	0.197	30.0	53.3	5.9	0.20	68.7	26.8	2	16.74	1.6	119.1	10.20	1.7
	E8	110.2	5.91	0.197	30.0	52.9	5.7	0.29	98.3	37.5	2	16.74	2.2	119.1	14.27	2.4
Shakir-Khalil & Al-Rawdan, 1995	F1	110.2	5.91	0.197	30.0	47.9	5.3	0.17	44.9	17.5	1	8.37	2.1	119.1	6.67	1.1
	F2	110.2	5.91	0.197	30.0	47.9	6.6	0.11	33.9	15.0	1	8.37	1.8	119.1	5.71	1.0
	F3	110.2	5.91	0.197	30.0	48.2	6.3	0.17	43.8	18.7	1	8.37	2.2	119.1	7.13	1.2
	F4	110.2	5.91	0.197	30.0	48.2	6 .5	0.11	33.2	14.6	1	8.37	1.7	119.1	5.54	0.9

Table 6. CCFT Connection Tests																
Reference	Specimen	L (in.)	D (in.)	t (in.)	D/t	F_y (ksi)	f'_c (ksi)	β	$P_{applied}$ (kip)	$V'_{applied}$ (kip)	Number of Girders	$R_{n,AISC2010}$ (kip)	Test-to-Predicted	F_{in} (Eq. 8) (psi)	$L_{transfer}$ (in.)	$L_{transfer}/D$
Shakir-Khalil, 1993a, 1994a	A1	110.2	6.63	0.197	33.7	46.4	6.2	0.20	61.9	30.5	2	16.55	1.8	137.6	11.31	1.7
	A2	110.2	6.63	0.197	33.7	46.8	6.5	0.20	57.7	29.0	2	16.55	1.8	137.6	10.76	1.6
	A5	110.2	6.63	0.197	33.7	46.8	6.5	0.40	138.6	69.4	2	16.55	4.2	137.6	25.76	3.9
	A6	110.2	6.63	0.197	33.7	46.1	6.5	0.29	91.3	46.4	2	16.55	2.8	137.6	17.21	2.6
	C1	110.2	8.63	0.248	34.8	44.2	5.7	0.20	100.7	49.6	2	28.05	1.8	102.3	18.98	2.2
	C2	110.2	8.63	0.248	34.8	43.9	7.3	0.20	110.3	61.4	2	28.05	2.2	102.3	23.49	2.7

bound on the slip strength. The portion of the applied load that is transferred to the concrete core, $V'_{applied}$, is computed using Equation 9, which assumes secant stiffnesses based on the material strengths. Equation 9 is equivalent to provisions in the AISC *Specification* (AISC, 2010) that specify how much load is transferred to the concrete when all of the specimens have compact members:

$$V'_{applied} = P_{applied}\left(1 - \frac{A_s F_y}{A_s F_y + C_2 A_c f'_c}\right) \quad (9)$$

where

C_2 = 0.85 for RCFT and 0.95 for CCFT

The nominal bond strength based on current design provisions (AISC, 2010) is tabulated for each of the specimens and is used and along with $V'_{applied}$ to compute the test-to-predicted ratio (Tables 5 and 6). The current design provisions are seen to be very conservative for these specimens, with test-to-predicted ratios ranging from 1.2 to 5.1 for RCFTs and 1.8 to 4.2 for CCFTs, especially when noting that these ratios are a lower bound because few specimens exhibited a failure mode that included slip.

Effective Bond Transfer Length

The transfer length, the length along the column where significant bond stresses occur, varies with material and geometric properties of the CFT and increases with applied load. The length used in the bond strength formula must address two types of slip limit states. The first is slip along the entire length of the column, where, depending on the boundary conditions, a push-out type failure could occur. The second is slip occurring locally, near the point of load application. This type of slip failure is enabled by the formation of a plastic mechanism in either the steel tube or concrete core, allowing the relative motion. Other, more localized failure modes that include slip (e.g., failure of one face of a CFT column where load is framing in) should be addressed in connection design and are not discussed here.

The CFT connection tests provide some insight into an appropriate bond length. The transfer length at peak load, $L_{transfer}$, is computed for the CFT connections tests (Tables 5 and 6) using Equation 10, where p is the entire perimeter of the steel–concrete interface and F_{in} is the critical bond stress, as computed using Equation 6 for RCFTs and Equation 8 for CCFTs:

$$L_{transfer} = \frac{V'_{applied}}{p\,F_{in}} \quad (10)$$

Use of the formula for bond stress from push-out tests without shear tabs for RCFT (Equation 4) would result in transfer lengths approximately twice as large and could be justified because Equation 4 is recommended for design. However, the formula for bond stress from push-out tests with shear tabs is used for RCFTs, because it is a more accurate assessment for these specimens. The tabulated transfer lengths are of approximately the same magnitude as the lengths over which slip occurred, as reported by the researchers.

In Tables 5 and 6, the transfer length is seen to have a strong correlation with the ratio of load applied at the connection to total load, β (Figure 2). This is due to the fact that the specimens failed at loads near the cross-section strength, thus the specimens with larger β values had larger transferred loads at failure because a larger portion of the load was applied at the connection. The other specimens, with lower β values, presumably could have achieved the similar transferred loads at failure had a greater portion of the load been applied at the connection. Accordingly, the transfer length in Tables 5 and 6 should be considered a lower bound. The ratio of transfer length to tube width for specimens with a large proportion of the load applied at the connection ranges from 2.3 to 4.1 ($\beta \geq 0.4$; Table 5: specimens A1, A2, A3, B2, C1, D1, D2, D3 and D4 by Dunberry et al., 1987; Table 6: specimen A5 by Shakir-Khalil, 1993a). Based on these data, the current provisions for bond length for the case of load applied to the steel tube and the CFT extending to both sides of the point of force transfer (i.e., $C_{in} = 4$) (AISC, 2010) appear to be appropriate and safe for design.

While the CFT connection tests provide valuable information, they are limited by a lack of variety in geometric and material properties and loading configurations and because most specimens did not exhibit a slip related failure. A mechanistic analysis allows exploration of the effective bond transfer length for the range of properties and configurations seen in practice. A suitable bond length would account for both slip limit states: slip along the entire length and localized slip accompanied with overstressing and formation of a plastic mechanism in the steel tube or concrete core.

The normalized length (*L/H* for RCFT or *L/D* for CCFT) of the CFT push-out tests examined in this work varied from 1 to 6. The CFT connections tests exhibited normalized transfer lengths within the same range. While no definite trends were identified in the CFT push-out test results between the normalized length and bond stress, the bond stress as derived from the push-out tests may not be active along the entire length for longer columns. Thus, utilizing the entire length of the column to assess bond strength (i.e., $L_{bond} = L$, extending from mid-height of the column above the connection to mid-height of the column below the connection) may be inappropriate even for the case of slip occurring along the entire length of the column.

For localized slip, the length of the column that slips is relatively small, but to enable this failure mode, a plastic

mechanism needs to develop in either the steel tube or concrete core (depending on where the load is applied). The applied force required to develop the plastic mechanism assuming strengths consistent with current provisions (AISC, 2010) is given in Equation 11a for the case of load applied to the steel tube and the CFT extending to both sides of the point of force transfer, Equation 11b for the case of load applied to the steel tube and the CFT extending to only the compressive side of the point of force transfer, and Equation 11c for the case of load applied to the concrete core regardless of which sides the CFT extends.

$$P_{applied} = A_s F_{cr} + A_s F_y \tag{11a}$$

$$P_{applied} = A_s F_{cr} \tag{11b}$$

$$P_{applied} = C_2 A_c f'_c \tag{11c}$$

where F_{cr} is the critical compressive stress of the steel tube ($F_{cr} \leq F_y$) (AISC, 2010).

Note that when load is applied to the steel tube and the CFT extends to both sides, the compressive strength on one side and the tensile strength on the other side need to be met simultaneously to form a plastic mechanism. Thus, depending on the proportioning of the section, this limit state may be precluded by the cross-section strength of the composite column.

To determine an appropriate value for the bond length when a localized overstressing failure controls, the transfer length is computed when the applied load is equal to the limit (Equation 11). The transfer length is computed using Equation 12a for the case of load applied to the steel tube and Equation 12b for the case of load applied to the concrete core. These equations are as given in the AISC *Specification* (AISC, 2010), with the exception that F_{cr} is used instead of F_y to determine the portion of the load supported by the steel tube. This change was necessary to yield realistic results for slender tubes. Note that $F_{cr} = F_y$ in the controlling cases presented here; thus, this deviation from the AISC *Specification* has no effect on the proposed recommendations.

$$P_{applied}\left(1 - \frac{A_s F_{cr}}{P_{no}}\right) = pF_{in}L_{transfer} \tag{12a}$$

$$P_{applied}\left(\frac{A_s F_{cr}}{P_{no}}\right) = pF_{in}L_{transfer} \tag{12b}$$

where P_{no} is the nominal compressive strength of zero length CFT (AISC, 2010).

The computed transfer length is normalized by the outside dimension of the steel tube (H for RCFT; D for CCFT) to be comparable with the parameter C_{in}. The minimum normalized transfer lengths for practical ranges of material parameters ($F_y \geq 36$ ksi, $E_s = 29{,}000$ ksi, $f'_c \geq 3$ ksi) and geometric parameters ($H \geq 4$ in., $H/B \leq 2$, $B/t \geq 10$, $H/t \leq 400$ for RCFT; $D \geq 4$ in., $10 \leq D/t \leq 400$ for CCFT) and only for cases where the plastic mechanism was not precluded by the cross-section strength are presented in Table 7 for RCFTs and Table 8 for CCFTs for the various configurations. Based on these results, an appropriate value for C_{in} in the bond strength equation is 4 for the case of load applied to the steel tube and the CFT extending to both sides of the point of force transfer and 2 otherwise. The value of 4 for the case of load applied to the steel tube and steel tube and the CFT extending to both sides of the point of force transfer is in agreement with results of the CFT connection tests described earlier; there is no experimental evidence for the other configurations. These recommendations regarding C_{in} represent a minor change from the current provisions, where $C_{in} = 4$ when the CFT extends to both sides of the point of force transfer regardless of whether the load is applied to the steel or to the concrete. It is further recommended that in cases where the nominal bond length ($C_{in}H$ for RCFTs; $C_{in}D$ for CCFTs) of adjacent connection regions overlaps (e.g., columns with a low length-to-depth ratio or with beams framing in a staggered pattern), the bond length should be taken as a reduced value computed such that no overlap occurs.

An alternative form of the bond length could include the height of the shear tab. This form would have the advantage of being more consistent with the definition of the load transfer region used for detailing shear connectors in composite columns (AISC, 2010). If such a form was chosen, the value of C_{in} would need to be adjusted accordingly.

Effective Bond Transfer Width

Current design provisions in the AISC *Specification* allow only a portion of the perimeter of the steel–concrete interface to be used when computing the transfer strength (AISC, 2010). This is unique among the existing and proposed design provisions examined in this paper (Tomii, 1985; Roeder et al., 1999; Parsley et al., 2000; CEN, 2004). Based on observations of friction marks on tested and disassembled push-out specimens, Shakir-Khalil (1993b) noted that for CCFTs the entire perimeter is engaged in bond transfer, whereas for RCFTs only the corner regions participate. There is limited evidence regarding the portion of the width that is active when various numbers of girders frame into either a CCFT or a RCFT column because the majority of tests have been completed with two girders. The CFT

Table 7. RCFT Minimum Transfer Lengths from Mechanistic Analysis									
Case		H (in.)	B (in.)	t (in.)	H/t	F_y (ksi)	f'_c (ksi)	$L_{transfer}$ (in.)	$L_{transfer}/H$
Square CFT	Load on steel, column extends both sides	4.00	4.00	0.067	59.5	36.0	3.0	48.43	12.11
	Load on steel, column extends below only	4.00	4.00	0.132	30.3	36.0	3.0	16.06	4.02
	Load on concrete	4.00	4.00	0.132	30.3	36.0	3.0	16.06	4.02
RCFT	Load on steel, column extends both sides	4.00	4.00	0.067	59.5	36.0	3.0	48.43	12.11
	Load on steel, column extends below only	6.96	4.00	0.400	17.4	36.0	3.0	22.91	3.29
	Load on concrete	6.96	4.00	0.400	17.4	36.0	3.0	22.91	3.29

Table 8. CCFT Minimum Transfer Lengths from Mechanistic Analysis							
Case	D (in.)	t (in.)	D/t	F_y (ksi)	f'_c (ksi)	$L_{transfer}$ (in.)	$L_{transfer}/D$
Load on steel, column extends both sides	4.00	0.075	53.5	36.0	3.0	19.13	4.78
Load on steel, column extends below only	4.00	0.104	38.4	36.0	3.0	7.94	1.99
Load on concrete	4.00	0.104	38.4	36.0	3.0	7.94	1.99

connection tests conducted by Shakir-Khalil and Al-Rawdan (1995) with only one girder framing in had experienced lower transfer loads than the other specimens (Table 5), but it is important to note that the specimen did not suffer a bond failure and would likely have resisted higher transfer loads if the specimen were designed to mitigate non-slip-related failure. The experimental bond stress for push-out tests, including those with shear tabs, is computed assuming the full perimeter is engaged in slip. All of the push-out tests with shear tabs in Tables 3 and 4 have two girders framing on opposite sides. This implies that, for columns with at least two girders framing in on opposite sides, the bond stress can be achieved for the entire perimeter. For the cases of edge and corner columns where one girder or two girders on adjacent sides frame in, it is unclear whether or not the entire perimeter is engaged. However, these configurations will induce bending moments into the columns, thus increasing the bond strength. Therefore, using the entire perimeter for corner columns is likely justified and is proposed for use in this work.

PROPOSED DESIGN FORMULA

Based on the preceding analyses of critical bond stress, longitudinal bond transfer length and circumferential bond transfer width, the formula for nominal bond strength is proposed as:

(a) For RCFT:

$$R_n = 2\left(B+H\right)L_{bond}F_{in} \tag{13a}$$

$$L_{bond} = C_{in}H \tag{13b}$$

$$F_{in} = 12.1\left(t/H^2\right) \le 0.1 \tag{13c}$$

(b) For CCFT:

$$R_n = \pi D L_{bond} F_{in} \tag{14a}$$

$$L_{bond} = C_{in}D \tag{14b}$$

Table 9. Computation of Resistance and Safety Factors					
Type	Number of Experiments	R_m/R_n	V_R	ϕ	Ω
RCFT	18	0.91	0.43	0.45	3.37
CCFT	127	1.26	0.51	0.55	2.74

$$F_{in} = 30.7\left(t/D^2\right) \le 0.2 \quad (14c)$$

where

R_n = nominal bond strength, kips
F_{in} = nominal bond stress, ksi
t = design wall thickness of steel section, in.
B = overall width of rectangular steel section ($B \le H$), in.
H = overall height of rectangular steel section ($H \ge B$), in.
D = outside diameter of round steel section, in.
L_{bond} = length of the bond region (the bond region of adjacent connections shall not overlap)
C_{in} = 4 if load is applied to the steel tube and the CFT extends to both sides of the point of force transfer
= 2 otherwise

For simplicity in design, the perimeter of the steel–concrete interface is approximated using the outside dimensions of the steel tube (i.e., $p = 2(B + H)$ for RCFT and $p = \pi D$ for CCFT). The error introduced from this simplification is small in comparison to the scatter in the results.

An upper bound is placed on the bond stress based on the bond stress observed in experimental results of the stockiest tubes for each shape. For very large cross-sections and thin steel tubes, the bond stress approaches zero, essentially requiring an alternate force transfer mechanism when significant loads are applied.

The proposed formula differs from the current formula (AISC, 2010) in the bond strength, bond length, and bond width. In the proposed equation, the bond width is the entire perimeter of the interface, regardless of the number of girders framing in. The resulting strength should be compared against the force transfer demand from all girders framing in, as opposed to checking each girder individually as implied by the current design formula (AISC, 2010).

The proposed formula for bond stress is based on geometric properties of the tube only. It is noted that concrete quality (e.g., the shrinkage/expansive potential) also affects the bond stress. This was not included in the proposed formula because the concrete quality is not typically known at the time of design. However, higher and more reliable bond strengths could be obtained if there were requirements placed on the quality of the concrete (Roeder et al., 1999).

To compute a resistance factor for load and resistance factor design, the recommendations of Ravindra and Galambos (1978) are used. The proposed formula for the resistance factor (Equation 15) depends on the desired reliability index, β_o; coefficient of variation of the resistance, V_R; and the mean test-to-predicted ratio, R_m/R_n:

$$\phi = \frac{R_m}{R_n} e^{(-0.55\beta_o V_R)} \quad (15)$$

Unfortunately, no suitable set of tests exists to compute reliable statistics on the resistance or test-to-predicted ratio for the bond strength. The CFT connection tests results have unnaturally high variation because the peak applied loads do not always reflect bond failures (i.e., other failure modes govern the peak strength). An approximate result can be obtained by computing the resistance factor for the bond stress. The nominal bond stress given by Equations 13b and 14b is compared to the experimentally observed bond stress for the specimens in Tables 1 and 2. The resulting mean and coefficient of variation of the test-to-predicted ratio are presented in Table 9. In this case, only uncertainty from the bond stress will be included. Assuming a reliability index of 3.0, as is recommended for members (Ravindra and Galambos, 1978), the resistance factor is computed as 0.45 for RCFT and 0.55 for CCFT. A value of 0.45 is recommended for both shapes. The corresponding safety factor for allowable stress design is computed as 3.33 ($\Omega = 1.5/\phi$). These values are consistent with those in the current AISC *Specification* (2010).

DISTRIBUTION OF BOND STRESS ALONG COLUMN HEIGHT

The current (AISC, 2010) and the proposed design equations assume that the bond stress is uniform over a given height of the column. However, distribution of bond stress is known to vary both along the perimeter of the interface and along the height of the columns. This complex three-dimensional behavior is most accurately analyzed using detailed continuum finite element models (Roeder et al., 1999; Johansson, 2003). One-dimensional analysis, assuming constant behavior around the perimeter of the interface, complements the more detailed analyses and provides a valuable link between the complex three-dimensional behavior and

simple design equations. The derivation presented here is essentially a simple case of the bond model developed by Hajjar et al. (1998), applicable only to concentrically loaded columns with negligible geometric nonlinearity. This section thus assesses the nonlinear distribution of bond stress using one-dimensional analysis and justifies the use of a uniform bond stress in design calculations.

The distribution of bond stress along the height of the column depends on the response of the steel tube and the concrete core, as well as the interface between the two. A differential equation can be formed to describe the slip behavior by assessing equilibrium on an infinitesimal length of a CFT column. A free-body diagram of the CFT segment is shown in Figure 5. Equilibrium can be assessed for the steel and concrete components (Equation 16):

$$\Sigma F_{concrete} = A_c\sigma_c(x) - A_c\sigma_c(x+dx) - p\,dx\,\tau(x) = 0 \quad (16a)$$

$$\Sigma F_{steel} = A_s\sigma_s(x) - A_s\sigma_s(x+dx) + p\,dx\,\tau(x) = 0 \quad (16b)$$

where

A_s = cross-sectional area of the steel tube
A_c = cross-sectional area of the concrete core
p = perimeter of the steel–concrete interface
x = variable defined by the length along the CFT
dx = length of the segment of CFT analyzed (Figure 5)
$\sigma_s(x)$ = longitudinal stress in the steel tube
$\sigma_c(x)$ = longitudinal stress in the concrete core
$\tau(x)$ = bond stress

If elastic behavior is assumed (i.e., steel and concrete stresses are linear functions of strain and bond stress is a linear function of slip), the general solution of the resulting differential equation is Equation 17 (Denavit, 2012).

$$\tau(x) = C_1e^{Cx} + C_2e^{-Cx} \quad (17)$$

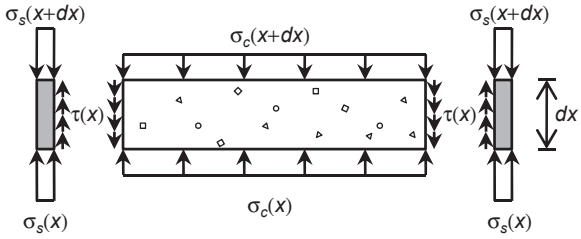

Fig. 5. Free-body diagram of CFT section.

where

$$C = \sqrt{\frac{p\kappa}{E_cA_c} + \frac{p\kappa}{E_sA_s}}$$

E_s = elastic modulus of the steel tube
E_c = elastic modulus of the concrete core
κ = elastic stiffness of the bond-slip relation
C_1 and C_2 = constants that depend on boundary conditions

The specific solution depends on the boundary conditions of the column. One representative case—one side of a shear connection where the peak bond stress is just reached and the column is of sufficient length to completely transfer the load—will be examined further. The boundary conditions for this case can be described by Equation 18:

$$\tau(0) = F_{in} \quad \tau(\infty) = 0 \quad (18)$$

Solving for the constants, the distribution of the bond stress is described by Equation 19. The equation indicates that the bond stress exponentially decays away from the point of load applications. The force transfer between materials persists along the full length of the column, although after a relatively short distance the bond stress is negligibly small. This behavior has been noted previously in analyses performed by Roeder et al. (1999).

$$\tau(x) = F_{in}e^{-Cx} \quad (19)$$

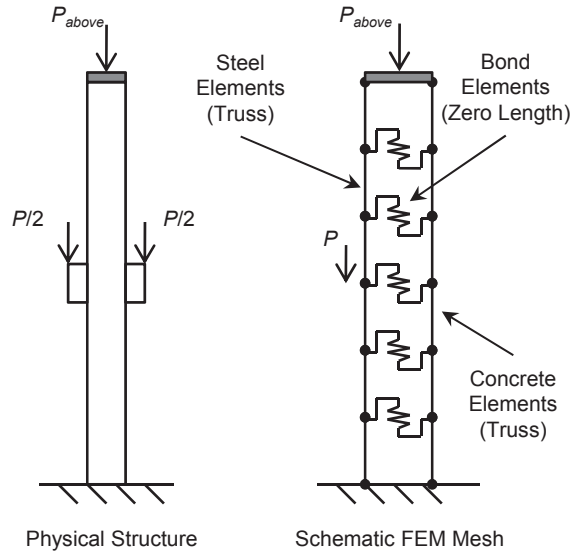

Fig. 6. Schematic of FEM mesh.

The load transferred can be computed by integrating along the length of the column and is found to be pF_{in}/C.

Examining the elastic behavior gives insight into the distribution of bond stress; however, nonlinearity in the steel tube, concrete core and bond behavior is expected at the ultimate limit state. A material nonlinear analysis was conducted using existing structural analysis formulations, noting that the governing differential equations can be modeled with two strands of linked truss elements. The steel tube and concrete core are modeled with truss elements, and the interface is modeled with zero length springs located at the nodes. This configuration is shown schematically in Figure 6. Typically, 200 elements along the length of the column were used in the analyses; the large number of elements provided for smooth results along the length of the column. When elastic materials are used, the analytical results (Equation 18) are captured exactly by this computational model. Suitable uniaxial material models have been developed in previous studies for RCFT (Tort and Hajjar, 2010) and CCFT (Denavit and Hajjar, 2012). An elastic–perfectly plastic model is used to describe the load-slip relationship with peak stress computed by Equation 13b for RCFT and Equation 14b for CCFT and the initial stiffness taken as 66 kip/in^3, based on recommendations by Hajjar et al. (1998).

Analyses were performed on column segments representing half the story height above and below a simple connection. Slip was constrained to be zero at the top and bottom of the column segment so that the introduction of load at the connection could be investigated without any influence of slip elsewhere in the column. The columns were subjected to a load applied at the top representing load in the column from upper stories and a load applied at the connection (midheight of the segment) equal to the nominal bond strength (Equation 13a for RCFTs and Equation 14a for CCFTs). Results include the distribution of slip, bond stress and axial load in the steel tube and concrete core along the height of the column. Sample results from one analysis are shown in Figure 7 for a 10-ft-long segment of a CCFT column constructed from an HSS 7.500×0.250 (F_y = 42 ksi, t_{design} = 0.233 in, F_{in} = 127.2 psi) and normal-strength concrete (f'_c = 4 ksi). A load of 74.2 kips ($0.2P_{no}$) was applied at the top, and a load of 211.9 kips was applied at the connection.

The horizontal dashed lines denote the nominal bond length ($C_{in}D$) in which the bond stress is assumed active in the design formulation. The nonlinear analysis confirms that the majority of the force transfer occurs in this region, although not all, with some slip extending both above and below this region. The distribution of slip is not symmetric about the connection, with the equilibrium achieved in a shorter length below the connection than above. This is due to the gradual decrease in stiffness of the steel tube and concrete core as loads are increased. The variation in stiffness with loading is also seen in the load sharing in the equilibrium regions. Above the connection the steel carries 52% of the axial load, while below the connection the steel carries 60% of the axial load. The percentage below the connection is in agreement with the AISC *Specification* (Equation 9), but because the percentage above is lower, the transferred

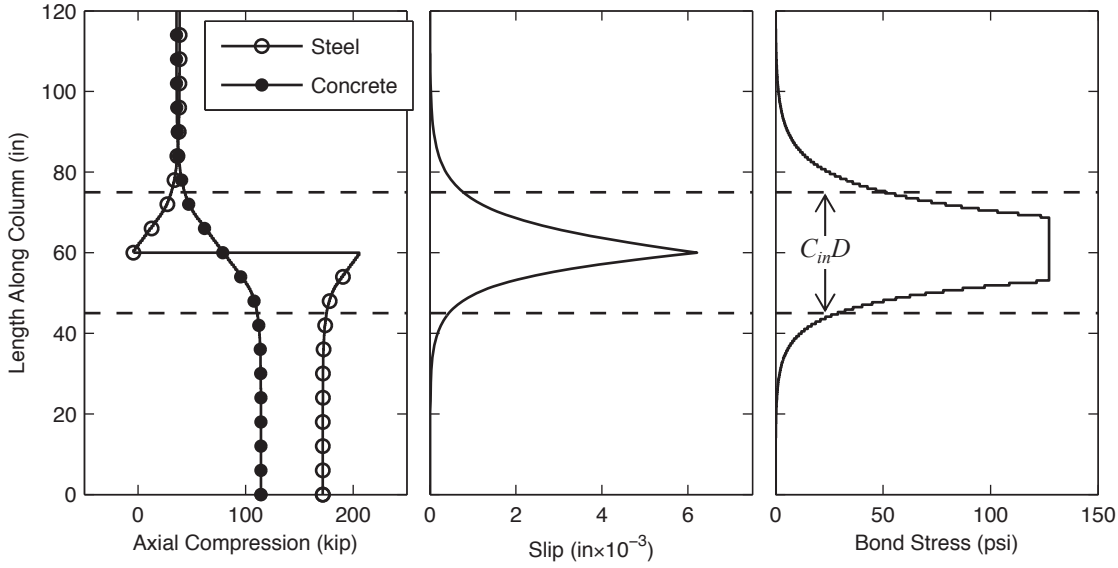

Fig. 7. Sample results of nonlinear bond analysis.

load is slightly underpredicted. The magnitude of slip at the nominal bond strength is rather small (on the order of one-hundredth of an inch), confirming that natural bond strength should not be superimposed with other force transfer mechanisms that may not develop their full strength at these low levels of deformation.

CONCLUSIONS

Current design provisions for the natural bond strength are overly simple and are found to be conservative for the cases examined. A new formula for nominal bond strength of CFT structures is proposed in this paper. The critical bond stress, given as a function of tube dimensions, is derived from results of push-out test and varies between RCFT and CCFT. The effective bond transfer area is determined based on an examination of experimental observations and results from specially instrumented connection tests. The resistance factor is computed as 0.45, and the safety factor is computed as 3.33, based on the bond stress formula. Using a one-dimensional model, the behavior of the connection region of a column was examined. The distribution of bond stress and the load deformation response at the joint both indicate that the proposed design formula is safe.

Finally, it is noted that because the proposed formula is based on experimental results that do not generally exhibit a bond slip failure, there is a degree of conservatism in the design recommendations. Thus, future experimental and analytical research is warranted to explore the behavior of CFT columns subjected large transfer forces.

NOTATION

A_c, A_s	Cross-sectional area of the concrete and steel
B	Overall width of rectangular steel section ($B \leq H$)
C	Constant in bond stress formula (Equation 16)
C_{in}	Coefficient for longitudinal bond height
D	Outside diameter of round steel section
E_c, E_s	Modulus of elasticity of the concrete and steel
F_{cr}	Critical compressive stress of the steel ($F_{cr} \leq F_y$)
F_{in}	Nominal bond stress
F_y	Steel yield strength
H	Overall height of rectangular steel section ($H \geq B$)
L	Specimen length
L_{bond}	Length used when determining bond strength
$L_{transfer}$	Length along the column where significant bond stresses occur
$P_{applied}$	Applied force
P_{no}	Nominal CFT section compressive strength
R_n	Nominal bond strength
$V'_{applied}$	Portion of applied force that is transferred
d_c, d_s	Displacement of the concrete and steel
f'_c	Concrete compressive strength
p	Perimeter of the steel–concrete interface
s	Slip
t	Thickness of steel tube
Ω	Safety factor
β	Applied load ratio
ϕ	Resistance factor
κ	Bond stiffness
σ_c, σ_s	Longitudinal stress of the concrete and steel
τ	Shear stress at steel–concrete interface

ACKNOWLEDGMENTS

Funding for this research was provided by the National Science Foundation under Grant No. CMMI-0619047, the American Institute of Steel Construction, the National Natural Science Foundation of China (90815029, 51021140006), China Scholarship Council (2007102420) and the University of Illinois at Urbana-Champaign. The authors thank Steven Palkovic, Matthew Eatherton and Luis Pallarés for their assistance with this research.

REFERENCES

AISC (2010), *Specification for Structural Steel Buildings*, ANSI/AISC 360-10, American Institute of Steel Construction, Chicago, IL.

Aly, T., Elchalakani, M., Thayalan, P. and Patnaikuni, I. (2010), "Incremental Collapse Threshold for Pushout Resistance of Circular Concrete Filled Steel Tubular Columns," *Journal of Constructional Steel Research*, Vol. 66, No. 1, pp. 11–18.

Bridge, R. and Webb, J. (1993), "Thin Walled Circular Concrete Filled Steel Tubular Columns," *Composite Construction in Steel and Concrete II*, American Society of Civil Engineers, New York, pp. 634–649.

CEN (2004), *Eurocode 4: Design of Composite Steel and Concrete Structures*, EN1994-1-1, European Committee for Standardization, Brussels, Belgium.

Denavit, M.D. (2012), "Characterization of Behavior of Steel–Concrete Composite Members and Frames with Applications for Design," Ph.D. Dissertation, Department of Civil and Environmental Engineering, University of Illinois at Urbana–Champaign, Urbana, IL.

Denavit, M.D. and Hajjar, J.F. (2012), "Nonlinear Seismic Analysis of Circular Concrete-Filled Steel Tube Members and Frames," *Journal of Structural Engineering*, ASCE, Vol. 138, No. 9, pp. 1089–1098.

Dunberry, E., LeBlanc, D. and Redwood, R.G. (1987), "Cross-Section Strength of Concrete-Filled HSS Columns at Simple Beam Connections," *Canadian Journal of Civil Engineering*, Vol. 14, No. 2, pp. 408–417.

Hajjar, J.F., Schiller, P.H. and Molodan, A. (1998), "A Distributed Plasticity Model for Concrete-Filled Steel Tube Beam-Columns with Interlayer Slip," *Engineering Structures*, Vol. 20, No. 8, pp. 663-676.

Johansson, M. (2003), "Composite Action in Connection Regions of Concrete-Filled Steel Tube Columns," *Steel & Composite Structures*, Vol. 3, No. 1, pp 47–64.

Morishita, Y., Tomii, M. and Yoshimura, K. (1979a), "Experimental Studies on Bond Strength in Concrete Filled Circular Steel Tubular Columns Subjected to Axial Loads," *Transactions of the Japan Concrete Institute*, Vol. 1, pp. 351–358.

Morishita, Y., Tomii, M. and Yoshimura, K. (1979b), "Experimental Studies on Bond Strength in Concrete Filled Square and Octagonal Steel Tubular Columns Subjected to Axial Loads," *Transactions of the Japan Concrete Institute*, Vol. 1, pp. 359–366.

Parsley, M.A., Yura, J.A. and Jirsa, J.O. (2000), "Push-Out Behavior of Rectangular Concrete-Filled Steel Tubes," *Composite and Hybrid Systems*, ACI SP-196, American Concrete Institute, Farmington Hills, MI, pp. 87–107.

Ravindra, K.M. and Galambos, V.T. (1978), "Load and Resistance Factor Design for Steel," *Journal of Structural Division*, ASCE, Vol. 104, No. ST9, pp. 1337–1353.

Roeder, C.W., Cameron, B. and Brown, C.B. (1999), "Composite Action in Concrete Filled Tubes," *Journal of Structural Engineering*, ASCE, Vol. 125, No. 5, pp. 477–484.

Roeder, C.W., Lehman, D.E., and Thody, R. (2009), "Composite Action in CFT Components and Connections," *Engineering Journal*, AISC, Vol. 46, No. 4, pp. 229–242.

Shakir-Khalil, H. (1991), "Bond Strength in Concrete-Filled Steel Hollow Sections," *International Conference on Steel and Aluminum Structures*, Singapore, May 22–24, pp. 157–168.

Shakir-Khalil, H. (1993a), "Full-Scale Tests on Composite Connections," *Composite Construction in Steel and Concrete II*, American Society of Civil Engineers, New York, pp. 634–649.

Shakir-Khalil, H. (1993b), "Pushout Strength of Concrete-Filled Steel Hollow Sections," *The Structural Engineer*, Vol. 71, No. 13, pp. 230–233.

Shakir-Khalil, H. (1993c), "Resistance of Concrete-Filled Steel Tubes to Pushout Forces," *The Structural Engineer*, Vol. 71, No. 13, pp. 234–243.

Shakir-Khalil, H. (1993d), "Connection of Steel Beams to Concrete-Filled Tubes," *Proc. 5th International Symposium on Tubular Structures*, Nottingham, England, UK, August 25–27, pp. 195–203.

Shakir-Khalil, H. (1994a), "Finplate Connections to Concrete-Filled Tubes," *Proc. 4th International Conference on Steel-Concrete Composite Structures*, Kosice, Slovakia, June 20–23, pp. 181–185.

Shakir-Khalil, H. (1994b), "Beam Connections to Concrete-Filled Tubes," *Proc. 6th International Symposium on Tubular Structures*, Melbourne, Australia, December 14–16, pp. 357–364.

Shakir-Khalil, H. and Al-Rawdan, A. (1995), "Behavior of Concrete-Filled Tubular Edge Columns," *Proc. 3rd International Conference on Steel and Aluminum Structures*, Istanbul, Turkey, May, pp. 515–522.

Tomii, M. (1985), "Bond Check for Concrete-Filled Steel Tubular Columns," *Composite and Mixed Construction*, American Society of Civil Engineers, New York, pp. 195–204.

Tomii, M., Yoshimura, K. and Morishita, Y. (1980a), "A Method of Improving Bond Strength Between Steel Tube and Concrete Core Cast in Square and Octagonal Steel Tubular Columns," *Transactions of the Japan Concrete Institute*, Tokyo, Vol. 2, pp. 327–334.

Tomii, M., Yoshimura, K. and Morishita, Y. (1980b), "A Method of Improving Bond Strength Between Steel Tube and Concrete Core Cast in Circular Steel Tubular Columns," *Transactions of the Japan Concrete Institute*, Tokyo, Vol. 2, pp. 319–326.

Tort, C. and Hajjar, J. F. (2010), "Mixed Finite-Element Modeling of Rectangular Concrete-Filled Steel Tube Members and Frames under Static and Dynamic Loads," *Journal of Structural Engineering*, ASCE, Vol. 136, No. 6, pp. 654–664.

Virdi, K.S. and Dowling, P.J. (1980), "Bond Strength in Concrete Filled Steel Tubes," *IABSE Periodical*, August, pp. 125–139.

Xu, C., Chengkui, H., Decheng, J. and Yuancheng, S. (2009), "Push-Out Test of Pre-Stressing Concrete Filled Circular Steel Tube Columns by Means of Expansive Cement," *Construction and Building Materials*, Vol. 23, pp. 491–497.

Yin, X. and Lu, X. (2010), "Study on Push-Out Test and Bond Stress-Slip Relationship of Circular Concrete Filled Steel Tube," *Steel and Composite Structures*, Vol. 10, No. 4, pp. 317–329.

Beam Deflections and Stresses During Lifting

R.H. PLAUT, C.D. MOEN and R. COJOCARU

This paper first appeared in the proceedings of the Structural Stability Research Council Annual Stability Conference in Pittsburgh, PA, May 10–14, 2011.

ABSTRACT

The behavior of horizontally curved beams during lifting is analyzed. The beams are circularly curved, doubly symmetric, prismatic and linearly elastic, and they are suspended at two symmetric locations. The two cables lifting the beams may be vertical or inclined symmetrically. Numerical results are presented for steel I-beams. Weak-axis and strong-axis deflections, roll angle and cross-sectional twist, internal forces, bending and twisting moments, and longitudinal stresses are calculated using newly derived analytical solutions implemented as a freely available spreadsheet at http://www.moen.cee.vt.edu. Lifting locations along the beam that minimize displacements and stresses are identified.

Keywords: lifting beams, twisting, deflections.

INTRODUCTION

When a horizontally curved beam is lifted by two cables, it tends to roll (rotate) about an axis above the beam. If the lift points are not approximately one-fifth of the beam's length from the near end, the beam may roll significantly. This causes weak-axis bending and cross-sectional twist to occur. Excessive roll and twist may cause difficulties when the beam is put into place, e.g., on permanent or temporary bridge supports. The objectives of the present study are to obtain analytical solutions for a basic class of beams and to determine the effects of various parameters, such as the locations of the lift points. For suspended beams that are intentionally curved, or are meant to be straight but have an imperfection in shape, the displacements and stresses are of concern, but lateral buckling is typically not an issue (Petruzzi, 2010; Plaut and Moen, 2011).

In the analysis, the beams are circularly curved (horizontally), the curvature is small, and the cross-sectional dimensions are small compared to the radius of curvature. The cross-section is uniform and doubly symmetric, and its center of gravity coincides with its shear center. The analytical formulation is also accurate for singly symmetric sections when the center of twist (shear center) is close to the cross-section centroid (Cojocaru, 2012). The cross-section is rigid and does not change shape as the beam rolls and deforms. The material behavior is linearly elastic and the displacements are small. The beam is subjected to its self-weight and to the two supporting cable forces that are symmetric with respect to midspan.

Investigations on the lifting of straight or curved beams include Mast (1989), Dux and Kitipornchai (1990), and Stratford and Burgoyne (2000). Additional references are listed in Plaut and Moen (2012). A recent research project at the University of Texas at Austin studied the behavior of curved steel I-beams during lifting with vertical cables (e.g., Farris, 2008; Schuh, 2008; Petruzzi, 2010; Stith, 2010). Results of some tests were presented, and the analysis was mainly conducted using the finite element software ANSYS. A software program called UT Lift was developed along with another program called UT Bridge that relates to bridge construction.

This current investigation complements the University of Texas research. The focus is not solely on steel I-beams and the supporting cables may be inclined. Instead of applying the finite element method, the results are obtained from new analytical equations (Plaut and Moen, 2012) implemented as a freely available spreadsheet at http://www.moen.cee.vt.edu/. However, this study is more restricted in some aspects because it does not include nonprismatic beams, nonsymmetric lift points, or the effect of attached cross frames.

FORMULATION

The beam is depicted in Figure 1. A perspective with inclined cables is shown in Figure 1a; a top view in Figures 1b and 1c; a side view (from the center of curvature) in Figure 1d; and another perspective in Figure 1e. The unstrained beam has radius of curvature R, length L, cross-sectional

R.H. Plaut, D. H. Pletta Professor of Engineering (Emeritus), Virginia Tech, Blacksburg, VA. E-mail: rplaut@vt.edu

C.D. Moen, Assistant Professor, Virginia Tech, Blacksburg, VA (corresponding). E-mail: cmoen @vt.edu

R. Cojocaru, Graduate Research Assistant, Virginia Tech, Blacksburg, VA. E-mail: cojocaru@vt.edu

area A, modulus of elasticity E, shear modulus G, torsional constant J, warping constant C_w and self-weight q per unit length.

The subtended angle of the beam is 2a, and the cylindrical coordinate θ is zero at midspan. The connection points D and K of the two cables are located at the lift points $\theta = -\gamma$ and γ, respectively, at a distance a from the near end of the beam and at a height H above the shear center and parallel to the y-axis (the weak axis). The line passing through D and K, which is dashed in Figure 1e, is called the roll axis (or axis of rotation). The inclination angle of the cables from the vertical is y toward midspan, and the offset of the center of the beam from the chord through the ends is denoted δ.

Figure 1a shows the principal axes y and z of the cross-section and the longitudinal x-axis, which is tangential to the curved axis of the member through the shear center. The origin is at midspan, so that $x = R\theta$. The longitudinal deflection is U, the strong-axis deflection is V, the weak-axis deflection is W (positive if radially outward) and the angle of twist is ϕ. The moments of inertia for strong-axis and weak-axis bending, respectively, are I_z and I_y.

The center of gravity of the unstrained beam lies along the central ray $\theta = 0$ and at a radial distance (eccentricity) e from the roll axis, as shown in Figure 1c. If the center of gravity of the entire beam does not lie in the vertical plane that includes the roll axis, then the beam exhibits a rotation about the roll axis, as shown in Figure 1e, until its center of gravity lies in that vertical plane. If the beam were rigid, the roll angle would be $\beta_{rigid} = \arctan(e/H)$ (Schuh, 2008). The deformation causes the actual roll angle β to be different.

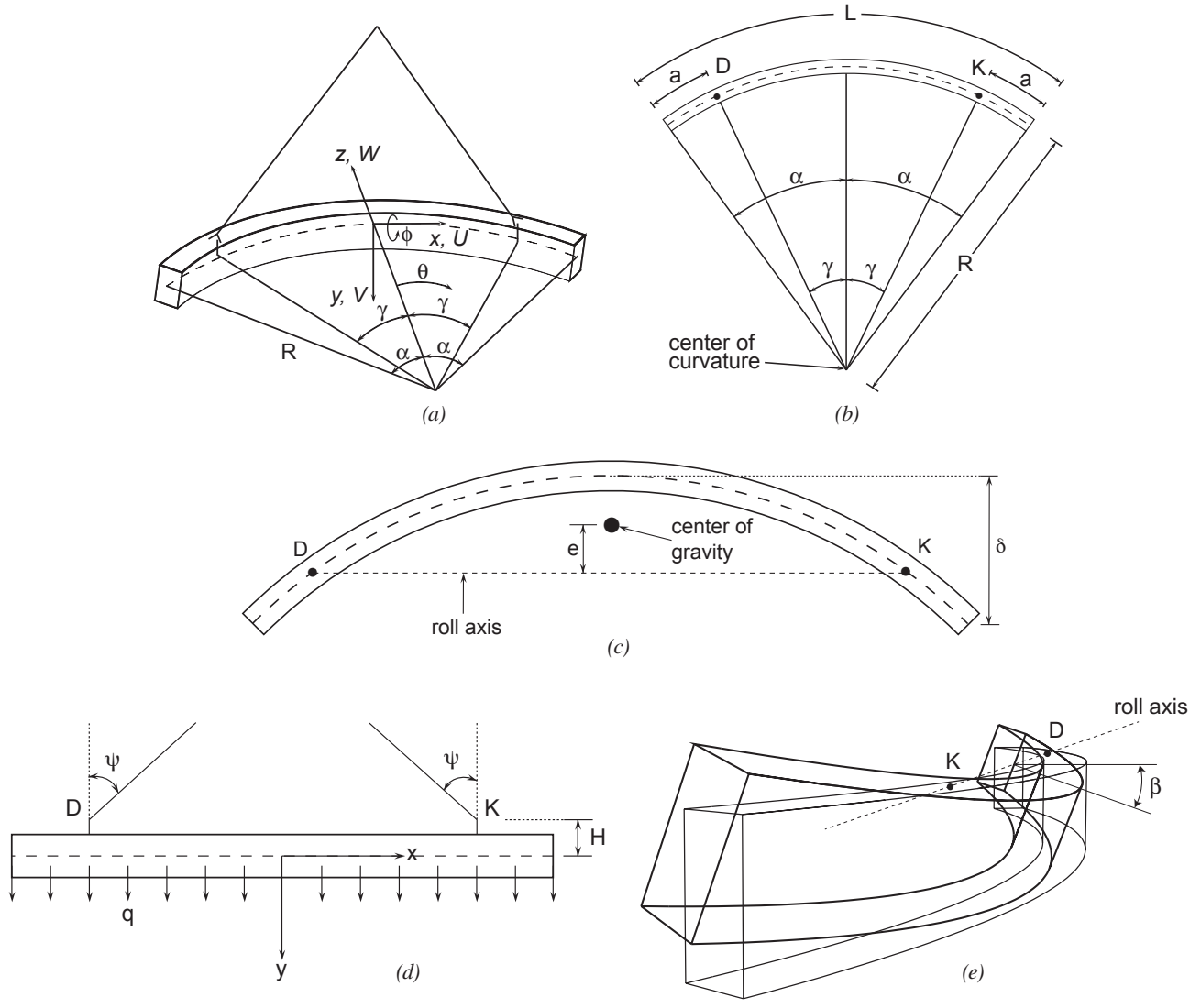

Fig. 1. Geometry of beam: (a) perspective; (b) top view; (c) top view; (d) side view; (e) rotation about roll axis.

Table 1. Properties of Steel I-Beams						
b_f (in.)	A (in.^{2})	q (kip/ft)	I_y (in.^{4})	I_z (in.^{4})	J (in.^{4})	C_w (in.^{6})
12	87.75	0.299	434	65,300	36.7	0.537×10^6
18	105.75	0.360	1,460	87,600	50.2	1.812×10^6
24	123.75	0.421	3,458	110,000	63.7	4.294×10^6

The total rotation of the plane of the cross-section at location θ is $\beta\cos(\theta) - \phi$, and it is assumed that V, W and ϕ are zero at the lift points [so that the total rotation there is $\beta\cos(\gamma)$]. The equation for β, along with analytical equations that furnish the internal forces and moments, deflections, twist and stresses, are given in Plaut and Moen (2012).

The roll angle β is usually zero when a/L is approximately 0.21 (Schuh, 2008; Plaut and Moen, 2012). For smaller values of a/L, β is positive, and for larger values of a/L, β is negative. As a/L decreases or increases from 0.21, the magnitude of the roll angle increases.

EXAMPLE

Three steel I-beams, similar to ones in Schuh (2008), are considered. The beams have $\delta/L = 0.01$, $L = 90$ ft, $R = 1{,}125$ ft, web depth $h_w = 69$ in., web thickness $t_w = 0.75$ in., flange thickness $t_f = 1.5$ in., $H = 66$ in., $E = 29{,}000$ ksi, Poisson's ratio = 0.3 and specific weight = 490 lb/ft^3. The cables are vertical ($\psi = 0$). Three flange widths, $b_f = 12$ in., 18 in. and 24 in., are considered, and the corresponding values of A, q, I_y, I_z, J and C_w are listed in Table 1. The effect of the normalized overhang length is examined for the range $0.1 \le a/L \le 0.4$.

Figure 2 shows how the roll angle β varies with a/L. For small overhang lengths a, the roll angle β is positive and the cross-section tilts so that its top edge moves outward (away from the center of curvature), as shown in Figure 1e. For large overhang lengths, it tilts in the opposite direction. The magnitude of the roll angle tends to decrease slightly as the flange width increases from 12 in. to 24 in.

The twist ϕ at midspan is plotted in Figure 3. It is positive for an intermediate range of the overhang length and negative otherwise. Figure 4 depicts how the overhang length affects the twist at the end of the beam ($x = L/2$). For a given value of a/L, as the flange width increases, the magnitudes of the midspan and end twist usually decrease.

It has been recommended that the magnitude of the total rotation, $|\beta\cos(\theta) - \phi|$, be less than 1.5° (Farris, 2008). The overhang length is critical with regard to this criterion. For

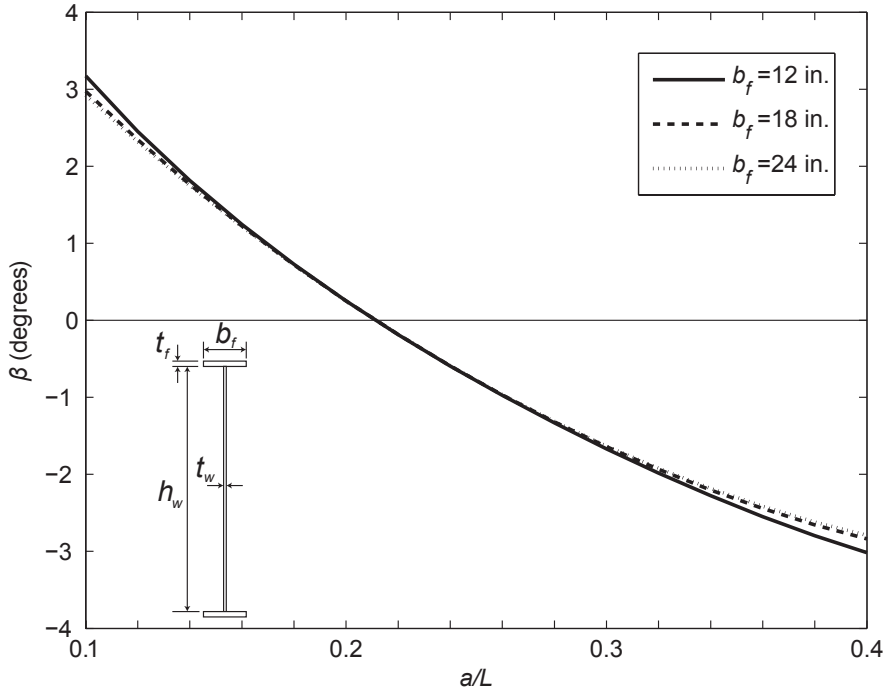

Fig. 2. Roll angle versus normalized overhang length a/L.

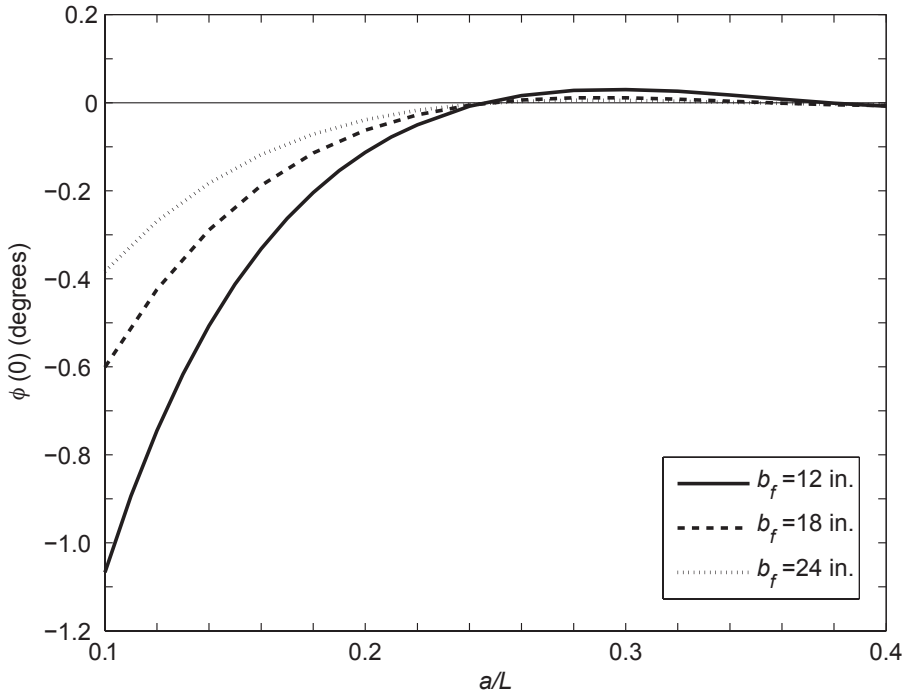

Fig. 3. Twist at midspan versus a/L.

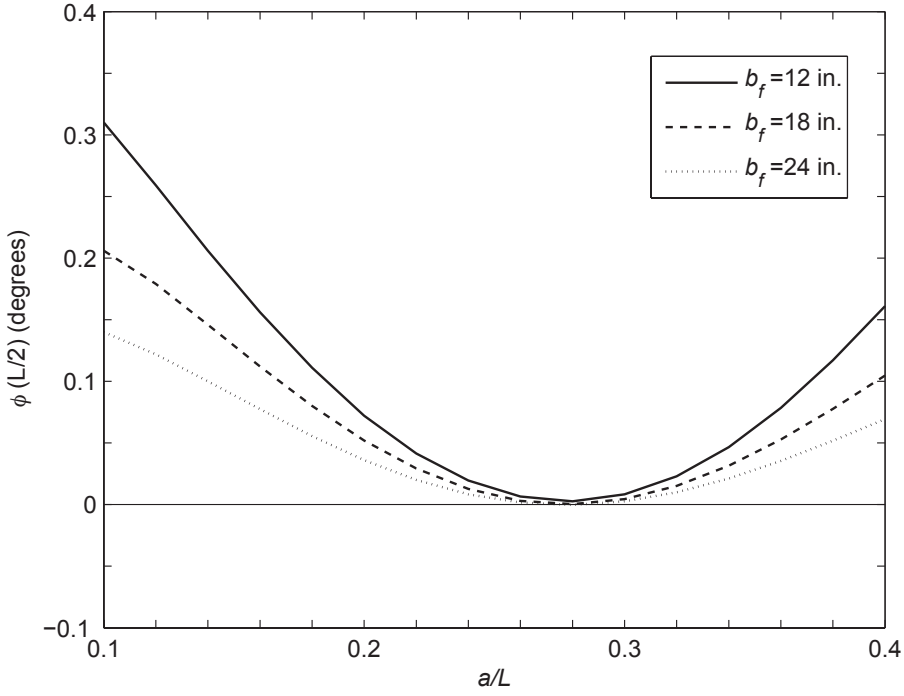

Fig. 4. Twist at end versus a/L.

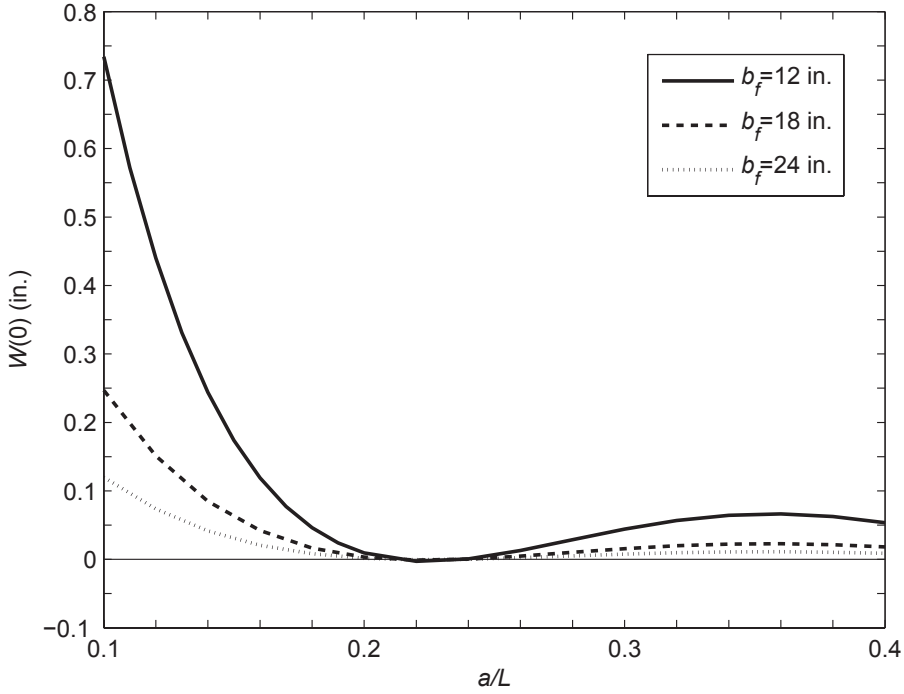

Fig. 5. Weak-axis deflection at midspan versus a/L.

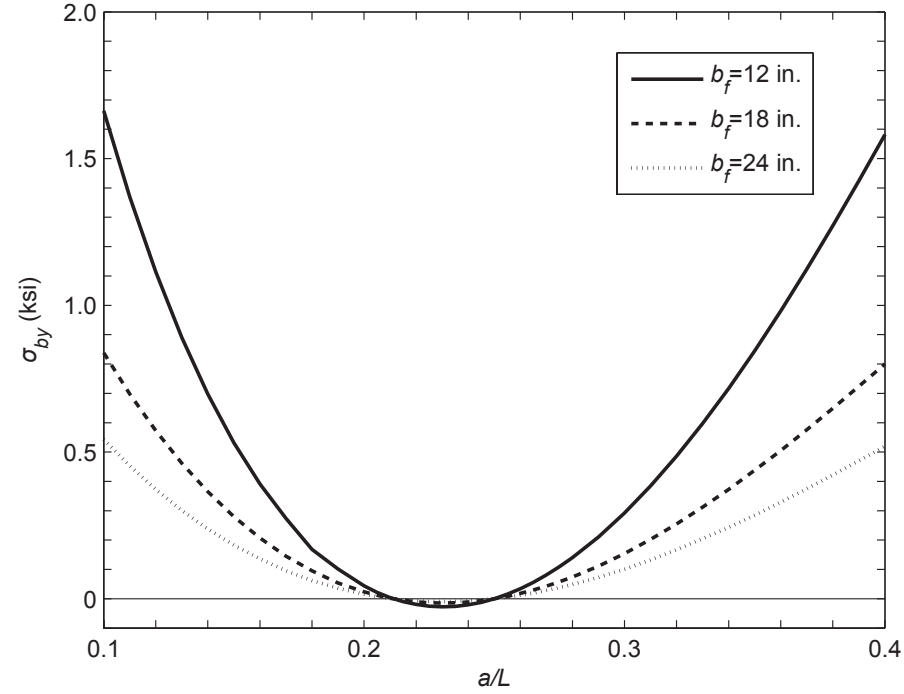

Fig. 6. Longitudinal stress at midspan tip due to weak-axis bending versus a/L.

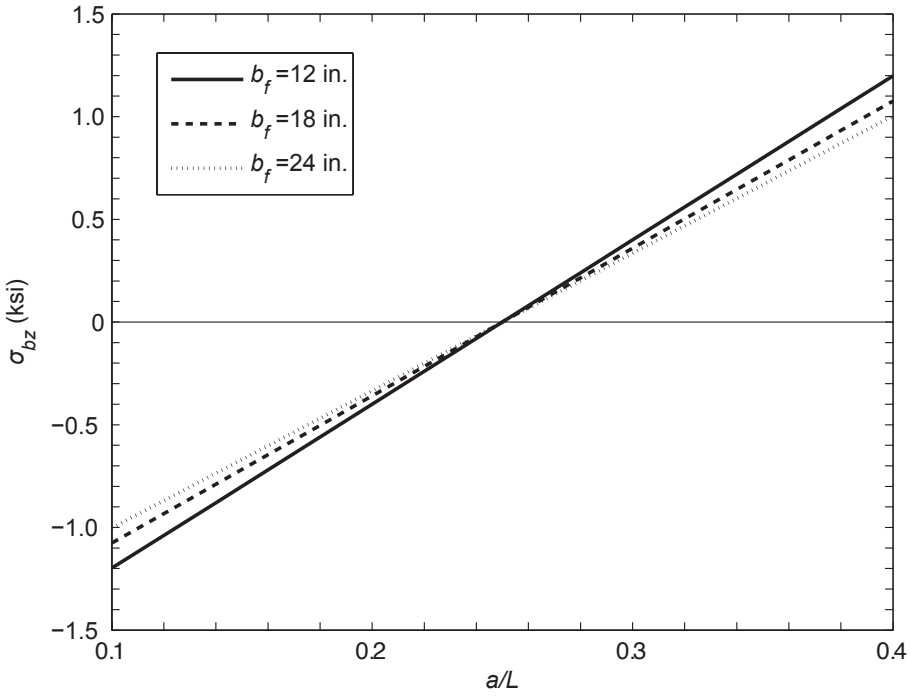

Fig. 7. Longitudinal stress at midspan tip due to strong-axis bending versus a/L.

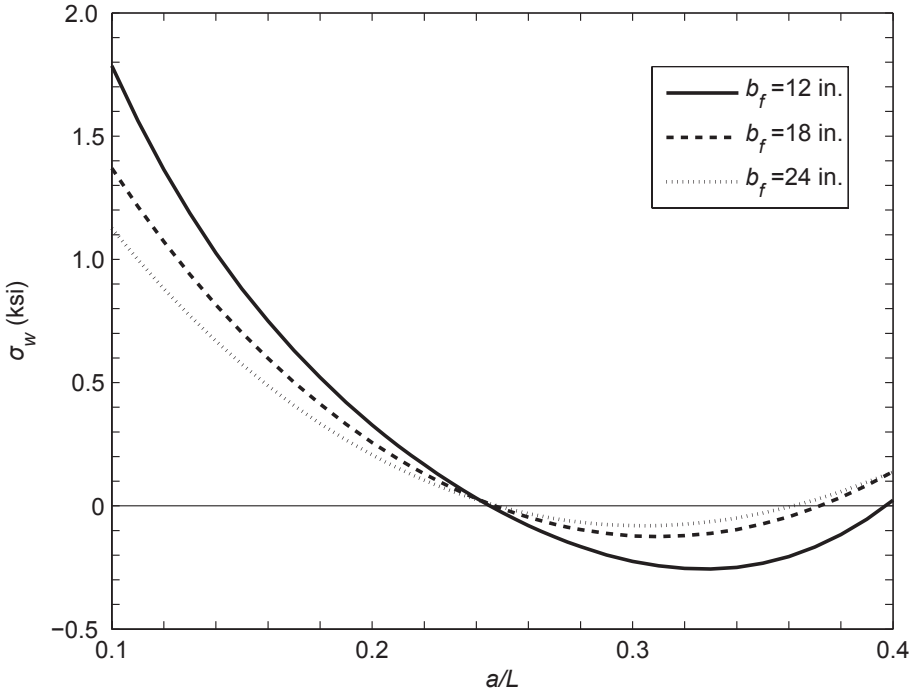

Fig. 8. Longitudinal stress at midspan tip due to warping versus a/L.

the three flange widths considered, the criterion is satisfied at midspan if $0.17 < a/L < 0.29$ and at the end of the beam if $0.14 < a/L < 0.29$.

In Figure 5, the weak-axis deflection W at midspan is plotted versus a/L. The roll angle is zero when $a/L = 0.211$, and this deflection $W(0)$ becomes slightly negative for a small range around $a/L = 0.22$. As the flange width increases, the midspan deflection tends to decrease.

With regard to possible buckling of the flange due to compression, it is important to know the magnitude of the longitudinal (normal) stress acting on the cross-section. The maximum value occurs at midspan and, in general, is a combination of stresses due to axial load, weak-axis bending, strong-axis bending and warping (Seaburg and Carter, 1997; Stith, 2010). The first of these stresses is zero here because the cables are vertical, i.e., $\psi = 0$. Summing the values of the maximum magnitudes of each of the other stresses at the tips of the flanges, one can write an upper bound as $\sigma_n = |\sigma_{by}| + |\sigma_{bz}| + |\sigma_w|$, where the stress contributions at a tip at midspan are σ_{by} due to weak-axis bending, σ_{bz} due to strong-axis bending and σ_w due to warping normal stress.

The longitudinal stress σ_{by} due to weak-axis bending is shown in Figure 6 for the three steel I-beams. It is highest for $b_f = 12$ in. and lowest for $b_f = 24$ in. For all three cases, $\sigma_{by} = 0$ at $a/L = 0.21$ and 0.25, and σ_{by} is very small if the lift points lie between those locations.

Figure 7 depicts the longitudinal stress σ_{bz} due to strong-axis bending. This stress is zero at $a/L = 0.25$. The highest magnitude occurs for $b_f = 12$ in., the case with the highest ratio A/I_z.

In Figure 8, the midspan stress σ_w due to warping normal stress is plotted. It is zero at $a/L = 0.25$ for the three cases, and again at $a/L = 0.40$, 0.37 and 0.36, respectively, for $b_f =$ 12, 18 and 24 in. In comparing Figures 6, 7 and 8, the magnitude of σ_w is larger than the magnitudes of σ_{by} and σ_{bz} for all three cases if a/L is small.

Finally, the sum σ_n of the magnitudes of these three normal stresses is depicted in Figure 9. It is zero at $a/L = 0.25$, and elsewhere is highest for $b_f = 12$ in. In the range shown, and for these three steel I-beams, the longitudinal stresses are not very large. Similar magnitudes were found in tests reported in Schuh (2008).

CONCLUSION

The locations of the lift points are most important. If the distance between each lift point and the near end of the beam is not approximately one-fifth of the beam's length, the beam may rotate significantly and exhibit undesirably large displacements and stresses. It is also important that the torsional constant and the weak-axis moment of inertia not be too small, so that the weak-axis deflection and cross-sectional twist are not too large.

Lateral buckling is possible if the beam is perfectly straight, but even then it will not occur for reasonably designed beams and lift points (i.e., if the bending stiffness and torsional stiffness are not extremely small and the

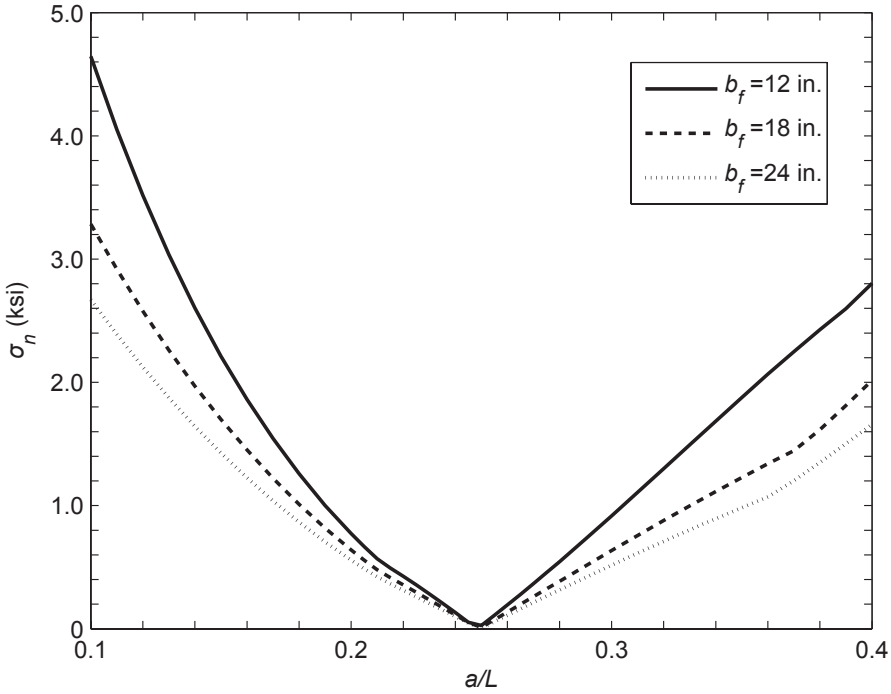

Fig. 9. Upper bound on magnitude of longitudinal stress at midspan versus a/L.

beam is not lifted near its ends). The governing equations for lateral buckling are presented in Plaut and Moen (2011). For the steel I-beams considered here, the corresponding 90-ft-long straight beam would have a critical specific weight that is larger than the specific weight of steel by factors 2.2, 4.4 and 7.4, respectively, if b_f = 12, 18 and 24 in. and if the lift points are at the ends ($a = 0$). The factors are larger if the lift points are not at the ends ($a > 0$).

Results were presented here for steel beams with length L = 90 ft, web depth h_w = 69 in., offset ratio δ/L = 0.01 and vertical cables ($\psi = 0$). In Plaut and Moen (2011), larger steel beams are analyzed, with L = 124.1 ft, h_w = 84 in., δ/L = 0.01276 and $\psi = 0$. In addition, results are given for beams with rectangular cross-section and small initial curvature (i.e., an imperfection from a straight beam). The beams have L = 150 ft, depth d = 60 in., width b = 12 in. and δ/L = 0.001. Cable inclination angles from $\psi = 0$ to 45° are considered. An increase in ψ tends to induce compression in the internal portion of the beam and to increase the deformations.

A spreadsheet that implements the Plaut and Moen (2012) analytical solution is freely available at http://www.moen.cee.vt.edu.

REFERENCES

Cojocaru, R. (2012), *Lifting Analysis of Precast Prestressed Concrete Beams*, Master's Thesis, Virginia Tech, Blacksburg, VA.

Dux, P.F. and Kitipornchai, S. (1990), "Stability of I-Beams under Self-Weight Lifting," *Journal of Structural Engineering*, ASCE, Vol. 116, No. 7, pp. 1877–1891.

Farris, J.F. (2008), *Behavior of Horizontally Curved Steel I-Girders During Construction*, Master's Thesis, University of Texas at Austin, Austin, TX.

Mast, R.F. (1989), "Lateral Stability of Long Prestressed Concrete Beams, Part 1," *PCI Journal*, PCI, Vol. 34, No. 1, pp. 34–53.

Petruzzi, B.J. (2010), *Stabilizing Techniques for Curved Steel I-Girders During Construction*, Master's Thesis, University of Texas at Austin, Austin, TX.

Plaut, R.H. and Moen, C.D. (2011), *Theory and Applications of the Lifting of Elastic, Doubly Symmetric, Horizontally Curved Beams*, Technical Report CE/VPI-ST11/04, Structural Engineering and Materials, Department of Civil and Environmental Engineering, Virginia Tech, Blacksburg, VA.

Plaut, R.H. and Moen, C.D. (2012), "Analysis of Elastic, Doubly Symmetric, Horizontally Curved Beams During Lifting," *Journal of Structural Engineering,* ASCE, in press.

Schuh, A.C. (2008), *Behavior of Horizontally Curved Steel I-Girders During Lifting*, Master's Thesis, University of Texas at Austin, Austin, TX.

Seaburg, P.A. and Carter, C.J. (1997), *Torsional Analysis of Structural Steel Members*, Steel Design Guide Series 9, American Institute of Steel Construction, Chicago, IL.

Stith, J.C. (2010), *Predicting the Behavior of Horizontally Curved I-Girders During Construction*, Ph.D. thesis, University of Texas at Austin, Austin, TX.

Stratford, T.J. and Burgoyne, C.J. (2000), "The Toppling of Hanging Beams." *International Journal of Solids and Structures*, Vol. 27, No. 26, pp. 3569–3589.

Current Steel Structures Research

No. 32

REIDAR BJORHOVDE

INTRODUCTION

This issue of "Current Steel Structures Research" for the *Engineering Journal* focuses on a selection of research projects at three European universities. The descriptions will not discuss all of the current projects at the schools. Instead, selected studies provide a representative picture of the research work and demonstrate the importance of the schools to the home countries—and indeed to the efforts of industry and the profession worldwide.

The universities and many of their researchers are very well known in the world of steel construction: the University of Sheffield in Sheffield, England; Luleå University of Technology in Luleå, Sweden; and the University of Trento in Trento, Italy. The studies presented here reflect elements of the projects as well as other significant ongoing activities. As has been typical of European engineering research projects for many years, most of the projects are multiyear efforts and many are multipartner efforts. This calls for very careful planning, cooperation and implementation of research needs and applications, including the education of graduate students and advanced researchers. As is also the case for American research work, the outcomes of the projects focus on industry needs and implementation of the results in design standards.

The lead researchers have been active for many years, as evidenced by their prominent roles in research and development in their respective countries, but they have also been frequent participants in projects elsewhere. Many English-language technical papers and conference presentations have been published, contributing to a collection of studies that continues to offer solutions to complex problems for designers, fabricators and erectors. Many of these projects complement past and current work from around the globe.

References are provided throughout this paper, whenever such are available in the public domain. However, much of the work is still in progress, and in some cases reports or other publications have not yet been prepared for public dissemination.

Reidar Bjorhovde, Dr.-Ing., Ph.D., P.E., Research Editor of the *Engineering Journal.* Tucson, AZ. Email: rbj@bjorhovde.com

SOME CURRENT RESEARCH WORK AT THE UNIVERSITY OF SHEFFIELD IN SHEFFIELD, ENGLAND

The University of Sheffield has been active in steel structures research for many years. For the past 20 years, the university has been a worldwide leader in the complex subject of the response of steel and composite structures to fire, with Professor Ian Burgess as the lead researcher. Research that began with the behavior of individual beams and columns is now focused on the performance of building structures as a whole. Attention to the subject was significantly expanded through the full-scale fire tests conducted on a composite frame at the Building Research Establishment at Cardington, England, during the 1990s, where the Sheffield group participated. The initial studies focused on analytical solutions that continue to be the main emphasis of the Sheffield fire research. However, a number of recent projects have involved major physical tests, using unique, purpose-built facilities.

The group has been working for a number of years toward establishing a practical robustness analysis for steel and composite buildings. This is very much in line with the recommendations that were made after the World Trade Center disaster in New York. Efforts are now being directed toward the development of a general performance-based fire resistance design approach, moving away from the current prescriptive rules. Because connections are recognized as the most vulnerable parts of a structure, the state-of-the-art reflects modeling of their behavior as integral elements of the structural models. This is facilitated by progressive failure analyses of the components, incorporating limit states of local or overall building collapse. A significant advance is the development of component-based models of various types of connections that are suitable for use in fire engineering structural analysis. Some current research projects are presented in the following sections.

Design of Beam to Composite Column Connections for Improved Fire Robustness: This is part of the European Union funded project COMPFIRE, a joint effort of the universities of Sheffield and Manchester in England, the University of Coimbra in Portugal (lead institution), Luleå Technological University in Sweden and the Czech Technical University in Prague in the Czech Republic. Additional work is provided by the steel producer Tata Steel Research, Development and Technology. The project director in

Sheffield is Professor Ian Burgess; additional Sheffield researchers are Drs. Buick Davison and S.-S. Huang.

The project addresses the behavior and robustness of practical connections between steel or composite beams and two types of composite columns: concrete-filled tubes and partially encased W-shapes with concrete infilled between the flanges. The Sheffield work includes physical tests of flush end-plate and so-called reverse-channel connections and includes the development of component-based analytical models for such connections. Large rotation tests of full-scale connections have been tested at constant temperatures using combinations of tensile and shear forces. The loading conditions simulate realistic cases for connections in building fires. The scope of the series of tests has provided the basis for a limited parametric study, with experimental data that validate the component-based models. The test setup is shown in Figure 1.

Figure 2 shows two typical test specimens. Figure 3 shows the failure of a reverse-channel connection. The researchers noted that the reverse-channel connection not only provides a practical construction-site solution for connecting steel beams to composite or hollow-section columns, but it also offers significant ductility and high strength when compared to other more conventional connection types, as documented in Figure 4. It is particularly important to note that the high ductility allows the extra connection forces and moments that are normally generated in a fire to be reduced to very low levels; this increases the connection fire resistance without requiring it to be extremely strong. Finally, a component-based finite element model was created for the connection using component characteristics developed in this and previous projects (Spyrou, 2002; Block, 2006; Yu et al., 2009).

Progressive Collapse Modeling of Steel-Framed Structure in Fire: Going beyond the COMPFIRE project, modeling and analysis of progressive collapse has been facilitated with the development of a software package called Vulcan. The research team has the same staffing, with the addition of Professor R.J. Plank. The main objective has

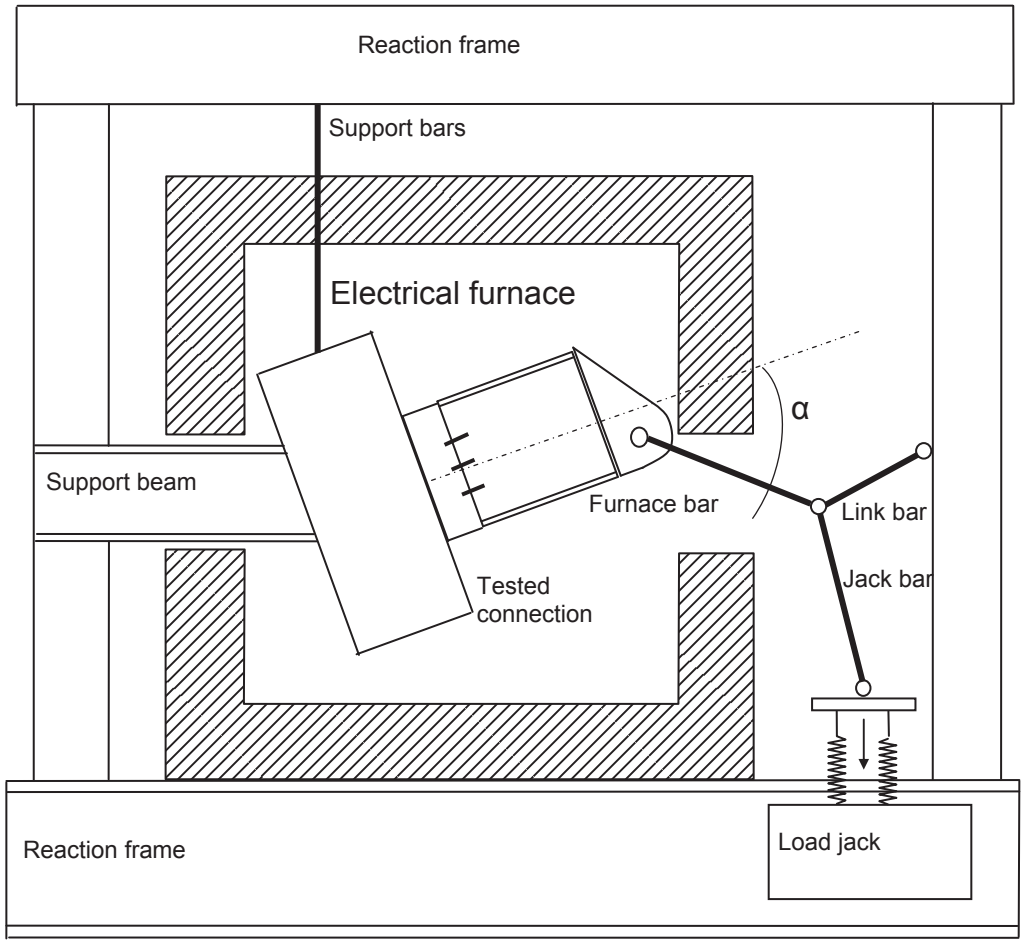

Fig. 1. Fire test setup for a beam-to-column connection (drawing courtesy of Professor Ian Burgess).

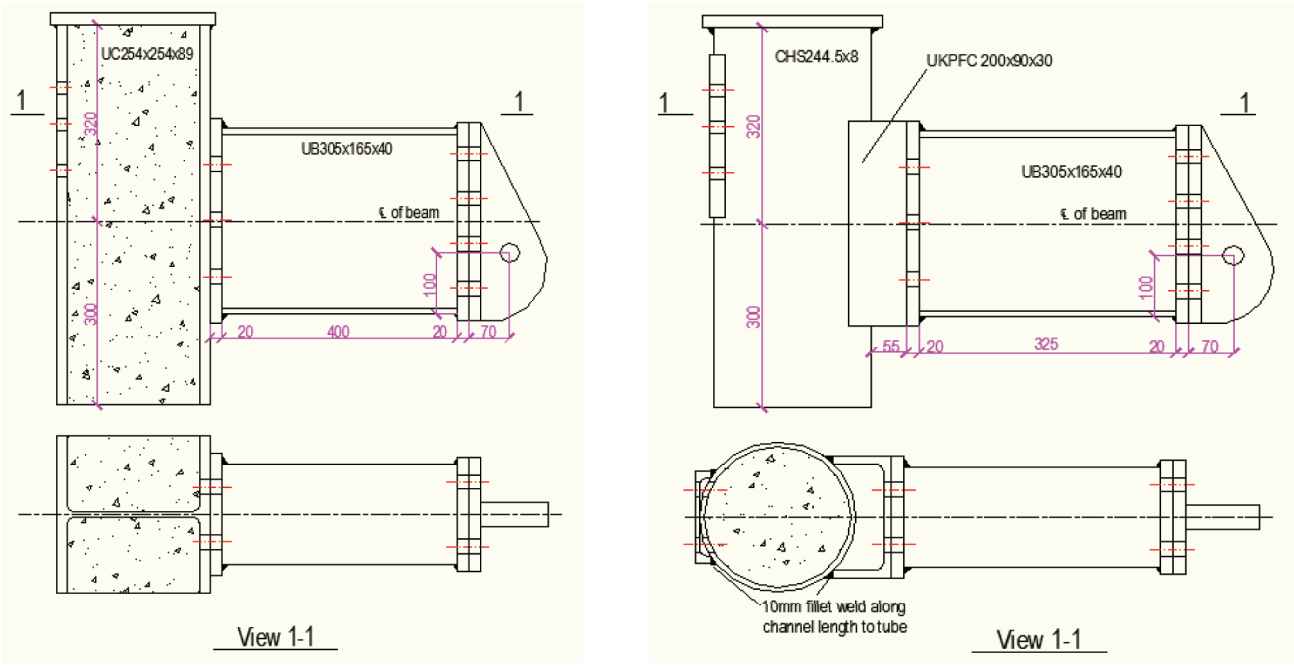

(a) (b)

Fig. 2. (a) Flush end-plate test specimen; (b) reverse channel test specimen (drawings courtesy of Professor Ian Burgess).

Fig. 3. Typical failure mode of a reverse-channel connection (photograph courtesy of Professor Ian Burgess).

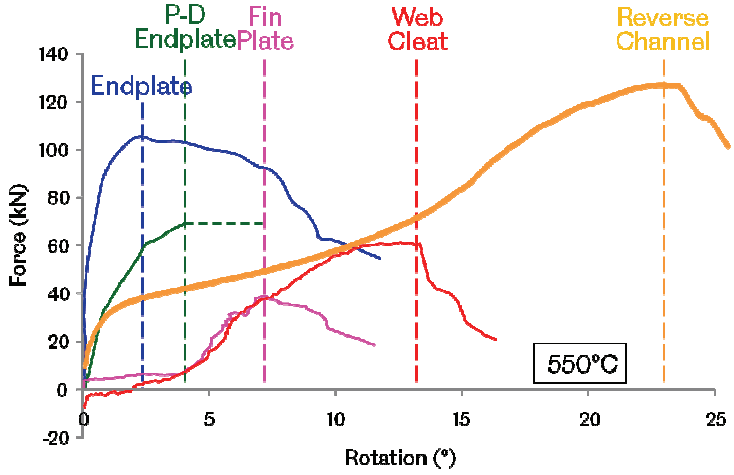

Fig. 4. Force-rotation relationships for various connections at 550 °C (1022 °F) (figure courtesy of Professor Ian Burgess).

been to develop a practical structural fire engineering analysis approach, allowing for the study of the mechanisms and principal phenomena of the progressive collapse process.

The numerical procedure used incorporates the complete structural behavior, including the progression from local buckling to overall collapse. The model combines alternate static and dynamic analyses as follows: Static analysis is used to trace the behavior of the structure at changing temperature until instability takes place. Beyond this point, a dynamic procedure is activated to track the motion of the system until stability is regained. This has been shown to work well in progressive collapse analyses that incorporate fire scenarios (Sun et al., 2012a). The process specifically allows for the identification of different forms of global failures and severe local failures, determining the sequence of the collapse mechanism. Several factors entering into the fire-induced progressive collapse are identified, including loading level, structural configuration and detailing, and type and location of the bracing system (Sun et al., 2012b). Figure 5 illustrates one such case of progressive collapse at increasing temperature levels.

Dynamic Behavior of Steel Connections with High Strain Rate and Noncyclic Dynamic Loading: Structural connections play a very important role in preventing progressive collapse in impact or explosion situations. Under such conditions, the connections must be capable of resisting high strain rates, meaning that high ductility is critical to help dissipate the energy through deformation without failure. The performance of connections under different types of loading using a wide range of strain rates was the motivation for a series of high-strain-rate tests on simple connections (Lau and Hancock, 1987). An example of a typical failure is shown in Figure 6.

In a follow-up study, numerical modeling was used to analyze the experimental results. Initially, a double-angle connection, which has a relatively complex geometry, was modeled as a base case for the development of other models. This approach has been validated by the experimental data, as illustrated in Figure 7 (p. 200). Additional models are now being developed for different types of connections. Parametric studies will be performed to evaluate the sensitivity of the models to geometric and material variations, particularly with reference to the effects of the strain rate.

Making the Case for Design for Deconstruction: This unique project reflects novel thinking about certain aspects of sustainability. Dr. Buick Davison is the director of the study, which explores what is required of the structural designer to take a structure down at the end of its useful life. Specifically, the study will investigate and quantify the environmental benefits of design for deconstruction. The strategy facilitates future reuse of structural and nonstructural materials by designing buildings to be systematically taken apart with no damage to their components. By reusing materials, the embodied energy and carbon of buildings can be reduced, and fewer natural resources need to be extracted from the earth. Steel is particularly suitable for reuse due to its durability as well as the fact that it is the most recycled of all materials. Steel elements do not necessarily have to be reused because contemporary steelmaking practice feeds recycled material into the steel production process.

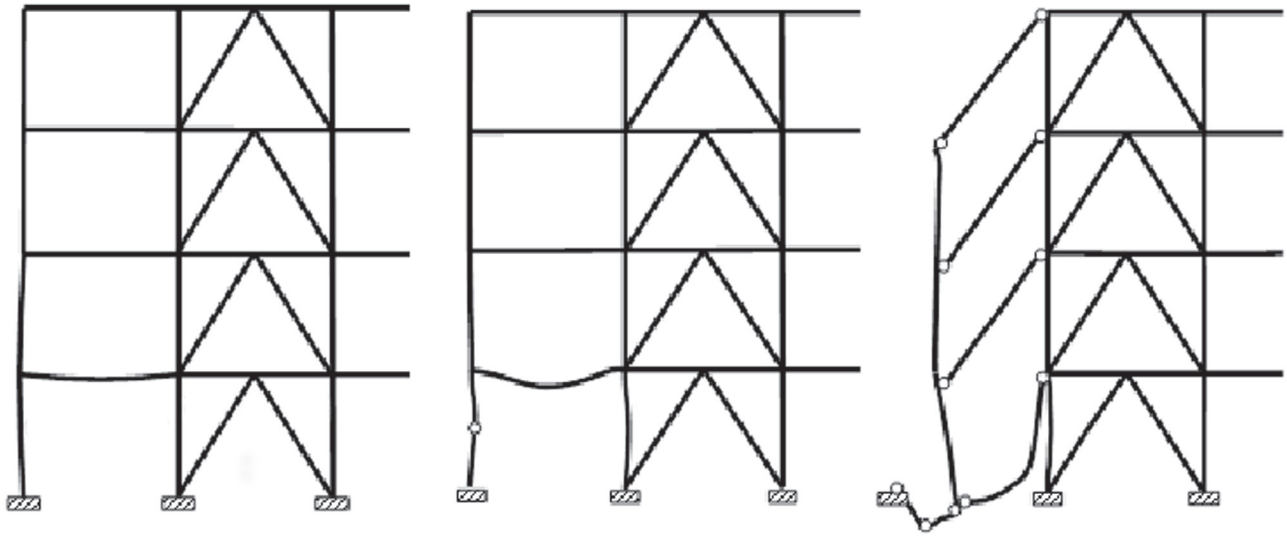

(a) 527 °C *(b) 698 °C* *(c) 745 °C*

Fig. 5. Progressive collapse mechanisms for a braced frame at increasing temperature (figure courtesy of Professors Ian Burgess and R.J. Plank).

Distortions, deflections and corrosion may have occurred in members during their service life. These effects can be measured, making it relatively simple to assess their suitability for reuse.

A methodology has been developed to account for designed-in future benefits (Densley Tingley and Davison, 2011a, 2011b). This involves sharing the environmental impact of a component between its predicted number of "structural lives." As an example, the benefits of designing a structural bay for deconstruction have been explored, showing that there can be a 60% increase in the embodied carbon of a structure if it has not been designed for deconstruction. Consequently, a web-based tool has been developed that facilitates calculation of the energy and carbon savings from designing for deconstruction, as well as the subsequent material reuse that will result. Named Sakura, the software allows designers to input information to explore the benefits to a specific project of designing for deconstruction. It is anticipated that the use of Sakura will promote and encourage design for deconstruction where appropriate, thus increasing future supply chains of reused materials and advancing sustainability.

SOME CURRENT RESEARCH WORK AT LULEÅ UNIVERSITY OF TECHNOLOGY IN LULEÅ, SWEDEN

The steel research group at Luleå University of Technology (LTU) is one of the most active in Europe and the only program in Sweden that has chair in steel structures. Professor Milan Veljkovic has been the director since 2007. To increase the relevancy of their work, the researchers include full-time faculty as well as part-time professors from industry and visitors from other countries. Naturally, doctoral candidates are critical to the success of research efforts, and in the last five years the program has grown from 2 to 13 participants. The group's expertise ranges from computational modeling to fire heat transfer to structural analysis and design.

The principal research subjects are:

- Behavior, strength and practical implementation of higher strength steel in construction; in applications for buildings, stadiums and other long span structures; and in towers for wind turbines.

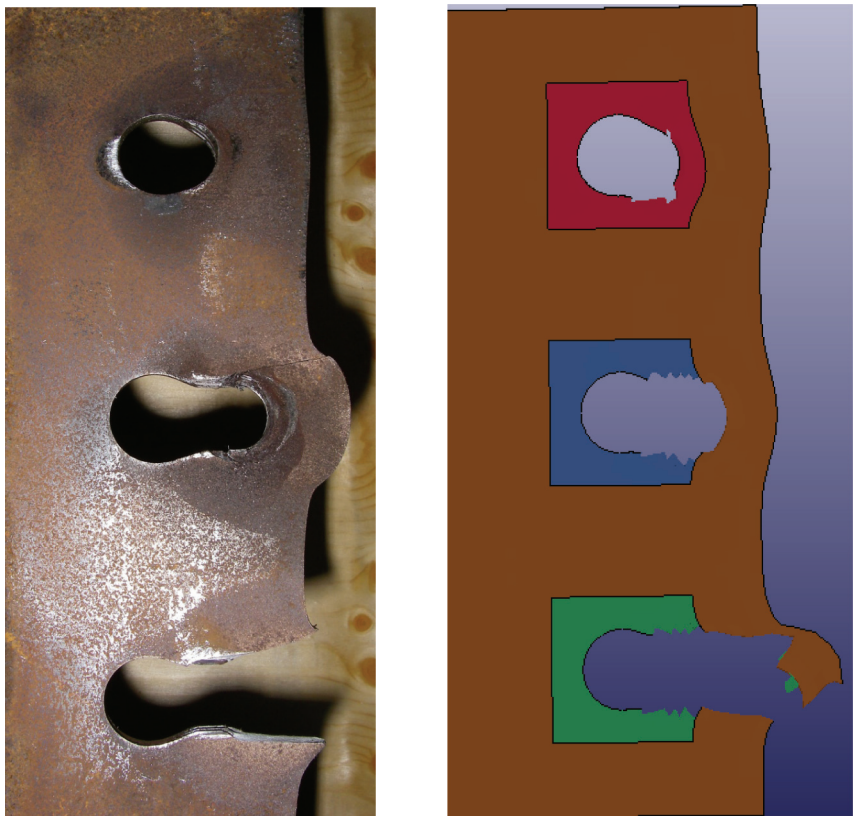

(a) (b)

Fig. 6. Failure of connection details due to high strain rates: (a) actual connection plate; (b) connection detail model (photographs courtesy of Professor Ian Burgess).

- Safety of structures exposed to fire, including fire development, heat transfer from the gas temperature to the structure and post-fire resistance of steel structures.

- Development of design recommendations for innovative bridges, such as composite bridges with integral abutments, where in-situ data are correlated with laboratory results and finite element analyses.

Recent work has added computational modeling of materials as well as stochastic material imperfections.

The group traditionally performs industry-oriented and applied research. Seven of the current eight projects are financed by the European Union. The majority of the projects receive funding from the Research Fund for Coal and Steel, and one is financed within the Framework Program 7, an EU-program for small and medium enterprises. As is now typical for European research efforts, multiple partners from academia and industry in several countries collaborate in each of the EU projects. The research funding to LTU of each project is approximately €100,000 per year.

Some of the current projects are described in the following.

High Steel Towers for Wind Turbines (HISTWIN): The first wind tower project was funded for a three-year period from 2006 to 2009. Professor Bernt Johannson (now retired) was the director. The research consortium consisted of Luleå Technological University (lead institution); the Technical University of Aachen (RWTH), Germany; the University of Coimbra, Portugal; Aristotle University of Thessaloniki, Greece; the steel company Rautaruukki OY, Finland; and the energy companies Martifer Energia, Portugal, and GLWind, Germany.

The main objective was to improve the competitiveness of tubular steel wind towers for hub-heights from 267 to 333 feet. The height limitation is required by transportation restrictions that limit the diameter of the bottom segment to about 15 feet. Traditional flange connections (Figure 8a) are labor intensive, expensive and require complex design models. Their fatigue resistance is low and is often the governing design criterion.

A breakthrough was achieved with an innovative solution that uses a slip-resistant connection with open-slotted holes. The idea is illustrated in Figure 8b. A series of small-scale physical tests were used to evaluate the feasibility of fabrication and to test the critical connection. The tests provided input data for finite element analysis and for design.

To facilitate assembly of the tubular sections, the lower segment has long, open-slotted holes, as indicated in Figure 8b. The bolts can be preinstalled in the standard holes in the upper section and then used for the angular alignment

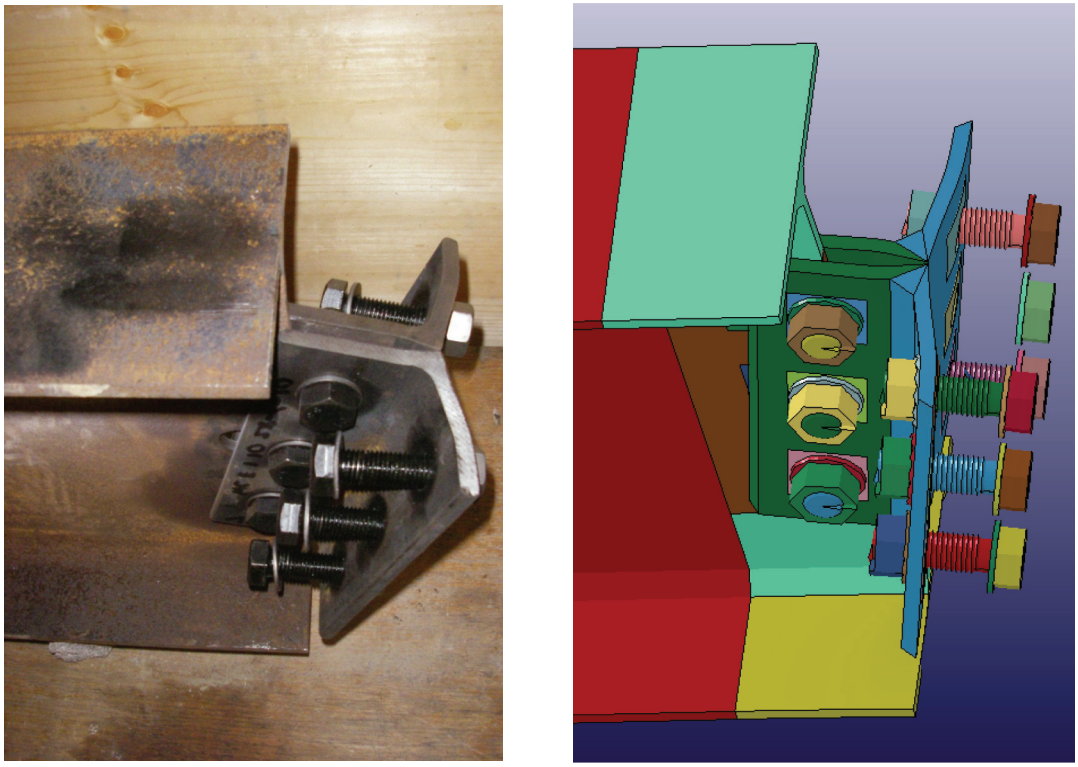

(a) *(b)*

Fig. 7. (a) Deformed angles of the physical test; (b) connection model (photographs courtesy of Professor Ian Burgess).

while the upper segment slides down. Slots weaken the lower section, giving lower sensitivity to assembly tolerances. The bending stiffness of the tubular shell is enhanced by the overlapping connection. Essentially, this connection allows for tight contact between the cylinders of the upper and lower tubular segments. Lastly, instead of using standard washers for each bolt, a common cover plate solution has been developed. Its purpose is to hold the bolt group together during assembly and to distribute the clamping force in a more uniform manner.

High Steel Towers for Wind Turbines—Second Project (HISTWIN 2): Due to the overall scope of the tubular wind tower project, it was decided that a follow-up project was needed. The funding period was three years, from 2010 to 2013. The academic and industry partners were the same as the first project, and Professor Milan Veljkovic was appointed project director.

The issue of local stability had been identified as critical to the success of the HISTWIN projects. To address this concern, the distances between the bolts in longitudinal connections and between modular segments have to be optimized. Numerical analysis and physical testing will be used to evaluate the effects on longitudinal bolted connections.

In the early segments of the project, it became clear that the stability issue would be more important for towers with slip-resistant connections. This subject is currently being addressed by considering alternative cross-sections. For example, using various numbers of folds to create a polygonal cross-section offers an attractive solution. Also, the foundations for the towers are critical, considering where the towers will be placed in the ocean. Traditional concrete slab foundations currently used in most onshore wind farms are not adequate for higher towers. A new type of hybrid slab foundation anchored with steel micro-piles has been developed, and this solution appears to offer significant advantages.

Optimization of Frames for Effective Assembly (Project FRAMEUP): The project is funded by the European Union's Research Fund for Coal and Steel for the period from 2011 to 2014. The research consortium consists of Luleå Technological University (lead institution); the University of Liège, Belgium; the Technical University of Aachen (RWTH), Germany; the University of Coimbra, Portugal; Aristotle University of Thessaloniki, Greece; and the construction companies Acciona Infrastructures S.A., Spain, PartConstruction AB, Sweden, and V&M Deutschland GmbH, Germany.

The three main objectives of the project are:

- *To develop the concept of a design process for a structural system primarily used for buildings with prefabricated steel 3D modules.* The process will be tested by computer simulations using a virtual engineering tool. Such a tool allows for the identification of all possible conflicts in the design, including the transfer of modules from delivery trucks to the structure. This is an integral part of the new design process. The procedure starts with the assembly of the roof and the top floor, providing a stiff structure that will be lifted by jacks. Each story will be assembled at the ground level and then lifted up to create space for the next story. This protects every story from precipitation and other moisture damage during the assembly. The process is based on using jacks

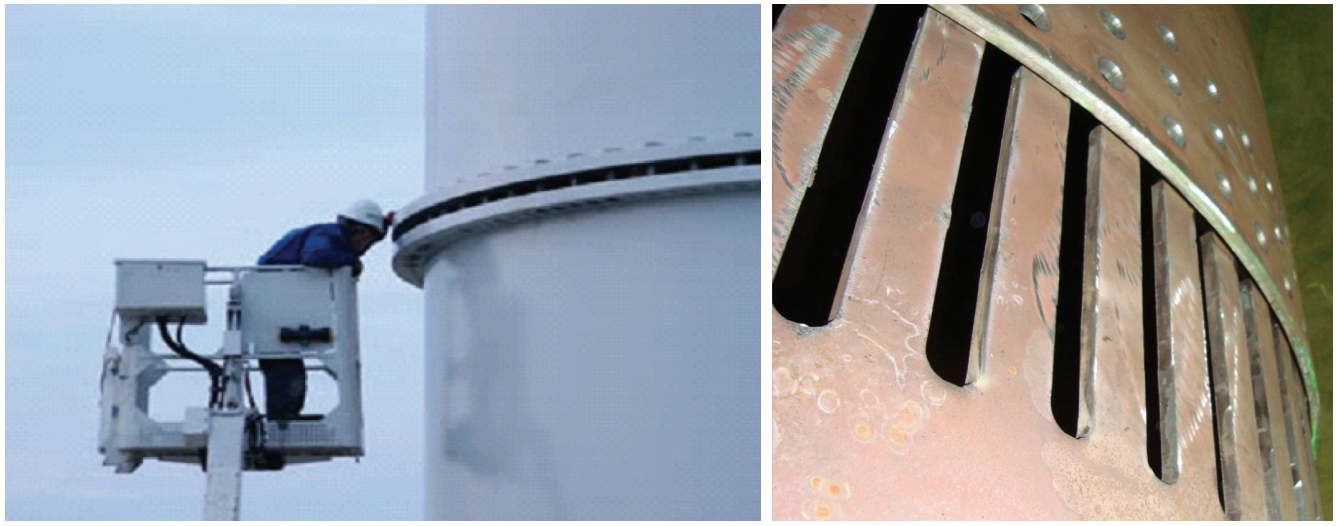

(a) *(b)*

Fig. 8. Wind turbine tower connections: (a) traditional flange connection; (b) slip-resistant connection (photographs courtesy of Professor Milan Veljkovic).

instead of cranes and is expected to be safer and drier. The construction site will also be smaller, with less noise and other disturbances for its neighbors. An example is shown in Figure 9.

- *To test and establish the performance of a new type of connection that uses a number of nonstandardized components.* The connections are developed for HSS columns and beams. They must satisfy the requirements for faster assembly and disassembly as well as the requirements for moment resistance specified by local design codes.

- *To achieve an optimized building technology with 3D modules using the innovative erection technique.* This is influenced by the architectural demands, which in turn influence the structural solution.

Design of Connections to Composite Columns for Improved Fire Robustness (COMPFIRE): This project is in partnership with the University of Sheffield, previously discussed.

Other Projects: Projects on High-Strength Long-Span Structures (HILONG) and Rules On High-Strength Steel (ROUSTE) have been approved for 2012 through 2015. Studies on composite bridge construction were conducted in the project Economic and Durable Design of Composite Bridges with Integral Abutments (INTAB+) and completed in 2011. Papers and reports are currently being prepared.

Significant educational efforts will also be pursued during the 2012 through 2015 time period, addressing the broad subject of sustainable structures under natural hazards and catastrophic events. These projects are funded by the European Union under the Erasmus Mundus educational program. Six universities are partnering for this activity.

SOME CURRENT RESEARCH WORK AT THE UNIVERSITY OF TRENTO IN TRENTO, ITALY

The structural engineering research group at the University of Trento was established in 1985 when the Faculty of Engineering was founded. Since the very beginning, the group has been active in the fields of steel and wood construction, generally associated with earthquake engineering. Most recently, the fields of smart structures and structural monitoring and control have been explored.

The research group has seven faculty members related to steel structures. Their current activities focus on three main areas of research:

- Dynamic and seismic response of steel and composite (steel-concrete) structural systems.

- Stability of complex engineering systems.

- Structural robustness.

In addition, the group is heavily involved in industry-based research projects. These projects include a nearly 20-year effort supporting Italian rack manufacturers. The

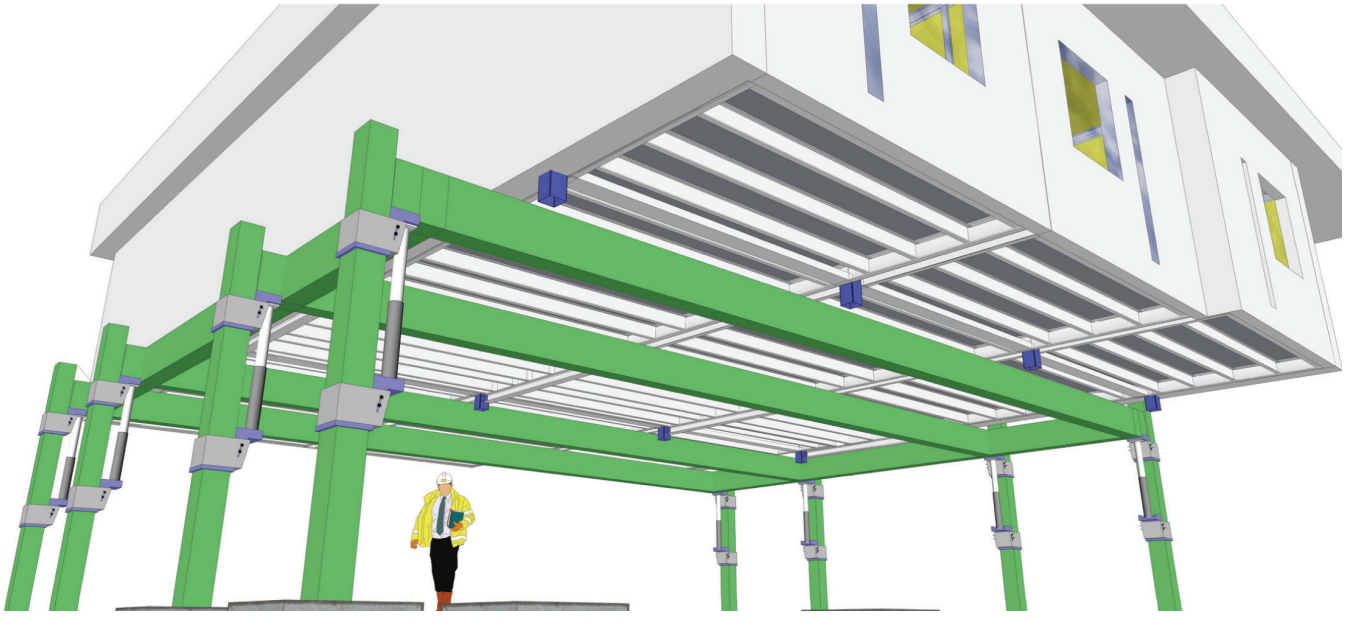

Fig. 9. Erection phase of the FRAMEUP pilot building (figure courtesy of Professor Milan Veljkovic).

knowledge gained from rack research related to the performance of cold-formed systems led the group to develop a new prefabricated system for residential steel housing.

Extensive experimental facilities provide great flexibility in accommodating complex tests under static and dynamic loading, including full-scale specimens. The group is also active with Italian and European code committees, as well the committees of the European Convention for Constructional Steelwork (ECCS). A discussion of several of their current research projects follows.

Design and Integrity Assessment of High-Strength Tubular Structures for Extreme Loading Conditions (HITUBES): Funded by the European Union's Research Fund for Coal and Steel with the University of Trento as the lead institution, Professor Oreste Bursi is the project director. The project partners are the University of Liège, Belgium; the University of Thessaloniki, Greece; the Italian Center for Materials Development; the Portuguese Institute for Welding and Quality; the ITMA Foundation of Spain; and the Corrosion and Metals Research Institute of Sweden.

The HITUBES project was recently completed. The project goal was to develop performance-based design and assessment procedures for the use of high-strength steel tubes in a variety of applications, in steel grades as high as S700MC (a yield stress of 700 MPa or 100 ksi). The use of tubes in structures subjected to extreme repeated loads was also examined. The project's ambitious goals included increasing structural performance, reducing structural weight, and reducing construction and operating costs. Specifically, the following subjects were addressed:

- Structural identification and health monitoring of cable-stayed and arch footbridges.
- Simulation of welded and bolted connections under monotonic, low-cycle and high-cycle fatigue loadings.
- Reliability analysis for quantification of realistic performance scenarios.

Two types of structures were analyzed in detail for possible construction with steel tubes: slender pedestrian and bicycle bridges and the arch and hanger elements of railway bridges. Railway bridges in particular are commonly subjected to extreme repeated loads.

The Trento contribution was mainly associated with the dynamic identification and the finite element model updating. Reference was made to the Ponte del Mare, the bridge shown in Figure 10, which is a twin-deck, curved, cable-stayed pedestrian bridge. The outer deck is reserved for pedestrians, while the inner deck is for bicyclists. The decks have constant radii of approximately 267 feet and 330 feet.

The pedestrian bridge was redesigned using circular hollow sections in steel grade TS 590 (a yield stress of 590 MPa or 85 ksi). In the redesign, the high-strength steel and the circular cross-sections combine to reduce the visual impact of the bridge and to reduce the structure's weight. The research included both design and in-situ testing of the bridge. A comprehensive numerical analysis showed that a passive control system made of elastic and viscous-fluid dampers was necessary to mitigate pedestrian vibrations and to satisfy wind safety requirements relative to premature aeroelastic instability.

Performance-Based Approaches for High-Strength Tubular Columns and Connections under Earthquake and Fire Loads (ATTEL): The project is also funded by the Research Fund for Coal and Steel, with the University of Liège as the lead institution. The international partners are the University of Trento and the University of Thessaloniki, Greece, with industry partners the Italian Center for Materials Development and Italian fabricator Pichler. The Trento group is coordinated by Professor Oreste Bursi.

A capacity design approach, in which structures are designed to meet the strong column–weak beam concept, is usually achieved by overdesigning the columns. A substantial improvement to the structural performance using this approach may be achieved by the use of high-strength steel, provided the steel and the detailing meet ductility and energy absorption criteria. The adoption of high-strength circular hollow sections for such purposes has been limited, despite excellent structural properties. Even recent Eurocode 3 modifications permitting the use of steel grades up to 700 MPa (100 ksi) maintain strict limitations at the material, structural and design levels (ECCS, 2005, 2007).

The ATTEL project aims to provide the analytical and experimental knowledge necessary to develop design criteria for the high-strength steel and composite circular hollow sections for columns and connections subjected to seismic and fire loads. The focus is on structural tubes ranging from 7 in. to 14 in. in diameter with a D/t ratio greater than 30. This range is of great interest for onshore structures. The following subjects are addressed:

- Steel and concrete-filled tubular (CFT) columns made of high-strength steel.
- Welded or bolted composite beam-to-CFT column connections in high-strength steel.
- CFT column base connections made of high-strength steel.

In Trento, the study has focused on the cyclic performance both of column base connections for tubular composite columns and beam-to-column connections (Zanon et al., 2011). The first series of tests on standard and innovative column base connection solutions are shown in Figures 11 and 12. Both standard and innovative seismic connections exhibited

favorable hysteretic response without loss of strength and stiffness.

Stability of Industrial Steel Pallet Racks: Industrial racks are one of the most common structures for storing palletized goods. Examples of such structures are shown in Figure 13. A number of studies were carried out under the supervision of Professors Nadia Baldassino and Riccardo Zandonini to investigate key aspects of the performance of such systems.

Rack structures use thin-walled cold-formed steel shapes and, for this and many other reasons, exhibit very complex behavior. The main sources of complexity are the sensitivity of the columns (uprights) to buckling, the presence of perforations on the uprights that provide for the attachment of beams, the non-linear response of the connections, the frame sensitivity to the second-order effects and the influence of imperfections. The large variability in the geometry of the shapes, of the joints and of the perforations combined with the complexities of member behavior cannot be incorporated into practical design provisions at this time. Tests—preferably full-scale tests—are needed.

Relevant codes recognize the concept of design by testing and provide detailed recommendations for the testing of members, subsystems and joints (AISI, 2007). A thorough analysis of Eurocode 3 (ECS, 2005) identified a number of issues that are not adequately addressed (Baldassino and Zandonini, 2011). This triggered several studies of the buckling of perforated members, of base-plate connections and of the shear stiffness of upright frames.

The most recent work relates to the upright frames that typically ensure the stability of pallet racks in the cross-aisle direction (Gilbert et al., 2012). These frames are sensitive to second-order effects, and an accurate determination of their shear stiffness is essential for seismic design and

Fig. 10. The Ponte del Mare, a pedestrian and bicycle bridge in Pescara, Italy (photograph courtesy of Professor Oreste Bursi).

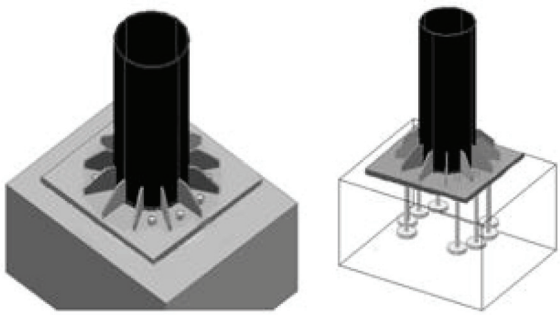

Fig. 11. Standard solution for a column base connection (courtesy of Professor Oreste Bursi).

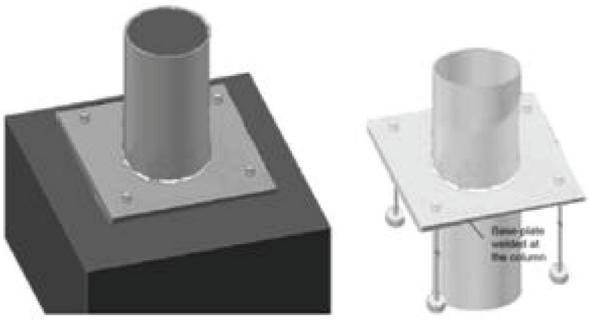

Fig. 12. Innovative solution for a column base connection (courtesy of Professor Oreste Bursi).

to ensure the stability of the rack, especially in the case of high-bay racks and racks supporting the building enclosure. The study compared two alternative methods, one of which is specified by the Eurocode, 3 and the other by the Australian standard. Figure 14 shows the assemblies of the two tests, as performed at the University of Sydney. A total of 36 tests of different frame configurations were performed, including numerical analyses to assess the accuracy of the two methods. The preliminary results show that the shear stiffness determined by these methods may vary by as much as a factor of two. Additional work will be pursued.

Base-Plate Connections for Rack Structures: Column base connections of rack frames are unique, and their response is significantly different from the corresponding connections in traditional steel frames. In Italian practice, the base connections are typically built up from base-plate elements that are bolted to the uprights and connected to the floor by means of special fixing systems. Figure 15 shows some representative examples.

Structural Robustness of Composite Frames: This project is funded by the European Union's Research Fund for Coal and Steel, as a joint effort between the University of Stuttgart, Germany (lead institution) and the University of Trento. Professor Ulrike Kuhlmann of the University of Stuttgart is the project director; Professor Riccardo Zandonini is the Trento coordinator.

Despite studies on robustness that began in the 1960s, only general strategies to achieve effective robust structural

Fig. 13. Typical steel storage pallet rack systems (photographs courtesy of Professors Nadia Baldassino and Riccardo Zandonini).

designs have been established. Recent failures have demonstrated the inadequacy of traditional design approaches when collapse has resulted from local damage caused by human accidental actions. Such issues call for design methodologies that allow verification of the safety of the structure in the statically modified condition so that local damage does not produce a chain reaction that may lead to partial or complete progressive collapse of the structure.

The tests conducted at the University of Trento were aimed at determining the performance of both the concrete slab and the steel connection, in accordance with the component method of connection design as specified by Eurocode 3 (ECS, 2005). In particular, the study focused on the response of connections subjected to combined axial, shear and moment stress resultants, as illustrated in Figure 16, and on T-stub components under combined axial and shear forces (Baldassino and Zandonini, 2009).

The testing assembly shown in Figure 17 was specifically designed to apply a wide range of axial and shear forces to the T-stub. By changing the location where the testing assembly is connected, it is possible to simulate rotation of the T-stub with respect to the load line. This rotation effectively allows for the application of different combinations of axial and shear forces, ranging from pure tension to pure shear. The tests on the full connection demonstrated the negative influence on both the ultimate load and deformation capacities of a loading history that combines shear, moment and axial force. The T-stub tests provided the data for the shear and axial force interaction domains. Both series confirmed the inherent high ductility.

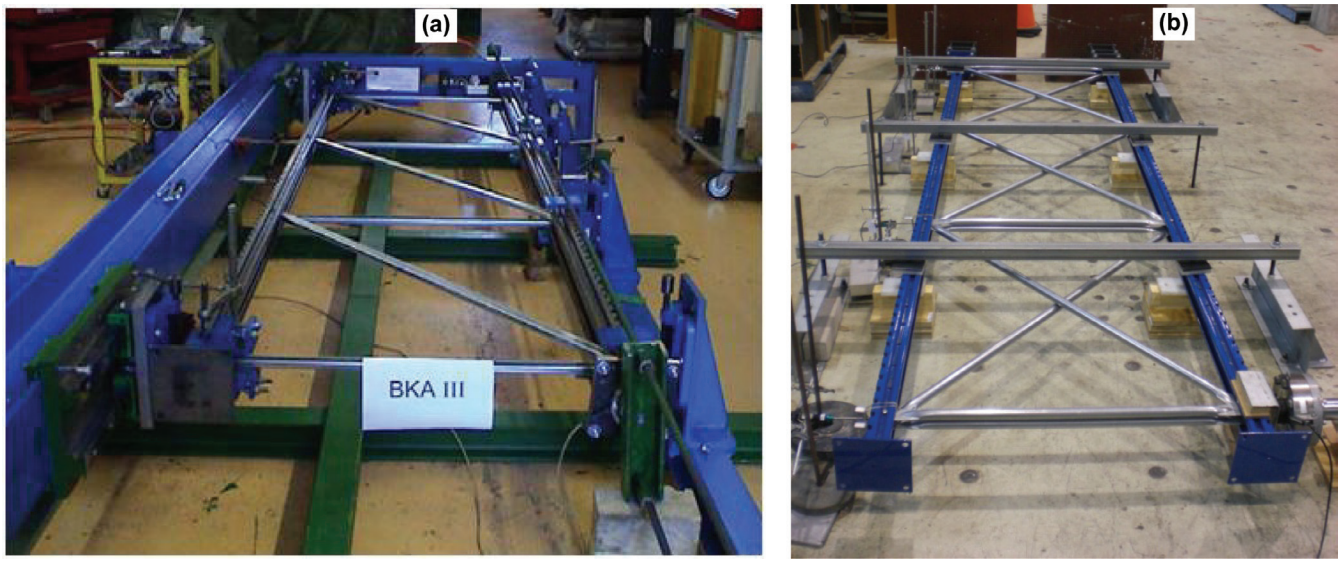

Fig. 14. Shear tests on upright frames: (a) Eurocode 3 method; (b) Australian standards method (photographs courtesy of Professor K.J.R. Rasmussen).

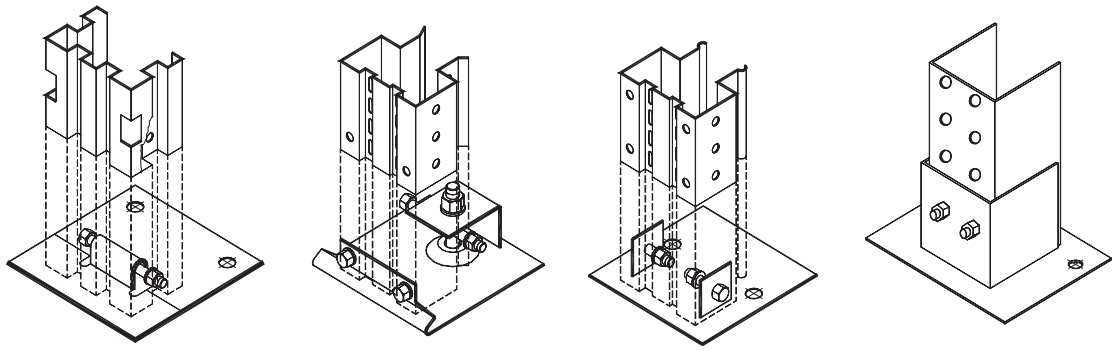

Fig. 15. Typical base connection details for Italian rack structures (figures courtesy of Professors Nadia Baldassino and Riccardo Zandonini).

A second project, about to start with the same partners, will primarily examine 3D action and the strain rate effect. The University of Trento will perform two full-scale tests on a flooring system as shown in Figure 18 to investigate the strain-rate effect on the T-stub response.

ACKNOWLEDGMENTS

Significant assistance has been provided by ISSRA member Professor Riccardo Zandonini of the University of Trento, and by his colleagues Professors Nadia Baldassino and Oreste Bursi. Professor Ian Burgess of the University

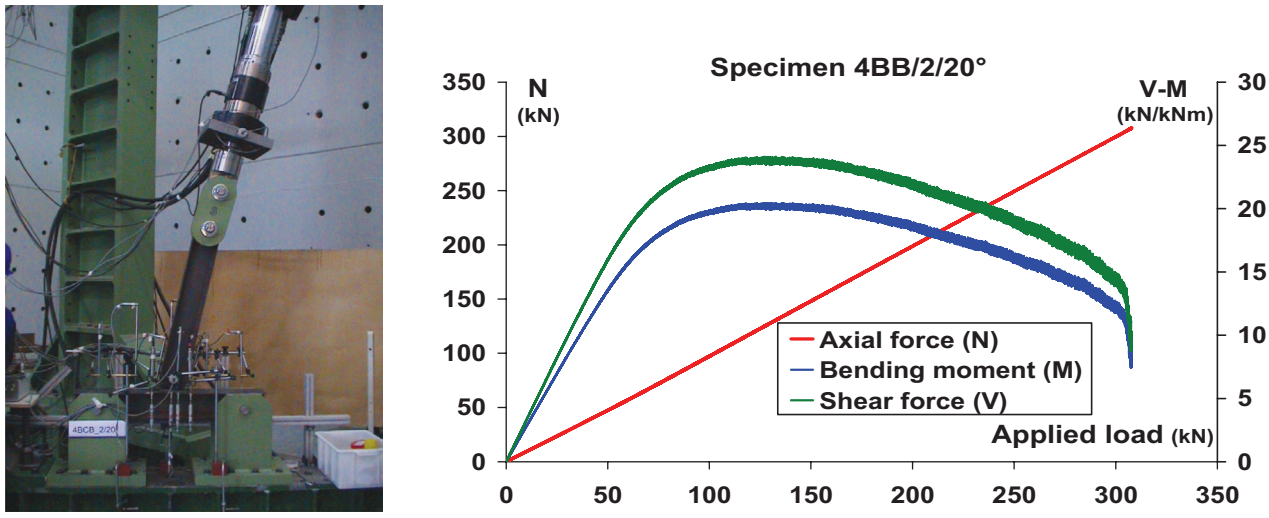

Fig. 16. Test on beam-to-column connection under combined axial and shear forces (figures courtesy of Professors Nadia Baldassino and Riccardo Zandonini).

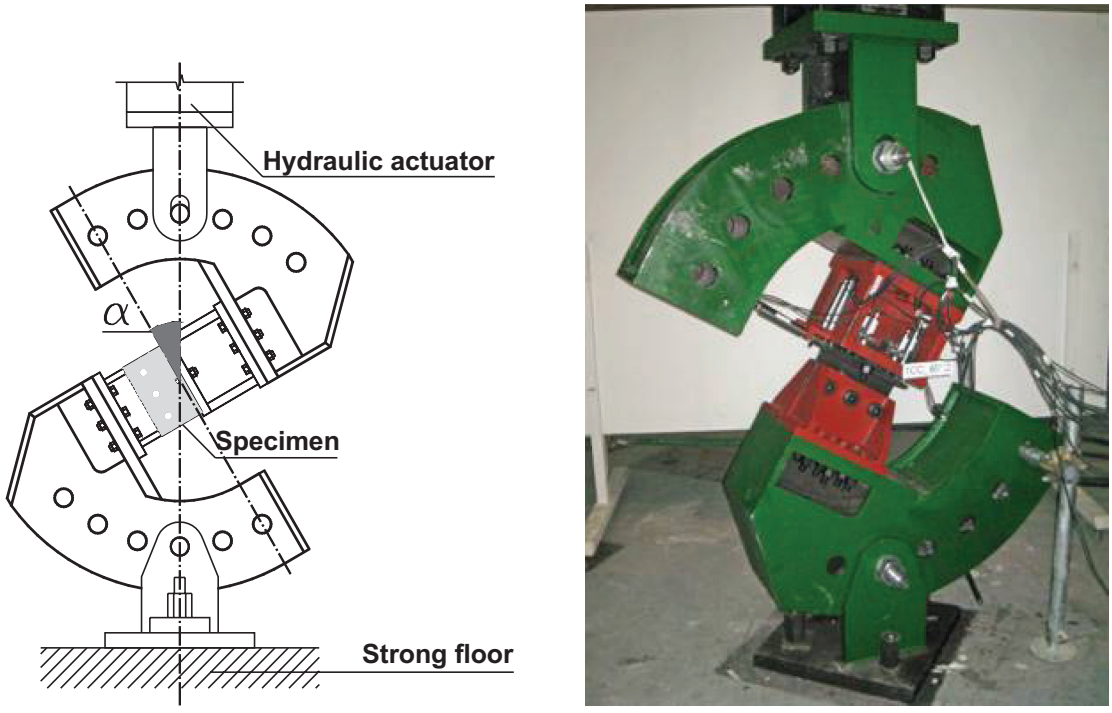

Fig. 17. Test set-up for T-stub tests under axial and shear force (figures courtesy of Professors Nadia Baldassino and Riccardo Zandonini).

of Sheffield and his colleagues R.J. Plank and Buick Davison were likewise very helpful, as were Professor Milan Veljkovic and his colleagues at the Luleå University of Technology. Their efforts are very sincerely appreciated.

REFERENCES

AISI (2007), *North American Specification for the Design of Cold-Formed Steel Structural Members*, ANSI/AISI Standard No. S100, American Iron and Steel Institute, Washington, D.C.

Baldassino, N. and Zandonini R. (2009), "Response of End-Plate Joints under Combined Forces," *Proceedings, ASCE Structures Congress,* Austin, TX, April 30–May 2, pp. 1821–1830.

Baldassino, N. and Zandonini R. (2011), "Design by Testing of Industrial Racks," *Advanced Steel Construction*, Vol. 7, No. 1, pp. 27–47.

Block, F.M. (2006), "Development of a Component-Based Finite Element for Steel Beam-to-Column Connections at Elevated Temperatures," Ph.D. Dissertation, University of Sheffield, United Kingdom.

Densley Tingley, D. and Davison, B. (2011a), "Supporting Design for Deconstruction through Environmental Assessment Methods," *Architectural Science*, No. 3, Special Issue, June, pp. 1–18.

Densley Tingley, D. and Davison, B. (2011b), "Design for Deconstruction and Material Reuse," *Proceedings of the Institution of Civil Engineers, Energy*, November, pp. 195–204.

ECS (2005), *Eurocode 3: Design of Steel Structures—Part 1-1: General Rules and Rules for Buildings,* Standard No. EN 1993-1-1, European Committee for Standardization, Brussels, Belgium.

ECS (2007), *Eurocode 3: Design of Steel Structures—Part 1-12: Additional Rules for the Extension of EN 1993 up to Steel Grades S700,* Standard No. EN 1993-1-12, European Committee for Standardization, Brussels, Belgium.

Gilbert, B.P., Rasmussen, K.J.R., Baldassino, N., Cudini, T. and Rovere, L. (2012), "Determining the Transverse Shear Stiffness of Steel Storage Rack Upright Frames," *Journal of Constructional Steel Research*, Vol. 78, pp. 107–116.

Lau, S.C.W. and Hancock, G.J. (1987), "Distortional Buckling Formulas for Channel Columns," *Journal of Structural Engineering*, ASCE, Vol. 113, No. 5, pp. 1063–1078.

Spyrou, S. (2002), "Development of a Component-Based Model of Steel Beam-to-Column Joints at Elevated Temperatures," Ph.D. Dissertation, University of Sheffield, United Kingdom.

Sun, R.R., Huang, Z.H. and Burgess, I.W. (2012a), "Progressive Collapse Analysis of Steel Structures under Fire Conditions," *Engineering Structures*, Vol. 34, pp. 400–413.

Sun, R.R., Huang, Z.H. and Burgess, I.W. (2012b), "The Collapse Behaviour of Braced Steel Frames Exposed to Fire," *Journal of Constructional Steel Research*, Vol. 72, pp. 130–142.

Yu, H.X., Burgess, I.W., Davison, J.B. and Plank, R.J. (2009), "Development of a Yield-Line Model for Endplate Connections in Fire," *Journal of Constructional Steel Research*, Vol. 65, No. 6, pp. 1279–1289.

Zanon, G., Kumar, A., Bursi, O.S., Ferrario, F., and Giacobbe, A. (2011), "High Strength Tubular Columns and Connections under Earthquake, Fire Loading and Fatigue," *Metallurgia Italiana*, Vol. 3, pp. 25–31.

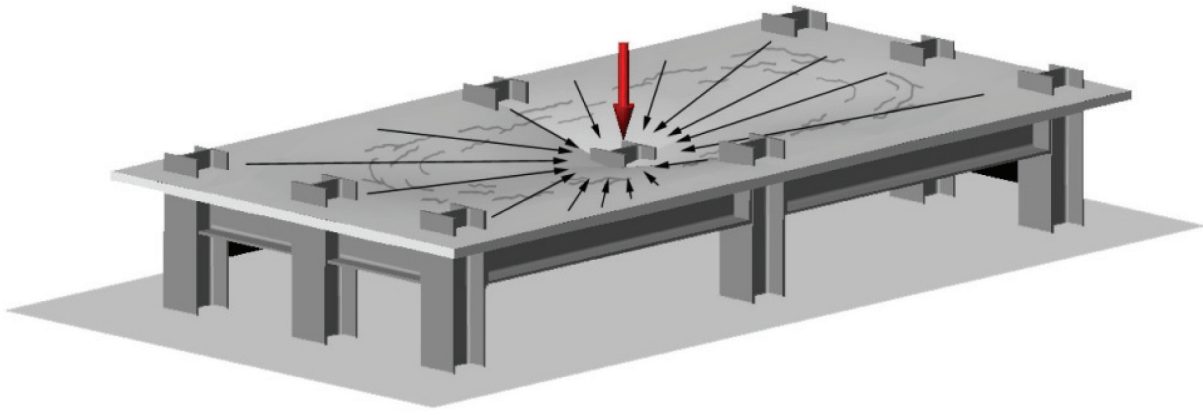

Fig. 18. Full-scale test on a floor system simulating the collapse of a column (figure courtesy of Professors Nadia Baldassino and Riccardo Zandonini).

GUIDE FOR AUTHORS

SCOPE: The ENGINEERING JOURNAL is dedicated to the improvement and advancement of steel construction. Its pages are open to all who wish to report on new developments or techniques in steel design, research, the design and/or construction of new projects, steel fabrication methods, or new products of significance to the uses of steel in construction. Only original papers should be submitted.

GENERAL: Papers intended for publication may be submitted by mail to the Editor, Keith Grubb, ENGINEERING JOURNAL, AMERICAN INSTITUTE OF STEEL CONSTRUCTION, One East Wacker Drive, Suite 700, Chicago, IL, 60601, or by email to grubb@aisc.org.

The articles published in the *Engineering Journal* undergo peer review before publication for (1) originality of contribution; (2) technical value to the steel construction community; (3) proper credit to others working in the same area; (4) prior publication of the material; and (5) justification of the conclusion based on the report.

All papers within the scope outlined above will be reviewed by engineers selected from among AISC, industry, design firms, and universities. The standard review process includes outside review by an average of three reviewers, who are experts in their respective technical area, and volunteers in the program. Papers not accepted will not be returned to the author. Published papers become the property of the American Institute of Steel Construction and are protected by appropriate copyrights. No proofs will be sent to authors. Each author receives three copies of the issue in which his contribution appears.

MANUSCRIPT PREPARATION: Manuscripts must be provided in Microsoft Word format. Include a PDF with your submittal. View our complete author guidelines at **www.aisc.org/ej**.

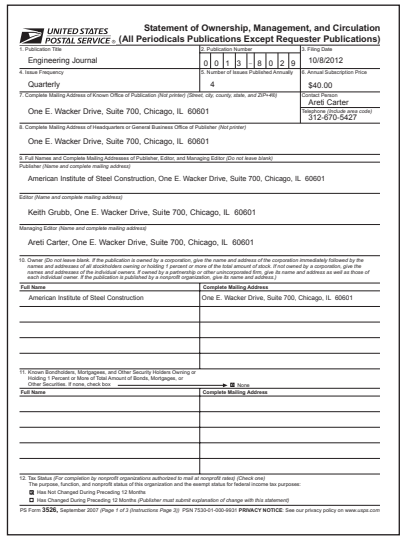

UNITED STATES POSTAL SERVICE® **Statement of Ownership, Management, and Circulation (All Periodicals Publications Except Requester Publications)**

1. Publication Title	2. Publication Number	3. Filing Date
Engineering Journal	0 0 1 3 - 8 0 2 9	10/8/2012
4. Issue Frequency	5. Number of Issues Published Annually	6. Annual Subscription Price
Quarterly	4	$40.00

7. Complete Mailing Address of Known Office of Publication (Not printer) (Street, city, county, state, and ZIP+4®): One E. Wacker Drive, Suite 700, Chicago, IL 60601 — Contact Person: Areti Carter; Telephone (Include area code): 312-670-5427

8. Complete Mailing Address of Headquarters or General Business Office of Publisher (Not printer): One E. Wacker Drive, Suite 700, Chicago, IL 60601

9. Full Names and Complete Mailing Addresses of Publisher, Editor, and Managing Editor (Do not leave blank)

Publisher (Name and complete mailing address): American Institute of Steel Construction, One E. Wacker Drive, Suite 700, Chicago, IL 60601

Editor (Name and complete mailing address): Keith Grubb, One E. Wacker Drive, Suite 700, Chicago, IL 60601

Managing Editor (Name and complete mailing address): Areti Carter, One E. Wacker Drive, Suite 700, Chicago, IL 60601

10. Owner (Do not leave blank. If the publication is owned by a corporation, give the name and address of the corporation immediately followed by the names and addresses of all stockholders owning or holding 1 percent or more of the total amount of stock. If not owned by a corporation, give the names and addresses of the individual owners. If owned by a partnership or other unincorporated firm, give its name and address as well as those of each individual owner. If the publication is published by a nonprofit organization, give its name and address.)

Full Name	Complete Mailing Address
American Institute of Steel Construction	One E. Wacker Drive, Suite 700, Chicago, IL 60601

11. Known Bondholders, Mortgagees, and Other Security Holders Owning or Holding 1 Percent or More of Total Amount of Bonds, Mortgages, or Other Securities. If none, check box → ☒ None

Full Name	Complete Mailing Address

12. Tax Status (For completion by nonprofit organizations authorized to mail at nonprofit rates) (Check one)
The purpose, function, and nonprofit status of this organization and the exempt status for federal income tax purposes:
☒ Has Not Changed During Preceding 12 Months
☐ Has Changed During Preceding 12 Months (Publisher must submit explanation of change with this statement)

PS Form **3526,** September 2007 (Page 1 of 3 [Instructions Page 3]) PSN 7530-01-000-9931 **PRIVACY NOTICE:** See our privacy policy on www.usps.com

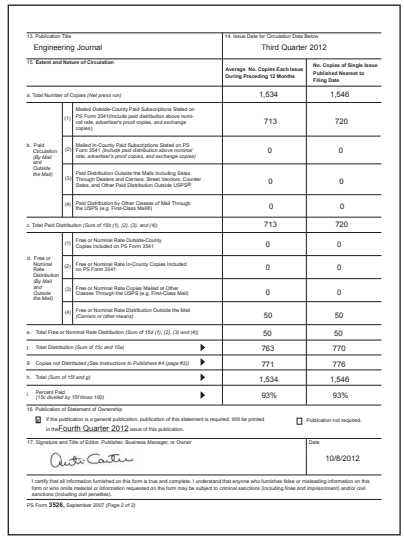

13. Publication Title	14. Issue Date for Circulation Data Below
Engineering Journal	Third Quarter 2012

15. Extent and Nature of Circulation			Average No. Copies Each Issue During Preceding 12 Months	No. Copies of Single Issue Published Nearest to Filing Date
a. Total Number of Copies (Net press run)			1,534	1,546
b. Paid Circulation (By Mail and Outside the Mail)	(1)	Mailed Outside-County Paid Subscriptions Stated on PS Form 3541(Include paid distribution above nominal rate, advertiser's proof copies, and exchange copies)	713	720
	(2)	Mailed In-County Paid Subscriptions Stated on PS Form 3541 (Include paid distribution above nominal rate, advertiser's proof copies, and exchange copies)	0	0
	(3)	Paid Distribution Outside the Mails Including Sales Through Dealers and Carriers, Street Vendors, Counter Sales, and Other Paid Distribution Outside USPS®	0	0
	(4)	Paid Distribution by Other Classes of Mail Through the USPS (e.g. First-Class Mail®)	0	0
c. Total Paid Distribution (Sum of 15b (1), (2), (3), and (4))			713	720
d. Free or Nominal Rate Distribution (By Mail and Outside the Mail)	(1)	Free or Nominal Rate Outside-County Copies included on PS Form 3541	0	0
	(2)	Free or Nominal Rate In-County Copies Included on PS Form 3541	0	0
	(3)	Free or Nominal Rate Copies Mailed at Other Classes Through the USPS (e.g. First-Class Mail)	0	0
	(4)	Free or Nominal Rate Distribution Outside the Mail (Carriers or other means)	50	50
e. Total Free or Nominal Rate Distribution (Sum of 15d (1), (2), (3) and (4))			50	50
f. Total Distribution (Sum of 15c and 15e)			763	770
g. Copies not Distributed (See Instructions to Publishers #4 (page #3))			771	776
h. Total (Sum of 15f and g)			1,534	1,546
i. Percent Paid (15c divided by 15f times 100)			93%	93%

16. Publication of Statement of Ownership
☒ If the publication is a general publication, publication of this statement is required. Will be printed in the Fourth Quarter 2012 issue of this publication. ☐ Publication not required.

17. Signature and Title of Editor, Publisher, Business Manager, or Owner: Areti Carter — Date: 10/8/2012

I certify that all information furnished on this form is true and complete. I understand that anyone who furnishes false or misleading information on this form or who omits material or information requested on the form may be subject to criminal sanctions (including fines and imprisonment) and/or civil sanctions (including civil penalties).

PS Form **3526,** September 2007 (Page 2 of 3)